Nearly Perfect Fluidity: From Cold Atomic Gases to Hot Quark Gluon Plasmas

Thomas Schäfer[1] **and Derek Teaney**[2,3]

[1]Department of Physics, North Carolina State University, Raleigh, NC 27695
[2]Department of Physics, State University of New York at Stony Brook, Stony Brook, NY 11794
[3] RIKEN-BNL Research Center, Brookhaven National Laboratory, Upton, NY 11973

Abstract. Quantum uncertainty suggests a lower bound on the internal friction – shear viscosity – of a fluid. The shear viscosity of a nearly perfect fluid approaches this bound. A measure of fluidity is provided by the ratio of shear viscosity η to entropy density s. In this review we summarize theoretical and experimental information on the structure of the three main classes of quantum fluids that are known to have values of η/s that are smaller than $\hbar/k_B$, where $\hbar$ is Planck's constant and k_B is Boltzmann's constant. These fluids are strongly coupled Bose fluids, in particular liquid Helium, strongly correlated ultracold Fermi gases, and the quark gluon plasma. We discuss the main theoretical approaches to transport properties of these fluids: kinetic theory, numerical simulations based on linear response theory, and holographic dualities. We also summarize the experimental situation, in particular with regard to the observation of hydrodynamic behavior in ultracold Fermi gases and the quark gluon plasma.

Contents

1 Introduction **3**

2 Strongly coupled quantum fluids **6**
2.1 Bose fluids: Dilute Bose gases 6
2.2 Bose fluids: Liquid helium 8
2.3 Fermi liquids: The dilute Fermi gas at unitarity 9
2.4 Gauge theories: QCD 13
2.5 Gauge theories: Superconformal QCD 16

3 Transport theory **18**
3.1 Hydrodynamics 19
3.1.1 Non-relativistic fluids 19
3.1.2 Superfluid hydrodynamics 21
3.1.3 Relativistic fluids 22
3.2 Diffusion 25
3.3 Dynamic universality 25
3.4 Kubo relations and spectral functions 26
3.5 Kinetic theory: Shear viscosity 28
3.5.1 Phonons in dilute Fermi gases 29
3.5.2 Phonons and rotons in liquid helium, pions in QCD 31
3.5.3 Non-relativistic atoms: Dilute Fermi gases and ^{4}He 32
3.5.4 Gauge fields in QCD 33
3.6 Kinetic theory: Other transport properties 36
3.6.1 Bulk viscosity 36
3.6.2 Diffusion 36
3.6.3 Thermal conductivity 37

4 Holography **38**
4.1 Shear viscosity and the stress tensor correlation function 39
4.2 The KSS bound 44
4.3 Other transport properties 45
4.4 Hydrodynamics and holography 46
4.5 Non-relativistic AdS/CFT correspondence 47

5 Experimental determination of transport properties **48**
5.1 Liquid helium 48
5.2 Cold atomic gases 49
5.3 The quark gluon plasma at RHIC 53
5.3.1 The Bjorken model 54
5.3.2 Estimates of viscous corrections 56
5.3.3 Hydrodynamic Simulations 58

6 Outlook **62**

1. Introduction

A fluid is a substance that can be described by the laws of fluid dynamics. These laws imply that the response of a fluid to slowly varying external perturbations is completely governed by conservation laws. In the case of simple fluids, such as water, the conserved quantities are mass, energy, and momentum.

The study of fluids is one of the oldest problems in physics [1]. Understanding why certain liquids make good fluids, and others do not, has nevertheless remained a very difficult question. The quality of a fluid can be characterized by its shear viscosity η. Shear viscosity can be defined in terms of the friction force F per unit area A created by a shear flow with transverse flow gradient $\nabla_y v_x$,

$$\frac{F}{A} = \eta \, \nabla_y v_x \, . \tag{1}$$

Viscosity causes dissipation which converts part of the kinetic energy of the flow to heat. A good fluid is therefore characterized by a small shear viscosity. Indeed, the inverse of shear viscosity, $\varphi = 1/\eta$, is sometimes called fluidity.

The molecular theory of transport phenomena in dilute gases goes back to Maxwell. Maxwell realized that shear viscosity is related to momentum transport by individual molecules. A simple estimate of the shear viscosity of a dilute gas is

$$\eta = \frac{1}{3} \, npl_{mfp} \, , \tag{2}$$

where n is the density, p is the average momentum of the molecules, and l_{mfp} is the mean free path. The mean free path can be written as $l_{mfp} = 1/(n\sigma)$ where σ is a suitable transport cross section. This implies that the shear viscosity of a dilute gas grows with temperature (as $p \sim T^{1/2}$) but is approximately independent of density. This counterintuitive result is confirmed by experiment, going back to experiments carried out by Maxwell himself [2].

At low temperature gases condense into the liquid (or solid) state. In a liquid transport is no longer governed by the motion of individual molecules. A simple picture, due to Frenkel, Eyring, and others, is that momentum transport is due to processes that involve the motion of vacancies [3]. These processes can be viewed as thermally activated transitions in which a molecule or a cluster moves from one local energy minimum to another. The viscosity scales as

$$\eta \simeq hne^{E/(k_B T)} \, , \tag{3}$$

where E is an activation energy and h is Planck's constant. This result shows that the viscosity of a liquid grows as the temperature is lowered. Taken together, the two estimates given in equ. (2) and (3) imply that the viscosity of a typical fluid has a minimum as a function of temperature, and that the minimum is likely to occur in the vicinity of the liquid-gas phase transition.

fluid	P [Pa]	T [K]	η [Pa·s]	η/n [$\hbar$]	η/s [$\hbar/k_B$]
H_2O	$0.1{\cdot}10^6$	370	$2.9 \cdot 10^{-4}$	85	8.2
^{4}He	$0.1{\cdot}10^6$	2.0	$1.2 \cdot 10^{-6}$	0.5	1.9
H_2O	$22.6{\cdot}10^6$	650	$6.0 \cdot 10^{-5}$	32	2.0
^{4}He	$0.22{\cdot}10^6$	5.1	$1.7 \cdot 10^{-6}$	1.7	0.7
^{6}Li ($a = \infty$)	$12{\cdot}10^{-9}$	$23{\cdot}10^{-6}$	$\leq 1.7 \cdot 10^{-15}$	≤ 1	≤ 0.5
QGP	$88{\cdot}10^{33}$	$2{\cdot}10^{12}$	$\leq 5 \cdot 10^{11}$		≤ 0.4

Table 1. Viscosity η, viscosity over density, and viscosity over entropy density ratio for several fluids. Data for water and helium taken from [4, 5] and [6], data for Li and the quark gluon plasma (QGP) will be explained in Sect. 5. For water and helium we show data at atmospheric pressure and temperatures just below the boiling point and the λ transition, respectively. These data points roughly correspond to the minimum of η/n at atmospheric pressure. We also show and data near the tri-critical point which roughly corresponds to the global minimum of η/s. Note that the quark gluon plasma does not have a well defined density.

Experimental results show that the minimum value of the viscosity of good fluids, like water, liquid helium and liquid nitrogen, differs by many orders of magnitude, see the data in Table 1. The SI unit for viscosity is Pascal second (Pa· s), the CGS unit is Poise (P). Note that 1 Pa·s = 10 Poise. Clearly, it is desirable to normalize the viscosity to a suitable thermodynamic quantity in order to make more useful comparisons. Equations (2) and (3) indicate that a suitable ratio is provided by η/n. We note that the ratio of viscosity over mass density $\rho = mn$ is known as the kinematic viscosity $\nu = \eta/\rho$. The behavior of solutions of the Navier-Stokes equation is governed by the Reynolds number

$$R = \left(\frac{\rho}{\eta}\right) uL\,, \tag{4}$$

which is the ratio of a property of the flow, its characteristic velocity u multiplied by its characteristic length scale L, over a property of the fluid, its kinematic viscosity. Good fluids attain larger Reynolds numbers, and are more likely to exhibit turbulent flow. Data for the ratio η/n are tabulated in Table 1. We observe that the ratios η/n for good fluids are indeed similar in magnitude.

A disadvantage of considering the ratio η/n is that it is not possible to include relativistic fluids in the comparison. In the case of relativistic fluids particle number is not conserved and the quantity n is not well defined. In Sect. 3.1 we will show that in relativistic hydrodynamics the quantity $\eta/(nm)$ is replaced by $\eta/(sT)$, where s is the entropy density and T is the temperature. This indicates that we should consider the ratio η/s. This quantity is well defined in both the relativistic and non-relativistic limit. In non-relativistic fluids the entropy per particle is typically order one (in units of Boltzmann's constant), and η/n is of the same order of magnitude as $\eta/(s/k_B)$. Data for η/s in units of $\hbar/k_B$ are also given in Table 1.

We observe that good fluids are characterized by $\eta/s \sim \hbar/k_B$. This is consistent with high temperature limit of Eyring's formula equ. (3). The value $\eta/s \sim \hbar/k_B$ may

also be considered as the strong coupling limit of the dilute gas result given in equ. (2). In the strong coupling limit the mean free path becomes very small, but the uncertainty relation suggests that $pl_{mfp} \geq \hbar$ [7]. Using $s/n \sim k_B$ then gives $\eta/s \sim \hbar/k_B$.

These observations raise a number of interesting questions:

- Is there a fundamental limit on η/s, or can this ratio become arbitrarily small? Does quantum mechanics, or quantum field theory, play a role in establishing such a bound?
- Is there a "perfect fluid", i.e. a fluid that saturates the lower bound on η/s? If yes, what are the characteristics of such a fluid?
- How is η/s correlated with other transport properties, like bulk viscosity, diffusion constants, conductivities? Are there bounds on other transport properties?

We will not be able to provide definitive answers to these questions in this review. There are, however, a number of recent results, from both theory and experiment, that shed light on these issues:

- The experimental realization of new classes of quantum fluids. Prior to 1995 the only bulk quantum fluids that could be studied in the laboratory were the two isotopes of liquid helium, ^{4}He and ^{3}He. In 1995 several groups achieved quantum degeneracy is dilute atomic Bose gases. In 1999 experimentalists also succeeded in producing degenerate atomic Fermi gases [8, 9]. Using Feshbach resonances it is possible to experimentally control the interaction between the atoms, and to study equilibrium and transport properties as a function of the interaction strength.
- The experimental discovery of almost ideal hydrodynamic flow in a completely different physical system, the quark gluon plasma created in heavy ion collisions at the relativistic heavy ion collider (RHIC) at Brookhaven National Laboratory [10, 11, 12]. The quark gluon plasma also exhibits a large energy loss for high energy colored particles, and a very small heavy quark diffusion constant.
- Progress in non-equilibrium field theory culminated in the calculation of transport coefficients of weakly coupled gauge theory plasmas [13, 14, 15]. These results complete the program of using kinetic theory to calculate the transport properties of the three main classes of quantum liquids: Bose gases, Fermi gases, and gauge theory plasmas.
- The theoretical discovery of a completely new method for computing the transport properties of very strongly coupled fluids [16]. This method is based on the holographic duality between certain strongly coupled field theories in $d = 4$ space-time dimensions and weakly coupled string theory in $d = 10$ [17]. For gauge theories that have a weakly coupled string dual the shear viscosity to entropy density ratio at infinite coupling is $\eta/s = \hbar/(4\pi k_B)$. It was also shown that the first correction to this result at finite but large coupling increases η/s [18], and it was conjectured that $\eta/s = \hbar/(4\pi k_B)$ is a universal lower bound [19].

It is the goal of this review to summarize these recent developments. For this purpose we shall concentrate on three representative fluids: ^{4}He, a strongly coupled Bose fluids; atomic Fermi gases near a Feshbach resonance, which are the most strongly coupled Fermi liquids; and the quark gluon plasma near the critical temperature for condensation into hadron gas, which is a very strongly coupled plasma. The review is structured as follows: In Sect. 2 we discuss the thermodynamics of these quantum fluids. In Sect. 3 we review theoretical approaches to transport properties. We briefly summarize the hydrodynamic description of relativistic and non-relativistic fluids, as well as superfluids in Sects. 3.1-3.3. A general connection between transport coefficients and the underlying field theory is provided by Kubo relations, which we introduce in Sect. 3.4. In Sect. 3.5 we concentrate on fluids that can be described in terms of weakly coupled quasi-particles. In this case transport properties can be computed using kinetic theory. In Sect. 4 we summarize results for transport coefficients that have been obtained using holographic dualities. Finally, in Sect. 5 we discuss experimental results for the viscosity and other transport properties of strongly coupled quantum fluids.

Needless to say, a review of this size cannot adequately summarize all the work that has been done on the transport properties of quantum fluids. A standard reference on the properties of liquid Helium is [6], a recent review on strongly coupled Fermi gases is [20], and the physics of the strongly coupled quark gluon plasma is discussed in [21]. The kinetic theory of dilute Bose and Fermi gases is covered in textbooks, see [22, 23], and the kinetic theory of gauge fields was reviewed in [24]. A review of the AdS/CFT correspondence with an emphasis on transport theory is [25], and reviews of relativistic hydrodynamics can be found in [26, 27].

2. Strongly coupled quantum fluids

In this section we will discuss equilibrium properties of strongly interacting quantum fluids. We will specify the effective action for bosonic, fermionic, and gauge theory fluids, identify the relevant physical scales, and discuss the nature of low energy excitations.

2.1. Bose fluids: Dilute Bose gases

The effective action for a spinless bosonic field $\psi(\mathbf{x},t)$ is given by

$$S = \int dt \int d^3x\, \psi^*(\mathbf{x},t)\left(i\partial_t + \frac{\hbar^2\boldsymbol{\nabla}^2}{2m}\right)\psi(\mathbf{x},t) \qquad (5)$$
$$- \frac{1}{2}\int dt \int d^3x_1 \int d^3x_2\, \psi^*(\mathbf{x}_1,t)\psi(\mathbf{x}_1,t)V(\mathbf{x}_1-\mathbf{x}_2)\psi^*(\mathbf{x}_2,t)\psi(\mathbf{x}_2,t)\,,$$

where m is the mass of the boson, and $V(\mathbf{x})$ is a potential. The action is invariant under Galilean transformations $\mathbf{x} \to \mathbf{x} - \mathbf{v}t$ which act on the field as $\psi(\mathbf{x},t) \to \exp(im\mathbf{v}\cdot\mathbf{x} - \frac{i}{2}m\mathbf{v}^2t)\psi(\mathbf{x}-\mathbf{v}t,t)$. The action is also invariant with respect to the $U(1)$ symmetry $\psi \to \exp(i\alpha)\psi$. The $U(1)$ symmetry corresponds to the conservation of the number of atoms.

If the typical momenta are small compared to $1/r_0$, where r_0 is the range of the potential, we can approximate the interaction by a local four-boson term. For very small momenta the leading term is an s-wave interaction

$$V(\mathbf{x}_1 - \mathbf{x}_2) = C_0 \delta(\mathbf{x}_1 - \mathbf{x}_2)\,, \tag{6}$$

where C_0 can be related to the scattering length a, $C_0 = (4\pi a)/m$. We are interested in many-body systems described by the effective action given in equ. (5). We first consider the relevant scales in a weakly interacting Bose gas governed by the s-wave scattering length. At high temperature the Bose gas is a classical Boltzmann gas. The average energy of the atoms is $\frac{3}{2}k_B T$, and the average momenta are of order $(mk_B T)^{1/2}$. The importance of quantum statistics is governed by the parameter nv_Q, where n is the density, $v_Q = \lambda^3$ is the quantum volume and

$$\lambda = \frac{2\pi\hbar}{\sqrt{2\pi m k_B T}} \tag{7}$$

is the thermal wave length. Quantum statistics becomes important for $nv_Q \sim 1$, and Bose condensation in an ideal gas occurs at $nv_Q = 2.61$, corresponding to a critical temperature

$$T_c = \frac{2\pi\hbar^2}{m k_B}\left(\frac{n}{\zeta(3/2)}\right)^{2/3}\,. \tag{8}$$

The effects of a non-zero scattering length can be taken into account order by order in an expansion in $an^{1/3}$. At high temperature this is the standard Virial expansion

$$P = n k_B T\left\{1 + b_2 n + O(n^2)\right\}\,, \tag{9}$$

where P is the pressure and b_2 is the second Virial coefficient. In the limit of small a the second Virial coefficient is given by

$$b_2 = -\frac{1}{4\sqrt{2}}\lambda^3 + 2a\lambda^2\,, \tag{10}$$

where the first term is due to quantum statistics, and the second term is related to the interaction. The second Virial coefficient is finite in the limit of a large scattering length. As $a \to \infty$ the interaction part approaches $-\sqrt{2}\lambda^3$, and the role of interactions is governed by the same parameter that controls the effects of quantum statistics.

The interaction also shifts the critical temperature for Bose condensation. The calculation of this shift is a non-perturbative problem, even if the scattering length is small. This is related to the fact that fluctuations become large in the vicinity of a second order phase transition, and perturbation theory breaks down. The shift can be computed numerically using the Landau-Ginzburg effective lagrangian. For repulsive scattering length ($a > 0$) one finds [28]

$$\Delta T_c = (1.32 \pm 0.02) a n^{1/3} T_c, \tag{11}$$

which implies that repulsive interactions increase the critical temperature. Dilute Bose gases in which the scattering length is attractive are not stable. Weak repulsive interactions increase the transition temperature but suppress the condensate fraction.

If $an^{1/3}$ is large no Bose condensation takes place. For dilute systems we expect a transition to a solid phase for $an^{1/3} \sim 1$.

An issue which is very important for transport properties is the nature of the quasi-particle excitations. At high temperature the mean free path of the atoms is large, $l_{mfp} \sim 1/(na^2)$, and the atoms are good quasi-particles. At very low temperature the system is superfluid and there is a Goldstone boson, the phonon, related to the breaking of the $U(1)$ phase symmetry. Goldstone bosons are derivatively coupled and the interaction at low energy is weak. This implies that the mean free path at low temperature, $T \ll T_c$, is large. The phonon dispersion relation in a weakly non-ideal ($na^3 < 1$) Bose gas was first computed by Bogoliubov. The result is

$$\epsilon_p = \frac{1}{2m}\sqrt{(p^2 + 8\pi an)^2 - (8\pi an)^2}\,. \tag{12}$$

For small momenta the dispersion relation is linear, $\epsilon_p \simeq c_s p$, and the phonon velocity is given by $c_s = \sqrt{4\pi an}/m$.

2.2. Bose fluids: Liquid helium

A simple s-wave interaction is sufficient for understanding the properties of trapped atomic Bose gases, but more accurate potentials are required for even a qualitative description of liquid ^{4}He. Accurate ^{4}He potentials consist of a short range contribution combined with a van der Waals tail

$$V(r) = V_{sr}(r) - \frac{C_6}{r^6}\,. \tag{13}$$

The coefficient C_6 defines the van der Waals length scale $l_{VdW} = (mC_6/\hbar^2)^{1/4}$. Accurate parametrizations of V_{sr} can be found [29, 30]. These potentials have a van der Waals length $l_{VdW} \simeq 10.2\, a_0$, an effective range $r \simeq 14\, a_0$, and a very large scattering length $a \simeq 189\, a_0$, where $a_0 = 0.529\, \mathring{A}$ is the Bohr radius. The large s-wave scattering length is related to the existence of a very weakly bound ^{4}He dimer. The binding energy of the dimer is $B = -1.1 \cdot 10^{-7}$ eV. There are many interesting universal effects governed by the large scattering length [31]. The density of liquid ^{4}He is too large for these phenomena to be important, but universal effects have been observed in dilute atomic gases in which the scattering length is large.

In the case of ^{4}He the interaction between the atoms is not weak, and it cannot be characterized in terms of the scattering length only. In the high temperature limit ^{4}He is a classical gas, and corrections to the ideal gas behavior are described by the Virial expansion. The Virial expansion provides a very accurate description of the equation of state at normal pressure for temperatures above 10 K. At temperatures below 10 K one has to rely on quantum Monte Carlo methods or variational many-body wave functions [32]. At atmospheric pressure ^{4}He liquefies at 4.22 K, and it becomes superfluid at 2.17 K. This temperature can be compared to the critical temperature for Bose condensation of an ideal gas with the density of liquid helium, $n = 1/(3.6\, \mathring{A})^3$, which is $T_c^0 = 3.1$ K. The rough agreement between these two numbers

is somewhat of a coincidence. The condensate fraction in superfluid helium at zero temperature is small [33], $f \simeq (7.25 \pm 0.75) \cdot 10^{-2}$, and the critical temperature drops with density, contrary to what one would expect for an ideal gas. The superfluid transition is in the universality class of the three dimensional $O(2)$ model. Renormalization group arguments predict a mild nonanalyticity in the specific heat, $c_v \sim t^{-\alpha}$ with $t = (T - T_c)/T_c$ and $\alpha = -0.0151(3)$ [34]. This prediction agrees reasonably well with micro gravity experiments which find $\alpha = -0.01285(4)$ [35].

The excitation spectrum of superfluid ^{4}He shows important differences as compared to the spectrum of a dilute Bose condensed gas. As expected, at small momentum there is a phonon branch with $\epsilon(p) = c_s p$, where the speed of sound at normal pressure is $c_s = 238$ m/sec. At larger momentum the dispersion relation has a second minimum, called the roton branch. The dispersion relation in the vicinity of the minimum is

$$\epsilon(p) = \Delta + \frac{(p - p_0)^2}{2m^*}\,, \tag{14}$$

where $\Delta/k_B = 8.7\,\mathrm{K}$, $m^* = 0.14\,m$ and $p_0/\hbar = 1.9\,\mathring{A}^{-1}$. The roton plays a significant role in determining the specific heat and transport properties near the critical temperature. The physical nature of the roton excitation is not entirely clear, but the location of the roton minimum is closely correlated with the first maximum of the static structure factor $S(q)$. In particular, Feynman proposed a variational wave function for which the excitation energy is $\epsilon(q) = q^2/(2mS(q))$ [36]. The static structure factor is the Fourier transform of the density correlation function

$$S(q) = \frac{1}{\rho}\int d^3x\, e^{-i\mathbf{q}\cdot\mathbf{x}} \left[\langle\rho(0)\rho(\mathbf{x})\rangle - \langle\rho(0)\rangle^2\right]\,. \tag{15}$$

Goldstone's theorem implies that $S(q) \simeq q/(2mc_s)$ for small q. The first peak of the static structure function, which leads to the roton minimum, reflects the existence of strong short range correlations, and is a characteristic feature of a liquid. The phonon-phonon and phonon-roton interaction is constrained by Galilean invariance and $U(1)$ symmetry [22]. We will discuss these constraint in more detail in the next section, in connection with superfluid Fermi gases.

About Units: Up to this point, we have explicitly displayed factors of $\hbar$, c and k_B. From now on we will work in natural units and set $\hbar = k_B = c = 1$.

2.3. Fermi liquids: The dilute Fermi gas at unitarity

In this section we consider non-relativistic Fermi liquids. Fermionic systems are interesting because it is possible to make strongly correlated liquids with only zero range interactions. Consider the lagrangian

$$\mathcal{L} = \psi^\dagger\left(i\partial_0 + \frac{\boldsymbol{\nabla}^2}{2m}\right)\psi - \frac{C_0}{2}\left(\psi^\dagger\psi\right)^2 + \frac{C_2}{16}\left[(\psi\psi)^\dagger(\psi\overleftrightarrow{\nabla}^2\psi) + h.c\right] + \ldots, \tag{16}$$

were ψ is a spin 1/2 fermion field with mass m, and $\ldots$ denotes terms with more derivatives or higher powers of the fermion field. The coupling constants $C_0, C_2, \ldots$ can

be related to the coefficients of the effective range expansion

$$C_0 = \frac{4\pi a}{m}, \quad C_2 = C_0 \frac{a r_0}{2}. \tag{17}$$

where a and r_0 are the s-wave scattering length and effective range. We will concentrate on dilute systems for which all terms except for C_0 can be neglected. We are particularly interested in the limit of large scattering lengths, $C_0 \to \infty$. One way to see that the many-body system governed by equ. (16) remains well defined in this limit is to introduce an auxiliary scalar field ϕ, and to eliminate the four-fermion interaction by performing a Hubbard-Stratonovich transformation. The result is

$$\mathcal{L} = \Psi^\dagger \left[i\partial_0 + \sigma_3 \frac{\boldsymbol{\nabla}^2}{2m} \right] \Psi + \mu \Psi^\dagger \sigma_3 \Psi + \left(\Psi^\dagger \sigma_+ \Psi \phi + h.c. \right) - \frac{1}{C_0} \phi^* \phi \ , \tag{18}$$

where $\Psi = (\psi_\uparrow, \psi_\downarrow^\dagger)^T$ is a Nambu-Gorkov spinor, σ_i are the Pauli matrices, and $\sigma_\pm = (\sigma_1 \pm i\sigma_2)/2$. We have also introduced a chemical potential μ. We observe that $a \to \infty$ corresponds to setting the quadratic coupling of the auxiliary field to zero.

Over the last ten years there has been truly remarkable progress in the study of cold, dilute gases of fermionic atoms in which the scattering length a of the atoms can be controlled experimentally. These systems can be realized in the laboratory using Feshbach resonances, see [37] for a review. A small negative scattering length corresponds to a weak attractive interaction between the atoms. This regime is known as the BCS (Bardeen-Cooper-Schrieffer) limit. As the strength of the interaction increases the scattering length becomes larger. It diverges at the point where a bound state is formed. The point $a = \infty$ is called the unitarity limit, because the scattering cross section saturates the s-wave unitarity bound $\sigma = 4\pi/k^2$. On the other side of the resonance the scattering length is positive. In the BEC (Bose-Einstein condensation) limit the interaction is strongly attractive and the fermions form deeply bound molecules.

In the high temperature limit the equation of state is again that of an ideal gas, and the leading correction is described by the Virial expansion. The second Virial coefficient is

$$b_2 = \frac{1}{8\sqrt{2}} \lambda^3 + \frac{1}{2} a \lambda^2 \, . \tag{19}$$

In the limit $a \to \infty$ the interaction term goes to $-\lambda^3/(2\sqrt{2})$. The Fermi gas becomes degenerate as $n\lambda^3 \sim 1$. In the limit in which the scattering length is large the Fermi gas becomes strongly interacting at the same temperature at which quantum effects become important.

In the BCS limit, $a < 0$ and $n^{1/3}|a| < 1$, the Fermi gas can be described as a Landau Fermi liquid. The excitations are weakly interacting particles and holes which carry the quantum numbers of the elementary fermions. At very low temperature the particle-particle interaction in the spin singlet channel becomes large, and the Fermi liquid undergoes a phase transition to a BCS superfluid. The transition temperature is [38]

$$T_c = \frac{8 e^\gamma E_F}{(4e)^{1/3} e^2 \pi} \exp\left(-\frac{\pi}{2 k_F |a|} \right), \tag{20}$$

where γ is the Euler constant. The Fermi momentum k_F is defined by the relation

$$n = \frac{k_F^3}{3\pi^2}\,, \tag{21}$$

and $E_F = k_F^2/(2m)$ is the Fermi energy. This relation defines a "Fermi momentum" even in the case that no sharp Fermi surface exists. Note that $T_F \equiv E_F$ is the degeneracy temperature (we have set $k_B = 1$). Also note that $n^{1/3}|a| < 1$ implies $T_c \ll T_F$.

In the Bose-Einstein limit the fermions form tightly bound molecules. The residual interaction between the molecules is repulsive, and the many-body system behaves as a weakly non-ideal Bose gas. The Bose gas condenses at the critical temperature given in equ. (8). Using the fact that the mass of molecules is $2m$, and that their density is $n/2$, we get

$$T_c = 0.21 E_F\,. \tag{22}$$

Variational calculations suggest that at zero temperature the evolution from weak to strong coupling is smooth [39]. The system is a pair condensate for all values of the coupling, but the size of the pairs evolves from being much smaller than the inter-particle spacing in the BEC limit to being much larger in the BCS limit. This idea is confirmed by quantum Monte Carlo calculations [40] and experimental observations [41].

Of particular interest is the crossover ("unitarity") regime where $a \to \infty$. In this limit the system possesses a number of interesting properties. First of all, the few and many body problem is scale invariant [42, 43]. This implies, for example, that all energy scales, like the critical temperature and the chemical potential, are proportional to the Fermi energy

$$T_c = \alpha E_F\,, \qquad \mu = \xi E_F\,. \tag{23}$$

Similarly, all length scales are given by numerical constants times the inverse Fermi momentum. The values of the universal constants $\alpha, \xi, \ldots$ can be determined using Quantum Monte Carlo (QMC) calculations, or from experiments on harmonically trapped Fermions. QMC calculations performed by Burovski et al. give $T_c = 0.152(7)E_F$ [44], and Carlson et al. obtained $\mu = 0.44(1)E_F$ [45]. A summary of experimental results was recently given by Luo and Thomas [46].

Second, the unitarity regime is the most strongly correlated simple many body system. The crossover regime is continuously connected to both the non-interacting Fermi gas and the non-interacting Bose gas, but neither limit provides a quantitatively accurate description. Very important for the purpose of this review is the observation hydrodynamic behavior and low viscosity in very dilute Fermi gases in the unitarity limit.

Before we end this section we briefly discuss the nature of excitations in the unitarity regime. In the high temperature limit the excitations are elementary fermions, even in the limit $a \to \infty$. This is related to the fact that the average cross section is of order λ^2, where $\lambda \sim T^{-1/2}$ is the thermal wave length. In the low temperature superfluid

phase the dominant excitation is the phonon, which is the Goldstone mode related to the breaking of $U(1)$ symmetry. The dispersion relation is

$$\epsilon_p = c_s p\,, \qquad c_s = \sqrt{\frac{\xi}{3}}\, v_F\,, \tag{24}$$

where $v_F = k_F/m$ is the Fermi velocity, and ξ is the universal parameter defined in equ. (23).

The phonon-phonon interaction can be described by an effective low energy lagrangian. The effective lagrangian provides an efficient tool to incorporate symmetry constraints on the phonon interaction. The Goldstone boson field is defined as the phase of the order parameter

$$\langle\psi\psi\rangle = |\langle\psi\psi\rangle| e^{2i\varphi}. \tag{25}$$

The effective theory is governed by the most general lagrangian which is consistent with the the symmetries of the problem, in particular Galilei invariance and $U(1)$ symmetry. The $U(1)$ symmetry acts as a shift on the Goldstone boson field, $\varphi \to \varphi + \alpha$. The $U(1)$ symmetry can be promoted to a local symmetry. The chemical potential behaves as a gauge field under this symmetry, $\mu \to \mu + \partial_0\alpha$. Under a Galilei transformation with boost parameter $\mathbf{v}$ the Goldstone boson field transforms as $\varphi(\mathbf{x},t) \to \varphi(\mathbf{x}-\mathbf{v}t) - m\mathbf{v}\cdot\mathbf{x} + O(\mathbf{v}^2)$. At leading order in derivatives of φ we can incorporate these symmetries by constructing an effective lagrangian that only depends on the variable

$$X = \mu - \partial_0\varphi - \frac{(\boldsymbol{\nabla}\varphi)^2}{2m}\,. \tag{26}$$

The functional form of the leading order lagrangian $\mathcal{L}(X)$ is fixed by the requirement that for constant fields the effective action $\Gamma(X=\mu) = V\mathcal{L}(\mu)$ reduces to the thermodynamic potential. We will see that this requirement also ensures that the effective lagrangian is equivalent to superfluid hydrodynamics. At zero temperature the thermodynamic potential is equal to the pressure and

$$\mathcal{L} = P(X) = \frac{2^{5/2} m^{3/2}}{15\pi^2\xi^{3/2}} \left(\mu - \partial_0\varphi - \frac{(\boldsymbol{\nabla}\varphi)^2}{2m}\right)^{5/2}\,, \tag{27}$$

where we have used the fact that, up to a numerical factor, the pressure of the interacting system is equal to that of a free gas. We have also used that this factor can be related to the ratio $\xi = \mu/E_F$. Goldstone bosons have energies $\omega < \mu$ and we can expand equ. (27) in powers of $\partial_0\varphi$ and $\nabla_i\varphi$. We find

$$\begin{aligned}\mathcal{L} = {} & \frac{1}{2}(\partial_0\phi)^2 - \frac{1}{2}c_s^2\,(\boldsymbol{\nabla}\phi)^2 - \alpha\left[(\partial_0\phi)^3 - 9c_s^2\partial_0\phi\,(\boldsymbol{\nabla}\phi)^2\right] \\ & - \frac{3}{2}\alpha^2\left[(\partial_0\phi)^4 + 18c_s^2\,(\partial_0\phi)^2\,(\boldsymbol{\nabla}\phi)^2 - 27c_s^4\,(\boldsymbol{\nabla}\phi)^4\right] + \cdots,\end{aligned} \tag{28}$$

where we have rescaled the field $\varphi \to \phi$ to make it canonically normalized. We have also defined $\alpha = \pi c_s^{3/2}\xi^{3/4}/(3^{1/4}8\mu^2)$. We observe that the three and four phonon vertices are completely fixed by the speed of sound c_s. We note that equ. (27) generates terms with arbitrary numbers of derivatives, but the number of derivatives is always equal to the

number of fields. Terms involving more derivatives than fields were constructed in [43]. These terms are interesting, because they involve non-trivial constraints from not just scale invariance, but from the full conformal symmetry of the Fermi gas at unitarity.

The spectrum of excitations with higher momenta is not well known. The static structure factor has been measured in quantum Monte Carlo simulations, and shows no liquid-like structures [47]. This suggests that there are no roton excitations, and that the phonon spectrum merges smoothly with the spectrum of weakly coupled particle-hole excitations at higher energy.

2.4. Gauge theories: QCD

Quantumchromodynamics (QCD) is governed by the lagrangian

$$\mathcal{L} = -\frac{1}{4}G^a_{\mu\nu}G^a_{\mu\nu} + \sum_f^{N_f} \bar{\psi}_f(i\not{D} - m_f)\psi_f \,, \tag{29}$$

where ψ_f is a Dirac fermion with flavor index f and m_f is the quark mass. We have suppressed the color ($A = 1, \ldots, N_c$) and spinor ($\alpha = 1, \ldots, 4$) indices of the fermion fields. The covariant derivative acting on the quark fields is

$$i\not{D}\psi = \gamma^\mu \left(i\partial_\mu + gA^a_\mu \frac{\lambda^a}{2} \right) \psi \,, \tag{30}$$

where A^a_μ is a gauge potential and λ^a ($a = 1, \ldots, N_c^2 - 1$) are the Gell-Mann matrices. The field strength tensor is defined by

$$G^a_{\mu\nu} = \partial_\mu A^a_\nu - \partial_\nu A^a_\mu + g f^{abc} A^b_\mu A^c_\nu \,, \tag{31}$$

where f^{abc} are the $SU(N_c)$ structure constants, and g is a coupling constant. In the standard model $N_c = 3$ and $N_f = 6$, but three out of the six flavors are too heavy too play much of a role in the dynamics of QCD, and we shall mostly concentrate on $N_f = 3$ flavors. The total quark density

$$\rho_q = \sum_f \psi^\dagger_f \psi_f \tag{32}$$

is conserved and we can introduce a chemical potential μ coupled to ρ_q. The phase structure and transport properties of QCD at finite μ are an interesting subject [48], but in this review we will concentrate on QCD at non-zero temperature and zero or very small small chemical potential. It is interesting to note that at low quark density the relevant degrees of freedom are protons and neutrons. In the low energy limit the interaction between neutrons and protons is governed by an effective lagrangian of the type given in equ. (16). The parameters $C_0, C_2, \ldots$ are functions of the quark masses. It is theoretically possible to tune the light quark masses to a point where the neutron-neutron scattering length diverges. The real world is close to this point, as the experimental value of the scattering is $a_{nn} \simeq -17$ fm is much larger than typical QCD scales. This implies that there is a point in the QCD phase diagram where the long distance physics is equivalent to that of a dilute atomic Fermi gas at unitarity.

For many purposes we can consider the first three flavors (up, down, and strange) to be approximately massless. In this limit the QCD lagrangian contains a single dimensionless parameter, the coupling constant g. If quantum effects are taken into account the coupling becomes scale dependent. At leading order the running coupling constant is

$$g^2(q) = \frac{16\pi^2}{b_0 \log(q^2/\Lambda_{QCD}^2)}\,, \qquad b_0 = \frac{11}{3}N_c - \frac{2}{3}N_f\,. \tag{33}$$

This result implies that as a quantum theory, QCD is not characterized by a dimensionless coupling, but by a dimensionful scale, the QCD scale parameter Λ_{QCD}. This phenomenon is called dimensional transmutation. We also observe that the coupling decreases with momentum. This is the phenomenon of asymptotic freedom.

At high temperature the dominant momenta are on the order of T, and for $T \gg \Lambda_{QCD}$ asymptotic freedom implies that bulk thermodynamics is governed by weak coupling. The weak coupling expansion of the equation of state is

$$P = T^4 \left\{ c_0 + c_2 g^2 + c_3 g^3 + (c_4' \log(g) + c_4) g^4 + \ldots \right\}\,, \tag{34}$$

where the first term is the Stefan-Boltzmann law and

$$c_0 = \frac{\pi^2}{90}\left(2\left(N_c^2 - 1\right) + 4N_c N_f \frac{7}{8}\right) \tag{35}$$

is proportional to the number of degrees of freedom ($2(N_c^2-1)$ gluons and $4N_cN_f$ quarks). We note that in a relativistic theory the equation of state is always sensitive to quantum statistics, even if the temperature is high. The first correction is [49]

$$c_2 = -\frac{N_c^2 - 1}{144}\left(N_c + \frac{5}{4}N_f\right)\,. \tag{36}$$

The perturbative expansion in equ. (34) is evaluated with g taken to be the running coupling constant evaluated at a scale $q \sim T$. The precise scale is not uniquely determined – changing the scale corresponds to reshuffling higher order corrections in the perturbative expansion. The scale is usually chosen to improve the apparent rate of convergence. This criterion gives a value close to $2\pi T$.

We note that the perturbative expansion is not a power series in the fine structure constant $\alpha_s = g^2/(4\pi)$. The expansion contains square roots and logarithms of α_s. Non-analytic terms in the expansion are related to infrared sensitive diagrams. For example, the g^3 term in equ. (34) is due to ring diagrams (also called the plasmon term). Ring diagrams are one-loop gluon diagrams in which the leading order gluon self energy has been summed to all orders. We also note that the weak coupling expansion cannot be extended to arbitrarily high powers in g. At $O(g^6)$ one encounters infrared divergent diagrams which can only be summed non-perturbatively, by computing the partition function of three-dimensional QCD at zero temperature.

In order to analyze the relevant scales in high temperature QCD in more detail we consider the current-current interaction

$$\mathcal{M} = j_\mu^a \Pi_{\mu\nu}^{ab} j_\nu^b\,, \tag{37}$$

where j^a_μ is a color current and $\Pi^{ab}_{\mu_\nu}$ is the gluon polarization function. The tensor structure of the gluon polarization function can be decomposed into a transverse and a longitudinal part

$$\begin{aligned}\Pi_{\mu\nu}(q) &= \Pi^T(q)P^T_{\mu\nu} + \Pi^L(q)P^L_{\mu\nu} \\ P^T_{ij} &= \delta_{ij} - \hat{q}_i\hat{q}_j\,, \qquad P^T_{00} = P^T_{0i} = 0\,, \\ P^L_{\mu\nu} &= -g_{\mu\nu} + \frac{q_\mu q_\nu}{q^2} - P^T_{\mu\nu}\,.\end{aligned} \tag{38}$$

We will consider the polarization function in the limit of weak coupling ($g < 1$), and for $\omega \ll q \ll T$, where ω, q are the energy and momentum transfer. We find

$$\Pi^{ab\,L}(q) = \frac{\delta^{ab}}{\mathbf{q}^2 + m_D^2}\,, \tag{39}$$

$$\Pi^{ab\,T}(q) = \frac{\delta^{ab}}{\mathbf{q}^2 - i\frac{\pi}{4}m_D^2\frac{\omega}{|\mathbf{q}|}}\,, \tag{40}$$

where

$$m_D^2 = g^2T^2\left(1 + \frac{N_f}{6}\right) \tag{41}$$

is called the Debye mass. The longitudinal term governs the Coulomb interaction between static charges. We observe that the Coulomb interaction is screened at distances $r \sim m_D^{-1} \sim 1/(gT)$. In perturbation theory the static magnetic interaction is unscreened. Nonstatic magnetic interactions are dynamically screened at a distance $r \sim (m_D^2\omega)^{-1/3}$. This phenomenon, known as Landau damping, also exists in ordinary plasma physics. Unlike classical plasmas the QCD plasma has a non-perturbative static magnetic screening mass $m_M \sim g^2T$. This is the scale that determines the non-perturbative g^6 term in the pressure. Modes below the magnetic screening scale contribute

$$P \sim T\int^{m_M} d^3k \sim g^6T^4\,. \tag{42}$$

The gluon polarization tensor also determines the propagation of gluonic modes. For this purpose we need the full energy and momentum dependence of $\Pi^{T,L}$, see [50]. For momenta $q \gg gT$ there are two transverse modes with dispersion relation $\omega \simeq q$. For momenta $q < gT$ there are two transverse and one longitudinal mode. The longitudinal mode is sometimes called the plasmon. The energy of both modes approaches $\omega = \omega_p = m_D/\sqrt{3}$ as $q \to 0$. The quantity ω_p is known as the plasma frequency. The gluon (and plasmon) decay constant in the limit $q \to 0$ is [51]

$$\gamma = 6.64\frac{g^2N_cT}{24\pi}\,. \tag{43}$$

An important issue is how small the coupling has to be in order for the perturbative estimates to be applicable. The convergence properties of the weak coupling expansion for the pressure are extremely poor. The series shows no signs of converging unless the coupling is taken to be much smaller than one, $g \ll 1$, corresponding to completely unrealistic temperatures on the order of 1 TeV. The problem is mostly due to the

nonanalytic terms in the expansion, and convergence can be improved significantly by considering resummation schemes or self-consistent quasi-particle expansions [52]. Convergence can also be improved by using a hierarchy of effective field theories for the hard ($p \sim T$), electric ($p \sim gT$), and magnetic ($p \sim g^2T$) sectors of the QCD plasma [53]. Ordinary perturbation theory corresponds to treating the electric sector perturbatively, but convergence can be improved by treating both the electric and the magnetic sector non-perturbatively [54].

Despite these advances accurate results at temperatures that can be reached in heavy ion collisions at RHIC have to rely on numerical simulations of the QCD partition function on a space-time lattice, see [55] for a review. Lattice simulations with realistic quark masses find a phase transition at the critical temperature $T_c = 192(8)$ MeV [56]. The transition is a rapid (but smooth) crossover from a low temperature phase that exhibits chiral symmetry breaking and confinement to a chirally restored and deconfined high temperature phase ‡. The energy density reaches about 85% of the ideal gas value at $T \simeq 2T_c$ and then evolves very slowly towards the non-interacting limit.

Below the critical temperature the degrees of freedom are hadrons. The lightest hadrons are pions, which are the Goldstone bosons associated with the spontaneous breaking of the approximate chiral symmetry of the QCD lagrangian. The masses of the charged and neutral pions are $m_{\pi^\pm} = 139$ MeV and $m_{\pi^0} = 135$ MeV. The masses of strange Goldstone bosons (kaons and etas) are around 500 MeV, and the mass of the lightest non-Goldstone boson, the rho, is 770 MeV. Chiral symmetry constrains the Goldstone boson scattering amplitudes. These constraints are obtained most easily from the low energy effective chiral lagrangian. At leading order we have

$$\mathcal{L} = \frac{f_\pi^2}{4}\mathrm{Tr}\left[\partial_\mu \Sigma \partial^\mu \Sigma^\dagger\right] + \left[B\mathrm{Tr}(M\Sigma^\dagger) + h.c.\right] + \dots , \tag{44}$$

where $\Sigma = \exp(i\phi^a\lambda^a/f_\pi)$ ($a = 1, \dots, 8$) is the chiral field, $f_\pi = 93$ MeV is the pion decay constant, B is proportional to the quark condensate, and $M = \mathrm{diag}(m_u, m_d, m_s)$ is the mass matrix. An expansion of Σ in powers of the pion, kaon and eta fields ϕ^a gives the leading low energy amplitudes for Goldstone boson scattering. Restricting ourselves to the $SU(2)$ flavor sector (pions only) we get

$$\mathcal{L} = \frac{1}{2}(\partial_\mu\phi^a)^2 - \frac{1}{2}m_\pi^2(\phi^a)^2 + \frac{1}{6f_\pi^2}\left[(\phi^a\partial_\mu\phi^a)^2 - (\phi^a)^2(\partial_\mu\phi^b)^2\right] + \dots , \tag{45}$$

where ϕ^a ($a = 1, 2, 3$) is the pion field.

2.5. Gauge theories: Superconformal QCD

QCD is a complicated theory, and a significant amount of effort has been devoted to the study of generalizations of QCD that possess a larger amount of symmetry, in particular supersymmetry. The most supersymmetric extension of QCD is a theory

‡ This issue is not completely settled. Aoki et al. find distinct crossover transitions at significantly lower temperatures, $T_\chi = 151$ MeV for chiral symmetry restoration, and $T_{dec} = 175$ MeV for deconfinement [57].

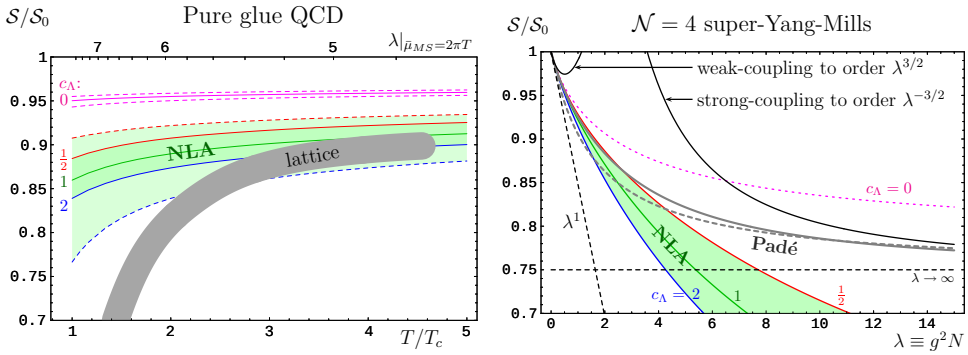

Figure 1. Entropy density in units of the Stefan-Boltzmann value for pure gauge QCD and $\mathcal{N} = 4$ supersymmetric QCD. The left panel shows the entropy density of pure gauge QCD as a function of T/T_c. The grey band is the lattice result. The solid lines show a resummed QCD calculation [52]. The different lines correspond to different choices for a non-perturbative parameter c_Λ. The dashed lines mark an error band determined by variations in the QCD renormalization scale. The right panel shows the entropy density of SUSY QCD as a function of the 't Hooft coupling λ. The curves are labeled as in the left panel.

with four supersymmetry generators, called $\mathcal{N} = 4$ SUSY QCD (theories with even more supersymmetry contain gravitational interactions). The lagrangian of the theory is

$$\mathcal{L} = -\frac{1}{4} G^a_{\mu\nu} G^a_{\mu\nu} - i\bar{\lambda}^a_i \sigma^\mu D_\mu \lambda^a_i + D^\mu \phi^{\dagger\, a}_{ij} D_\mu \phi^a_{ij} + \mathcal{L}_{\lambda\lambda\phi} + \mathcal{L}_{\phi^4} \,, \tag{46}$$

where $G^a_{\mu\nu}$ is the usual field strength tensor, λ^a_i is the gluino field, and ϕ^a_{ij} is a colored Higgs field. The gluino is a two-component (Weyl) fermion in the adjoint representation of the color group. The index i ($i = 1, \ldots, 4$) transforms in the fundamental representation of a global $SU(4)_R$ "R-symmetry". The Higgs is a scalar field in the adjoint representation of color, and in an anti-symmetric tensor (six dimensional) of $SU(4)_R$. Note that the total number of fermionic fields, $8(N_c^2 - 1)$, is indeed equal to the number of bosonic fields. We have not explicitly displayed the Yukawa couplings $\mathcal{L}_{\lambda\lambda\phi}$ and Higgs self couplings $\mathcal{L}_{\phi^4}$, see [58]. Both interaction terms only involve the dimensionless gauge coupling g.

$\mathcal{N} = 4$ SUSY QCD has a vanishing beta function and is believed to be a conformal field theory (CFT). As a consequence there is no dimensional transmutation, no confinement or spontaneous symmetry breaking, and no phase transition. The theory is an Coulomb phase for all values of the coupling g and the temperature T. However, if g is not small then there is no obvious way to compute thermodynamic or transport properties of the plasma.

An interesting new approach is provided by the duality between strongly coupled large N_c gauge theory and weakly coupled string theory on $\mathrm{AdS}_5 \times \mathrm{S}_5$ discovered by Maldacena [17]. We will have more to say about this approach in Section 4. For now we observe that the correspondence can be extended to finite temperature. In this case the relevant configurations is an $\mathrm{AdS}_5 \times \mathrm{S}_5$ black hole. The temperature of the gauge

theory is given by the Hawking temperature of the black hole, and the entropy is given by the Hawking-Beckenstein formula $S = A/(4G)$, where A is the surface area of the event horizon and G is Newton's constant.

Using the AdS/CFT correspondence we are in a position to compute the thermodynamic behavior in both the limit of small and large 't Hooft coupling $\lambda = g^2 N_c$. In a relativistic conformal theory we have $\epsilon = 3P$ and $s = 4P/T$, where ϵ is the energy density and s entropy density. It is conventional to state the result in terms of the entropy density in units of the entropy density of the non-interacting system. The result is [59, 60, 61]

$$\frac{s}{s_0} = \begin{cases} \frac{3}{4} + \frac{45\zeta(3)}{32}\lambda^{-3/2} + \dots & \lambda \gg 1 \\ 1 - \frac{3}{2\pi^2}\lambda + \frac{\sqrt{2}+3}{\pi^3}\lambda^{3/2} + \dots & \lambda \ll 1 \end{cases} . \tag{47}$$

This result has a number of remarkable features. First we observe that the entropy density at infinite coupling only differs by a factor 3/4 from the result in the free theory. We also note that the first non-trivial corrections in the strong and weak coupling limit are consistent with the idea that the evolution from weak to strong coupling is smooth. Equation (47) was compared with resummed perturbation theory and Pade approximants in [62], see Fig. 1. The authors argue that at the "QCD-like" point $s/s_0 = 0.85$ neither the strong nor the weak coupling expansion are quantitatively reliable, but that resummed perturbation theory is useful in this regime.

3. Transport theory

In this section we summarize theoretical approaches to transport phenomena in strongly coupled quantum fluids. The most general of these approaches is hydrodynamics. Hydrodynamics is based on the observation that correlation functions at low energy and small momentum are governed by the evolution of conserved charges. Conservation laws imply that the densities of conserved charges cannot relax locally, but have to propagate or diffuse out to large distance. This corresponds to hydrodynamic excitations with dispersion laws of the form $\omega \sim q$ (sound) or $\omega \sim iq^2$ (diffusion).

The hydrodynamic equations depend on the equation of state, and on a set of transport coefficients (shear viscosity, bulk viscosity, thermal conductivity, etc.). These coefficients can be extracted from experiment, or computed from an underlying field theory. The connection between transport coefficients and correlation functions in a (quantum) field theory is provided by linear response theory. Using linear response theory one can relate transport coefficients to the zero energy and zero momentum limit of a retarded correlation function. These relations are known as Kubo formulas, see Sect. 3.4.

The low energy behavior of correlation functions of conserved charges is complicated, and the calculation of transport coefficients based on the Kubo formula is difficult, even if the interaction is weak. The situation simplifies if the system allows a microscopic description in terms of quasi-particles. In that case we can use

an intermediate effective theory, known as kinetic theory, to relate the microscopic lagrangian to the hydrodynamic description. The calculation of transport coefficients in kinetic theory is reviewed in Sect. 3.5. If the interaction between quasi-particles is strong then the kinetic description breaks down. A new approach to extracting transport properties from a strongly coupled field theory is the holographic method which we will discuss in the next section. Using holography the calculation of the retarded correlator can be reduced to a classical computation in a suitable dual theory.

3.1. Hydrodynamics

3.1.1. Non-relativistic fluids The hydrodynamics of a non-relativistic fluid is governed by the conservation laws of energy, mass (particle number), and momentum,

$$\frac{\partial \epsilon}{\partial t} + \boldsymbol{\nabla} \cdot \mathbf{j}^{\,\epsilon} = 0\,, \tag{48}$$

$$\frac{\partial \rho}{\partial t} + \boldsymbol{\nabla} \cdot \mathbf{g} = 0\,, \tag{49}$$

$$\frac{\partial g_i}{\partial t} + \nabla_j \Pi_{ij} = 0\,. \tag{50}$$

Here, ϵ is the energy density, ρ is the mass density, $\mathbf{g}$ is the momentum density, and Π_{ij} is the stress tensor. The relations between the conserved currents and the hydrodynamic variables are called constitutive relations. These relations can be determined order by order in an expansion in derivatives of the flow velocity and the thermodynamic variables. The leading order result is called "ideal hydrodynamics". At this order the constitutive relations are completely fixed by Galilean invariance, rotational invariance, and conservation of entropy. The result is

$$\mathbf{j}^{\,\epsilon} = \mathbf{v}(\epsilon + P)\,, \tag{51}$$

$$\mathbf{g} = \rho \mathbf{v}\,, \tag{52}$$

$$\Pi_{ij} = P\delta_{ij} + \rho v_i v_j\,, \tag{53}$$

where $\epsilon = \epsilon_0 + \frac{1}{2}\rho v^2$ and ϵ_0 is the energy density in the rest frame of the fluid. There are six hydrodynamic variables, $\mathbf{v}$, ρ, ϵ and P, which are determined by the five conservation laws (48-50). In order for the equations to close we need to supply an equation of state $P = P(\epsilon, \rho)$. Since hydrodynamic variables evolve slowly, the equation of state is the one in thermal equilibrium.

In ideal hydrodynamics the equations of continuity and momentum conservation are

$$\frac{\partial \rho}{\partial t} + \boldsymbol{\nabla} \cdot (\rho \mathbf{v}) = 0\,, \tag{54}$$

$$\frac{\partial \mathbf{v}}{\partial t} + (\mathbf{v} \cdot \boldsymbol{\nabla})\,\mathbf{v} = -\frac{1}{\rho}\boldsymbol{\nabla} P\,. \tag{55}$$

The equation of momentum conservation is known as the Euler equation. In the case of ideal hydrodynamics the equation of energy conservation can be rewritten as

conservation of entropy,

$$\frac{\partial s}{\partial t} + \boldsymbol{\nabla} \cdot (\mathbf{v} s) = 0 \,. \tag{56}$$

At next order in the derivative expansion dissipative terms appear. The size of these terms is controlled by new parameters called transport coefficients. In the case of a non-relativistic fluid the relation $\mathbf{g} = \rho \mathbf{v}$ is not modified (it follows from Galilean invariance), but two new coefficients appear in the stress tensor. We can write $\Pi_{ij} = P\delta_{ij} + \rho v_i v_j + \delta\Pi_{ij}$ with

$$\delta\Pi_{ij} = -\eta \left(\nabla_i v_j - \nabla_j v_i - \frac{2}{3}\delta_{ij} \boldsymbol{\nabla} \cdot \mathbf{v} \right) - \zeta \delta_{ij} \left(\boldsymbol{\nabla} \cdot \mathbf{v} \right) \,. \tag{57}$$

Here, η is the shear viscosity and ζ is the bulk viscosity. The correction to the energy current has the form $j^\epsilon_i = v_i(\epsilon + P) + v_j \delta\Pi_{ij} + Q_i$ with

$$\mathbf{Q} = -\kappa \boldsymbol{\nabla} T, \tag{58}$$

where T is the temperature and κ is the thermal conductivity. The second law of thermodynamics implies that $\eta, \zeta, \kappa \geq 0$. The equation of momentum conservation with the viscous stresses (57) included is known as the Navier-Stokes equation.

The linearized hydrodynamic equations describe the propagation of sound and diffusive modes. In the case of a non-relativistic fluid there is a pair of sound modes that couple to the pressure/density and the longitudinal velocity, a pair of diffusive shear modes that couple to the transverse velocity, and a diffusive heat mode. The longitudinal and transverse components of the velocity are defined by $\mathbf{v} = \mathbf{v}^L + \mathbf{v}^T$ with $\boldsymbol{\nabla} \times \mathbf{v}^L = 0$ and $\boldsymbol{\nabla} \cdot \mathbf{v}^T = 0$. The hydrodynamic modes govern the hydrodynamic correlation functions. The transverse velocity correlation function is defined by

$$S^{vv}_{ij}(\omega, \mathbf{k}) = \langle \delta v^T_i \delta v^T_j \rangle_{\omega,\mathbf{k}} = \int d^3x\, dt\; e^{i(\omega t - \mathbf{k}\cdot\mathbf{x})} \langle \delta v^T_i(\mathbf{x}, t) \delta v^T_j(0,0) \rangle \,, \tag{59}$$

where $\delta v^T_i(\mathbf{x}, t) = v^T_i(\mathbf{x}, t) - \langle v^T_i(\mathbf{x}, t) \rangle$ is a fluctuation of the velocity. Linearized hydrodynamics gives

$$S^{vv}_{ij}(\omega, \mathbf{k}) = \frac{2T}{\rho} \left(\delta_{ij} - \hat{k}_i \hat{k}_j \right) \frac{\nu \mathbf{k}^2}{\omega^2 + \nu^2 \mathbf{k}^4} \,, \tag{60}$$

where $\nu = \eta/\rho$ is the kinetic viscosity. The dependence of the correlation function on ω and $\mathbf{k}$ is determined by the laws of hydrodynamics, equ. (48-50), and the overall normalization is fixed by the thermodynamic relation

$$\langle \delta v_i(\mathbf{x}, t) \delta v_j(\mathbf{x}', t) \rangle = \frac{T}{\rho} \delta_{ij} \delta(\mathbf{x} - \mathbf{x}') \,. \tag{61}$$

We observe that the transverse velocity correlation function has a diffusive pole, where the diffusion constant is given by the kinematic viscosity. The entropy correlation function has a diffusive pole governed by the thermal diffusion constant $\chi = \kappa/(c_p \rho)$, where c_p is the specific heat at constant pressure. The correlation function is

$$S^{ss}(\omega, \mathbf{k}) = \langle \delta s \delta s \rangle_{\omega,\mathbf{k}} = \frac{2c_p}{\rho} \frac{\chi \mathbf{k}^2}{\omega^2 + \chi^2 \mathbf{k}^4} \,. \tag{62}$$

The pressure correlation function contains the sound pole and is given by

$$S^{pp}(\omega,\mathbf{k}) = \langle \delta p \delta p \rangle_{\omega,\mathbf{k}} = 4\rho T c_s^3 \, \frac{\gamma c_s^2 \mathbf{k}^2 + \gamma_T(\omega^2 - c_s^2\mathbf{k}^2)}{(\omega^2 - c_s^2\mathbf{k}^2)^2 + 4\gamma^2 c_s^2 \omega^2} \,, \tag{63}$$

where $c_s = [(\partial P)/(\partial\rho)|_s]^{1/2}$ is the speed of sound and $\gamma = \gamma_{\eta,\zeta} + \gamma_T$ is the coefficient of sound absorption (the inverse sound attenuation length). The contributions to γ from viscosity and thermal conductivity are given by

$$\gamma_{\eta,\zeta} = \frac{\mathbf{k}^2}{2\rho c_s}\left(\zeta + \frac{4}{3}\eta\right) \,, \quad \gamma_T = \frac{\mathbf{k}^2 c_s \rho}{2T}\,\chi\left(\frac{\partial T}{\partial P}\right)_s \,. \tag{64}$$

3.1.2. Superfluid hydrodynamics Superfluidity is characterized by the spontaneous breakdown of the $U(1)$ symmetry associated with the conserved particle number. By Goldstone's theorem the spontaneous breaking of a continuous symmetry leads to the appearance of a gapless mode. This mode has to be included in the hydrodynamic description of the system. We introduced the Goldstone boson field φ in equ. (25). The quantity $\mathbf{v}_s = \boldsymbol{\nabla}\varphi/m$ can be interpreted as the superfluid velocity. Since $\mathbf{v}_s$ is the gradient of a phase the superfluid velocity is irrotational, $\boldsymbol{\nabla} \times \mathbf{v}_s = 0$.

We have to generalize the constitutive equations to include both the normal fluid velocity $\mathbf{v}_n$ and the superfluid velocity $\mathbf{v}_s$. In the ideal fluid case (no dissipation) the result is completely fixed by Galilean invariance and thermodynamic relations. The constitutive equations are

$$\mathbf{g} = \rho_n \mathbf{v}_n + \rho_s \mathbf{v}_s \,, \tag{65}$$

$$\Pi_{ij} = P\delta_{ij} + \rho_n v_{n,i} v_{n,j} + \rho_s v_{s,i} v_{s,j} \,, \tag{66}$$

$$\mathbf{j}^{\,\epsilon} = \rho s T \mathbf{v}_n + \left(\mu + \frac{1}{2}\mathbf{v}_s^2\right)(\rho_n \mathbf{v}_n + \rho_s \mathbf{v}_s) + \rho_n \mathbf{v}_n \mathbf{v}_n \cdot (\mathbf{v}_n - \mathbf{v}_s) \,, \tag{67}$$

where ρ_n and ρ_s are the normal and superfluid density of the system. The total density $\rho = \rho_n + \rho_s$ is the sum of the normal and superfluid contributions. The ratio ρ_s/ρ is a function of the temperature, the chemical potential, and the relative velocity $|\mathbf{v}_n - \mathbf{v}_s|$. This function, like the equation of state $P(\mu, T, |\mathbf{v}_n - \mathbf{v}_s|)$, depends on microscopic details. The conservation laws are given by equ. (48-50). These equations have to be supplemented by an equation of motion for the superfluid velocity. Euler's equation for the superfluid velocity is given by

$$\frac{\partial \mathbf{v}_s}{\partial t} + (\mathbf{v_s} \cdot \boldsymbol{\nabla})\mathbf{v}_s = -\boldsymbol{\nabla}\mu \,. \tag{68}$$

Using $\mathbf{v}_s = \boldsymbol{\nabla}\varphi/m$ this equation can be derived from the effective lagrangian given in equ. (27) [63, 64]. Because $\mathbf{v}_s$ is irrotational we can rewrite the convective derivative on the LHS of equ. (68) as a total derivative, $\mathbf{v}_s \cdot \boldsymbol{\nabla}\mathbf{v}_s = \frac{1}{2}\boldsymbol{\nabla}(\mathbf{v}_s^2)$.

As in the case of a normal fluid we may consider dissipative corrections to the constitutive equations. Viscous corrections to the energy momentum tensor are

$$\begin{aligned} \delta\Pi_{ij} = & -\eta\left(\nabla_i v_{n,j} + \nabla_j v_{n,i} - \frac{2}{3}\delta_{ij}\boldsymbol{\nabla}\cdot\mathbf{v}_n\right) \\ & - \delta_{ij}\Big(\zeta_1 \boldsymbol{\nabla}\cdot(\rho_s(\mathbf{v}_s - \mathbf{v}_n)) + \zeta_2(\boldsymbol{\nabla}\cdot\mathbf{v}_n)\Big) \,. \end{aligned} \tag{69}$$

We observe that viscous shear stresses only arise from the normal component of the flow. In addition to the normal bulk viscosity term proportional to ζ_2 there is a second contribution that involves the relative motion of the normal and superfluid components. Two additional bulk viscosities appear in the dissipative correction to the RHS of equ. (68). We replace $\boldsymbol{\nabla}\mu$ by $\boldsymbol{\nabla}(\mu + H)$ with

$$H = -\zeta_3 \boldsymbol{\nabla} \cdot (\rho_s (\mathbf{v}_s - \mathbf{v}_n)) - \zeta_4 \boldsymbol{\nabla} \cdot \mathbf{v}_n \,. \tag{70}$$

Onsager's symmetry principle requires that $\zeta_4 = \zeta_1$. The dissipative correction to the energy current is $\delta j_i^\epsilon = v_{n,j}\delta\Pi_{ij} + \rho_s(v_{s,i} - v_{n,i})H + Q_i$ where $Q_i = -\kappa\nabla_i T$ as in the case of a normal fluid.

Superfluid hydrodynamics contains two velocity fields, the normal flow velocity $\mathbf{v}_n$ and the superfluid (irrotational) flow velocity $\mathbf{v}_s$. This extra degree of freedom leads to an additional sound mode called second sound. The velocity of second sound depends strongly on temperature and vanishes at the critical temperature where $\rho_s/\rho \to 0$. If thermal expansion can be neglected second sound is an oscillatory motion of the superfluid against the normal fluid which does not lead to any mass transport and can be viewed as a pure entropy wave.

3.1.3. Relativistic fluids In a relativistic fluid the equations of energy and momentum conservation can be written as a single equation

$$\partial_\mu T^{\mu\nu} = 0 \,, \tag{71}$$

where $T^{\mu\nu}$ is the energy momentum tensor. In ideal fluid dynamics the form of $T_{\mu\nu}$ is completely fixed by Lorentz invariance,

$$T^{\mu\nu} = (\epsilon + P)u^\mu u^\nu + P\eta^{\mu\nu} \,, \tag{72}$$

where u^μ is the fluid velocity ($u^2 = -1$) and $\eta^{\mu\nu} = \mathrm{diag}(-1, 1, 1, 1)$ is the metric tensor. In a relativistic theory there need not be a conserved particle number. If a conserved particle number, for example baryon number, exists then there is a second hydrodynamic equation that express particle number conservation

$$\partial_\mu (n u^\mu) = 0 \,, \tag{73}$$

where n is the particle density. As in the non-relativistic case the hydrodynamic equations have to be supplemented by an equation of state $P = P(\epsilon)$ or $P = P(\epsilon, n)$. The four equations given in equ. (71) can be split into two sets using the longitudinal and transverse projectors

$$\Delta^{||}_{\mu\nu} = -u_\mu u_\nu, \qquad \Delta_{\mu\nu} = \eta_{\mu\nu} + u_\mu u_\nu \,. \tag{74}$$

With the help of the thermodynamic relations $d\epsilon = Tds$ and $\epsilon + P = sT$ the longitudinal equation is equivalent to entropy conservation

$$\partial_\mu (s u^\mu) = 0 \,, \tag{75}$$

and the transverse equation is the relativistic Euler equation

$$D u_\mu = -\frac{1}{\epsilon + P} \nabla^\perp_\mu P \,, \tag{76}$$

where $D = u \cdot \partial$ and $\nabla_\mu^\perp = \Delta_{\mu\nu}\partial^\nu$. Comparison with equ. (55) shows that the inertia of a relativistic fluid is governed by $\epsilon + P$.

The form of the dissipative terms depends on the precise definition of the fluid velocity. A useful choice is to define u^μ by the requirement that in the local rest frame $T^{00} = \epsilon$ and $T^{0i} = 0$ (Landau frame). In this case the dissipative correction to the energy momentum tensor in the rest frame has the same form as in the non-relativistic case, see equ. (57). A covariant definition is $T^{\mu\nu} = T_0^{\mu\nu} + \delta T^{\mu\nu}$ where

$$\delta^{(1)} T^{\mu\nu} = -\eta\sigma^{\mu\nu} - \zeta\Delta^{\mu\nu}\partial \cdot u \tag{77}$$

is the first order term and

$$\sigma^{\mu\nu} = \Delta^{\mu\alpha}\Delta^{\nu\beta}\left(\partial_\alpha u_\beta + \partial_\beta u_\alpha - \frac{2}{3}\eta_{\alpha\beta}\partial \cdot u\right) . \tag{78}$$

The dissipative correction to the conserved particle current is $j_\mu = n u_\mu + \delta j_\mu$ with

$$\delta^{(1)} j_\mu = -\kappa\left(\frac{nT}{\epsilon + P}\right)^2 \Delta_\mu^\perp\left(\frac{\mu}{T}\right) , \tag{79}$$

where κ is the thermal conductivity and μ is the chemical potential associated with the conserved density n. Alternatively, one can define the velocity via the particle current (Eckart frame). In that case there is no dissipative contribution to j_μ and the thermal conductivity appears in stress tensor.

The hydrodynamic equations determine the propagation of sound and diffusive modes. We consider the case without a conserved particle number. In this case all the modes can be found by considering correlation functions of the energy-momentum current $g^i = T^{0i}$. The longitudinal and transverse correlation functions are

$$S_{gg}^L(\omega, \mathbf{k}) = 2sT\,\frac{\Gamma_s\omega^2\mathbf{k}^2}{(\omega^2 - c_s\mathbf{k}^2)^2 + (\Gamma_s\omega\mathbf{k}^2)^2} , \tag{80}$$

$$S_{gg}^T(\omega, \mathbf{k}) = \frac{2\eta\mathbf{k}^2}{\omega^2 + (\frac{\eta}{sT}\mathbf{k}^2)^2} . \tag{81}$$

As in the non-relativistic fluid we find a pair of sound waves, and a pair of diffusive shear modes. The sound attenuation length is given by

$$\Gamma_s = \frac{\frac{4}{3}\eta + \zeta}{sT} , \tag{82}$$

and the analog of the kinematic viscosity is the ratio $\eta/(sT)$.

An new issue that arises in viscous relativistic hydrodynamics is the apparent lack of causality of the equations of motion. The problem can be seen by inspecting the linearized equation for the diffusive shear mode. The equation is first order in time, but second order in spatial gradients. As a result discontinuities in the initial conditions can propagate with infinite speed. This is not really a problem of the hydrodynamic description – the relevant modes are outside the domain of validity of hydrodynamics – but the acausal modes cause difficulties in numerical implementations. To overcome these difficulties one can include second order gradient corrections in the stress tensor. In general there is large number of second order terms. A complete classification of the

second order terms in a relativistic conformal fluid was recently given in [65]. Conformal symmetry implies that $\zeta = 0$ and $\delta^{(1)}T_{\mu\nu} = -\eta\sigma_{\mu\nu}$. The second order correction is

$$\begin{aligned}\delta^{(2)}T^{\mu\nu} = \eta\tau_{II}\left[{}^{\langle}D\sigma^{\mu\nu\rangle} + \frac{1}{3}\,\sigma^{\mu\nu}(\partial\cdot u)\right] \\ + \lambda_1\sigma^{\langle\mu}{}_{\lambda}\sigma^{\nu\rangle\lambda} + \lambda_2\sigma^{\langle\mu}{}_{\lambda}\Omega^{\nu\rangle\lambda} + \lambda_3\Omega^{\langle\mu}{}_{\lambda}\Omega^{\nu\rangle\lambda}\,,\end{aligned} \tag{83}$$

where $\sigma^{\mu\nu}$ is the first order shear tensor defined above,

$$A^{\langle\mu\nu\rangle} = \frac{1}{2}\Delta^{\mu\alpha}\Delta^{\nu\beta}\left(A_{\alpha\beta} + A_{\beta\alpha} - \frac{2}{3}\Delta^{\mu\nu}\Delta^{\alpha\beta}A_{\alpha\beta}\right) \tag{84}$$

denotes the transverse traceless part of $A^{\alpha\beta}$ and

$$\Omega^{\mu\nu} = \frac{1}{2}\Delta^{\mu\alpha}\Delta^{\nu\beta}\left(\partial_\alpha u_\beta - \partial_\beta u_\alpha\right) \tag{85}$$

is the vorticity. Equ. (83) defines four new second order transport coefficients, τ_{II} and $\lambda_{1,2,3}$. These coefficient can be determined using kinetic theory [66] or the AdS/CFT correspondence [65, 67].

Equation (83) is a constitutive relation that determines the stress tensor in terms of thermodynamic variables. Formally, we may replace time derivatives by spatial derivatives using the lower order equations of motion. Another option, inspired by the approach of Israel and Stewart [68], is to promote $\pi^{\mu\nu} = \delta T^{\mu\nu}$ to a hydrodynamic variable. The equation of motion for $\pi^{\mu\nu}$ is

$$\begin{aligned}\pi^{\mu\nu} = \; -\eta\sigma^{\mu\nu} - \tau_{II}\left[{}^{\langle}D\pi^{\mu\nu\rangle} + \frac{4}{3}\,\pi^{\mu\nu}(\partial\cdot u)\right] \\ + \frac{\lambda_1}{\eta^2}\pi^{\langle\mu}{}_{\lambda}\pi^{\nu\rangle\lambda} - \frac{\lambda_2}{\eta}\pi^{\langle\mu}{}_{\lambda}\Omega^{\nu\rangle\lambda} + \lambda_3\Omega^{\langle\mu}{}_{\lambda}\Omega^{\nu\rangle\lambda}\,,\end{aligned} \tag{86}$$

This equation describes the relaxation of $\pi^{\mu\nu}$ to the Navier-Stokes form $-\eta\sigma^{\mu\nu}$. There are also a number of more phenomenological approaches that include some subset of higher order terms, for example the already mentioned Israel-Stewart formalism [68] or the equations of Lindblom and Geroch [69], see [27] for a review. We note that whatever formalism is used, a necessary condition for the applicability of second order hydrodynamics is that higher order corrections are small, $\delta^{(2)}T^{\mu\nu} \ll \delta^{(1)}T^{\mu\nu} \ll T^{\mu\nu}$.

Remarks: The second order formalism was initially developed for non-relativistic fluids by Burnett [70, 71], see [72] for a review. Higher order hydrodynamic equations can be derived from kinetic theory by computing moments of the Boltzmann equation. This procedure is known as Grad's moment method [73]. It is not easy to find systems in which the second order theory provides a quantitative improvement over the Navier Stokes equation. An example is the work of Uhlenbeck, Foch and Ford on sound propagation in gases [74, 75]. Finally, we note that relativistic superfluid hydrodynamics was formulated by Carter, Khalatnikov and Lebedev [76, 77], see [78, 64, 79] for a more recent treatment that emphasizes the connection to effective field theory.

3.2. Diffusion

An important diagnostic of the properties of a fluid is the diffusion of a dilute gas of impurities suspended in the fluid. The number of impurity particles is conserved, and the number density satisfies the continuity equation

$$\frac{\partial n}{\partial t} + \boldsymbol{\nabla} \cdot \jmath = 0\,. \tag{87}$$

If the number density varies smoothly then the current can be expressed in terms of the thermodynamic variables. At leading order in derivatives of the density we can write $\vec{\jmath} = -D\boldsymbol{\nabla} n$, where D is the diffusion constant. Inserting this expression into the continuity equation gives the diffusion equation

$$\frac{\partial n}{\partial t} = D\boldsymbol{\nabla}^2 n\,. \tag{88}$$

A more microscopic view of diffusion is provided by studying the Brownian motion of an individual suspended particle. The motion is described by a stochastic (Langevin) equation

$$\frac{d\mathbf{p}}{dt} = -\eta_D \mathbf{p} + \xi(t), \qquad \langle \xi_i(t)\xi_j(t')\rangle = \kappa\delta_{ij}\delta(t-t'). \tag{89}$$

Here, $\mathbf{p}$ is the momentum of the particle, η_D is the drag coefficient, and $\xi(t)$ is a stochastic force. The coefficient κ is related to the mean square momentum change per unit time, $3\kappa = \langle(\Delta\mathbf{p})^2\rangle/(\Delta t)$. The Langevin equation can be integrated to determine the mean squared momentum. In the long time limit ($t \gg \eta_D^{-1}$) the particle thermalizes and we expect that $\langle \mathbf{p}^{\,2}\rangle = 3mT$. This requirement leads to the Einstein relation

$$\eta_D = \frac{\kappa}{2mT}. \tag{90}$$

The relation between η_D and the diffusion constant can be determined from the mean square displacement. At late times $\langle[\Delta\mathbf{x}(t)]^2\rangle = 6D|t|$ and

$$D = \frac{2}{m\eta_D} = \frac{2T^2}{\kappa}. \tag{91}$$

A particularly simple case is the diffusion of large spherical particles suspended in a non-relativistic fluid. In this case the drag coefficient can be computed using the Navier-Stokes equation and the drag is related to the shear viscosity of the fluid, $\eta_D = 6\pi\eta a/m$, where a is the radius of the particles. This leads to a relation between the diffusion constant and the shear viscosity, $D = T/(6\pi\eta a)$.

3.3. Dynamic universality

In the vicinity of a second order phase transition fluctuations of the order parameter relax slowly. This implies that order parameter fluctuations have to be included in the hydrodynamic description. The resulting hydrodynamic models describe universal features of transport phenomena near a continuous phase transition [80]. Dynamic universality classes, like the well-known static ones, depend on the symmetries of the order parameter and the number of dimensions. Universal aspects of transport also

depend on the nature of the order parameter, whether it is conserved or not, and on the presence of couplings (non-vanishing Poisson brackets) between the order parameter and the conserved fields.

In this section we will briefly review the hydrodynamic description of a simple fluid near the liquid-gas endpoint. This theory is known as model H. The hydrodynamic description of the superfluid-normal transition in liquid Helium and dilute atomic gases is known as model F. Near the critical point sound modes ($\omega \sim k$) are significantly higher in energy than diffusive modes ($\omega \sim k^2$), and the longitudinal components of the momentum density $\mathbf{g}$ can be neglected. A minimal model that describes the coupling of the order parameter ϕ to the transverse momentum density $\mathbf{g}_T$ is [80]

$$\frac{\partial \phi}{\partial t} = \lambda_0 \boldsymbol{\nabla}^2 \frac{\delta \mathcal{F}_T}{\delta \phi} - g_0 \boldsymbol{\nabla}\phi \cdot \frac{\delta \mathcal{F}_T}{\delta \mathbf{g}} + \zeta_\phi \,, \tag{92}$$

$$\frac{\partial g_i}{\partial t} = P^T_{ij} \left[\eta_0 \boldsymbol{\nabla}^2 \frac{\delta \mathcal{F}_T}{\delta g_j} + g_0 (\nabla_j \phi) \frac{\delta \mathcal{F}_T}{\delta \phi} + \zeta_{g_j} \right] . \tag{93}$$

where $P^T_{ij} = (\delta_{ij} + \nabla_i \nabla_j / \boldsymbol{\nabla}^2)$ is a transverse projector, ζ_ϕ and ζ_{g_j} are random forces, and the free energy $\mathcal{F}_T = \mathcal{F} - \mathcal{F}_h$ is given by

$$\mathcal{F} = \int d^d x \, \left[\frac{1}{2} (\boldsymbol{\nabla}\phi)^2 + \frac{r_0}{2}\phi^2 + u_0 \phi^4 + \frac{1}{2}\mathbf{g}^2 \right] , \tag{94}$$

$$\mathcal{F}_h = \int d^d x \, \left[h\phi + \mathbf{A} \cdot \mathbf{g} \right] , \tag{95}$$

where h and $\mathbf{A}$ are external fields. The coefficients λ_0 and η_0 are the bare values of the thermal conductivity and shear viscosity. Fluctuations cause the physical value of the zero frequency transport coefficients to diverge near the critical point. In order to study the critical behavior of the bulk viscosity the longitudinal component of $\mathbf{g}$ has to be included [81].

In a normal fluid the only conserved charges are the particle density, the energy density, and the momentum density. The order parameter is a suitable linear combination of the energy density and the particle density. In QCD the hydrodynamic variables include the chiral condensate, and the conserved energy density, baryon density, and isospin density. The situation was analyzed in more detail by Son and Stephanov [82] who argue that the QCD critical point is correctly described by model H. The values of the critical exponents can be determined using the epsilon expansion. The shear and bulk viscosity diverge with the correlation length ξ as [80, 81]

$$\eta \sim \xi^{x_\eta} \quad (x_\eta \simeq 0.06), \qquad \zeta \sim \xi^{x_\zeta} \quad (x_\eta \simeq 2.8). \tag{96}$$

The critical endpoint is in the same static universality class as the Ising model and $\xi \sim t^{-0.63}$, where $t = (T - T_c)/T$. We note that the divergence in the bulk viscosity is much stronger than the divergence in the shear viscosity.

3.4. Kubo relations and spectral functions

Hydrodynamics is an effective description of the low energy, long wavelength response of a fluid. The transport coefficients appear as unknown constants in the hydrodynamic

equations. These constants can be extracted from experiment, or computed from a more microscopic theory. The relationship between transport coefficients and correlation functions in a microscopic quantum field theory is provided by Kubo relations. We have seen that hydrodynamics fixes the low energy and low momentum behavior of the correlation functions of conserved charges, see equ. (60-63). In the field theory these correlation functions can be computed using linear response theory. The response is governed by the retarded correlation function. In the case of shear viscosity the relevant correlation function is

$$G_R^{xy,xy}(\omega,\mathbf{k}) = -i\int dt \int d^3x\, e^{i(\omega t-\mathbf{k}\cdot\mathbf{x})}\Theta(t)\langle[T^{xy}(\mathbf{x},t),T^{xy}(0,0)]\rangle\,, \tag{97}$$

where $T^{\mu\nu}$ is the energy momentum tensor. The imaginary part of the retarded correlator defines the spectral function, $\rho(\omega,\mathbf{k}) = -2\,\mathrm{Im}\,G_R(\omega,\mathbf{k})$. The spectral function is connected to the correlation function by the fluctuation-dissipation relation. In the low frequency limit $\rho(\omega,\mathbf{k}) = (\omega/T)S(\omega,\mathbf{k})$. Matching the correlation function from linear response theory to the hydrodynamic correlator gives the Kubo relation

$$\eta = \lim_{\omega\to 0}\lim_{k\to 0}\frac{\rho^{xy,xy}(\omega,\mathbf{k})}{2\omega}\,. \tag{98}$$

The formula for the bulk viscosity involves the trace of the energy momentum tensor

$$\zeta = \frac{1}{9}\lim_{\omega\to 0}\lim_{k\to 0}\frac{\rho^{ii,jj}(\omega,\mathbf{k})}{2\omega}\,, \tag{99}$$

and analogous results can be derived for the thermal conductivity and diffusion constants.

The spectral function contains information about the physical excitations that carry the response. We will discuss this issue in more detail when we compare the strong coupling (AdS/CFT) and weak coupling spectral functions in Sec. 4. Dispersion relations connect the spectral function to correlation functions with different analyticity properties. The Matsubara (imaginary energy) correlation function is

$$G_E(i\omega_n) = \int\frac{d\omega}{2\pi}\frac{\rho(\omega)}{\omega - i\omega_n}\,, \tag{100}$$

where $\omega_n = 2\pi nT$ is the Matsubara frequency. The imaginary time correlation function is given by

$$G_E(\tau) = \int\frac{d\omega}{2\pi}K(\omega,\tau)\rho(\omega)\,, \tag{101}$$

where the kernel $K(\omega,\tau)$ is defined by

$$K(\omega,\tau) = \frac{\cosh[\omega(\tau-1/(2T))]}{\sinh[\omega/(2T)]} = [1+n_B(\omega)]\,e^{-\omega\tau} + n_B(\omega)e^{\omega\tau}\,, \tag{102}$$

and $n_B(\omega)$ is the Bose distribution function. Equation (101) is the basis of attempts to compute transport coefficients using imaginary time quantum Monte Carlo data [83, 84, 85, 86]. The idea is to compute $G_E(\tau)$ numerically, invert the integral transform in equ. (101) to obtain $\rho(\omega)$, and then extract transport coefficients from $\rho'(0)$. The difficulty is that $G_E(\tau)$ is typically only computed on a small number of points, and

T	$1.02\ T_c$	$1.24\ T_c$	$1.65\ T_c$
η/s		0.102(56)	0.134(33)
ζ/s	0.73(3)	0.065(17)	0.008(7)

Table 2. Lattice QCD results for the ratio of shear and bulk viscosity to entropy density in a pure gluon plasma. The calculations were performed for three different temperatures, given in units of the critical temperature T_c. Data from [84, 88].

that the imaginary time correlator is not very sensitive to the slope of the spectral function at low energy. Many recent calculations make use of the maximum entropy method to obtain numerically stable spectral functions and reliable error estimates [87]. It was also observed that one can minimize the contribution from continuum states to the imaginary time Green function by studying the correlators of conserved charges, energy and momentum density, at non-zero spatial momentum [88]. In more physical terms this means that one is extracting the viscosity from the sound pole rather than the shear pole. In Table 2 we summarize some recent lattice QCD results on the shear and bulk viscosity in the high temperature phase of pure gauge QCD. We observe that the shear viscosity to entropy density ratio is close to the conjectured bound $1/(4\pi)$. The bulk viscosity is large in the vicinity of the phase transition but decreases quickly and becomes extremely small at $T = 1.64T_c$.

3.5. Kinetic theory: Shear viscosity

If the fluid can be described in terms of weakly interacting quasi-particles then the hydrodynamic variables can be written in terms of quasi-particle distribution functions $f_p(\mathbf{x}, t)$. In the case of a non-relativistic fluid the energy current, momentum current, and stress tensor are given by

$$j_i^\epsilon(\mathbf{x}, t) = \int \frac{d^3p}{(2\pi)^3} E_p v_{p,i} f_p(\mathbf{x}, t)\,, \tag{103}$$

$$g_i(\mathbf{x}, t) = \int \frac{d^3p}{(2\pi)^3} m v_{p,i} f_p(\mathbf{x}, t)\,, \tag{104}$$

$$\Pi_{ij}(\mathbf{x}, t) = \int \frac{d^3p}{(2\pi)^3} m v_{p,i} v_{p,j} f_p(\mathbf{x}, t), \tag{105}$$

where E_P is the quasi-particle energy, and $v_{p,i} = (\partial E_p)/(\partial p_i)$ is the quasi-particle velocity. The equation of motion for $f_p(\mathbf{x}, t)$ is the Boltzmann equation

$$\frac{\partial f_p}{\partial t} + \mathbf{v} \cdot \boldsymbol{\nabla} f_p + \mathbf{F} \cdot \boldsymbol{\nabla}_p f_p = C[f_p]\,, \tag{106}$$

where $\mathbf{F}$ is an external force and $C[f_p]$ is the collision term. In local thermal equilibrium the distribution function is determined by the local temperature, chemical potential, and flow velocity. We have

$$f_p^0(\mathbf{x}, t) = \frac{1}{\exp((E_p - \mathbf{v} \cdot \mathbf{p} - \mu)/T) \mp 1}\,, \tag{107}$$

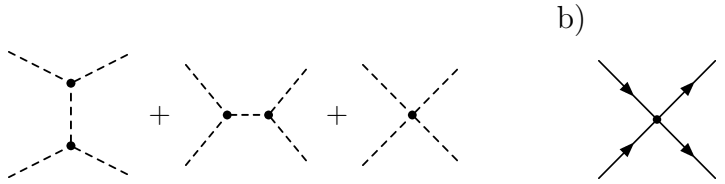

Figure 2. Leading order processes that contribute to the shear viscosity of the Fermi gas in the unitarity limit at low temperature (Fig. a) and high temperature (Fig. b). Dashed lines are phonon propagators and solid lines are fermion propagators.

where the $\mp$ sign corresponds to bosons/fermions. Transport coefficients characterize how the distribution function relaxes to its equilibrium value if it is perturbed slightly away from it. We can write

$$f_p(\mathbf{x},t) = f_p^0(\mathbf{x},t) + \delta f_p(\mathbf{x},t) \tag{108}$$

and linearize the Boltzmann equation in δf_p. In order to determine transport coefficients we also use a gradient expansion of the local velocity, temperature and chemical potential and linearize the Boltzmann equation in the "driving terms" $\nabla_i v_j$, $\nabla_i T$ and $\nabla_i \mu$. This procedure is known as the Chapman-Enskog method. In the next section we will describe the method in the case of phonon mediated transport in a superfluid, and then discuss some of the modifications that appear when studying high temperature Fermi and Bose gases as well as gauge theories.

3.5.1. Phonons in dilute Fermi gases In the following we will concentrate on the shear viscosity of the low temperature, superfluid, phase of the dilute Fermi gas at unitarity. The calculation is similar to the computation of the shear viscosity of superfluid helium, but as explained in Sect. 2.3 the low energy effective theory of the dilute Fermi gas is more tightly constrained. We discuss the shear viscosity of liquid helium, as well as the viscosity of the low temperature (chiral symmetry broken) phase of QCD in Sect. 3.5.2. The stress tensor of a phonon gas is

$$\Pi_{ij}(\mathbf{x},t) = c_s^2 \int \frac{d^3p}{(2\pi)^3} \frac{p_i p_j}{E_p} f_p(\mathbf{x},t)\,. \tag{109}$$

In order to study the shear viscosity we write $\delta f_p = -\chi(p) f_p^0(1+f_p^0)/T$ with

$$\chi(p) = g(p)\left(p_i p_j - \frac{1}{3}\delta_{ij}\mathbf{p}^2\right)\left(\nabla_i v_j + \nabla_j v_i - \frac{2}{3}\delta_{ij}\boldsymbol{\nabla}\cdot\mathbf{v}\right)\,. \tag{110}$$

Inserting this ansatz into the energy momentum tensor gives

$$\eta = \frac{4c_s^2}{15T}\int \frac{d^3p}{(2\pi)^3}\frac{p^4}{2E_p} f_p^0(1+f_p^0) g(p)\,. \tag{111}$$

The function $g(p)$ is determined by the linearized Boltzmann equation. Linearizing the LHS of the Boltzmann equation in derivatives of $\mathbf{v}, \mu, T$ gives

$$\frac{df_p}{dt} \simeq c_s^2 \frac{f_p^0(1+f_p^0)}{2E_p T} p_{ij} v_{ij}\,, \tag{112}$$

where we have defined

$$p_{ij} = p_i p_j - \frac{1}{3}\delta_{ij}\mathbf{p}^2, \quad v_{ij} = \nabla_i v_j + \nabla_j v_i - \frac{2}{3}\delta_{ij}\boldsymbol{\nabla}\cdot\mathbf{v}\,. \tag{113}$$

The RHS of the Boltzmann equation contains the collision term $C[f_p]$. In the present case the dominant contribution arises from binary $2 \leftrightarrow 2$ collisions. The linearized collision term is

$$\begin{aligned} C_{2\leftrightarrow 2}[f_p] &\simeq \frac{1+f_p^0}{2E_pT}\int d\Gamma(k;k',p')(1+f_k^0)f_{k'}^0 f_{p'}^0|\mathcal{M}|^2 \\ &\quad\times\left[g(p)p_{ij}+g(k)k_{ij}-g(k')k'_{ij}-g(p')p'_{ij}\right]v_{ij} \\ &\equiv \frac{f_p^0(1+f_p^0)}{2E_pT}C_{ij}[g(p)]v_{ij}, \end{aligned} \tag{114}$$

where $\mathcal{M}$ is the scattering matrix element,

$$d\Gamma(k;k',p') = \left(\prod_{q=k,k',p'}\frac{d^3q}{(2\pi)^3 2E_q}\right)\times(2\pi)^4\delta^{(4)}(p+k-k'-p') \tag{115}$$

is the phase space, and we have defined the linearized collision operator $C_{ij}[g(p)]$. The linearized Boltzmann equation can now be written as

$$C_{ij}[g(p)] = \frac{c_s^2}{T}\,p_{ij}. \tag{116}$$

This result can be used to rewrite the relation for the viscosity in equ. (111) as

$$\eta = \frac{2}{5}\int\frac{d^3p}{(2\pi)^3}\frac{f_p^0(1+f_p^0)}{2E_pT}p_{ij}g(p)C_{ij}[g(p)]\,. \tag{117}$$

The two relations equ. (111) and (117) can be used to derive a variational estimate of the shear viscosity. We can view equ. (111) as an inner product with measure $f^0(1+f^0)/(2E_p)$ and write

$$\eta = \frac{2}{5}\,\langle X|g\rangle\,, \tag{118}$$

where $X = (c_s^2/T)p_{ij}$ and $g = g(p)p_{ij}$. The linearized Boltzmann equation is $C|g\rangle = |X\rangle$ and equ. (117) can be written as $\eta = \frac{2}{5}\langle g|C|g\rangle$. The linearized collision operator C is a hermitean, negative semi-definite operator. The zero eigenvalues of C correspond to the conservation laws for energy, momentum, and particle number. Consider a variational ansatz $|g_{var}\rangle$ for the exact solution $|g\rangle$ of the linearized Boltzmann equation. The triangle equality implies

$$\langle g_{var}|C|g_{var}\rangle\langle g|C|g\rangle \geq \langle g_{var}|C|g\rangle^2 = \langle g_{var}|X\rangle^2\,. \tag{119}$$

Using $\eta = \frac{2}{5}\langle g|C|g\rangle$ we get

$$\eta \geq \frac{2}{5}\,\frac{\langle g_{var}|X\rangle^2}{\langle g_{var}|C|g_{var}\rangle^2}\,. \tag{120}$$

This result is, of course, not a lower bound on the exact value of η, but it is a bound within the approximation that is used to compute the collision term. A popular choice for g_{var} is X. This ansatz provides a good estimate in the case of non-relativistic particles

interacting via short range interactions, as well as for gauge boson exchanges in QCD, but not in the case of Goldstone boson scattering.

A systematic method for improving the variational estimate is based on orthogonal polynomials. We can construct a complete set of polynomials that are orthogonal with respect to the inner product defined in equ. (118). In non-relativistic physics these polynomials are known as Sonine polynomials [89] and suitable generalizations can been constructed for Bose and Fermi gases [90]. We now fix an integer N and expand the solution of the linearized Boltzmann equation in the first N polynomials. At finite N solving the Boltzmann equation reduces to the problem of inverting an $N \times N$ matrix. The solution provides a variational estimate for η which becomes exact as $N \to \infty$. Convergence is usually quite fast.

To complete the calculation of the shear viscosity we need to compute the scattering amplitude $\mathcal{M}$. The collision operator at leading order in T/μ is determined by the scattering amplitude at leading order in q/μ, where $q = p, p', k, k'$. The amplitude is given by the diagrams in Fig. 2a with vertices and propagators determined by the effective lagrangian given in equ. (28). The expression for $\mathcal{M}$ is not very instructive and can be found in [90]. The best estimate for η is obtained by using $g(p) \sim p^{-1}$. We find

$$\eta = 9.3 \times 10^{-6} \frac{\xi^5}{c_s^3} \frac{T_F^8}{T^5}\,, \tag{121}$$

where $\xi \simeq 0.4$ is the universal parameter we introduced in equ. (23). In the low temperature limit the entropy density is dominated by the phonon contribution

$$s = \frac{2\pi^2}{45} \frac{T^3}{c_s^3}\,. \tag{122}$$

The ratio η/s drops sharply with temperature. Extrapolating to $T = T_c \simeq 0.15 T_F$ gives $\eta/s \sim 0.8$, with very large uncertainties.

3.5.2. Phonons and rotons in liquid helium, pions in QCD The calculations of shear viscosity of liquid ^{4}He below the λ point is similar to the computation of η in the superfluid Fermi gas. The main difference is that close to T_c it is important to include the roton contribution. Rotons form a dilute gas, and unlike phonons, they are not derivatively coupled. As a consequence the roton viscosity is independent of the roton density. The roton momentum is determined by the roton minimum of the dispersion relation and depends only weakly on temperature. This implies that the roton viscosity is almost temperature independent. The value of the roton viscosity depend on the poorly known roton-roton interaction. A fit to experimental data for the shear viscosity below the lambda point gives $\eta_r \simeq 1.2 \cdot 10^{-5}$ poise. The leading correction to the roton term comes from phonon-roton scattering. Landau and Khalatnikov find [22]

$$\eta = \eta_r + \frac{A}{T^{1/2}} \exp\left(\frac{\Delta}{T}\right) \frac{10 + 8\bar{\Theta}/\Theta_{ph}}{1 + 8\bar{\Theta}/\Theta_{ph}}\,, \tag{123}$$

where Δ is the roton energy defined in equ. (14), A is a constant, and Θ/Θ_{ph} is the ratio of the roton-roton and roton-phonon relaxation rates. This ratio scales as $T^{4.5} \exp(\Delta/T)$.

For $T < 0.9$ K we can use $\bar{\Theta} \gg \Theta_{ph}$ and the temperature dependence of the phonon-roton term is governed by the $T^{-0.5}\exp(\Delta/T)$ term. For $T < 0.7$ K phonon-phonon scattering dominates and the viscosity scales as T^{-5}, as in the previous section. At even smaller temperature, $T \lesssim 0.5$ K, phonon splitting may become important and the temperature dependence is $\eta \sim T^{-1}$ [91]. The roton contribution to the entropy density is

$$s_r = \frac{2(m^*)^{1/2}p_0^2\Delta}{(2\pi)^{3/2}T^{1/2}}\left(1+\frac{3T}{2\Delta}\right)\exp\left(-\frac{\Delta}{T}\right), \tag{124}$$

where m^* and p_0 are given in equ. (14). The phonon contribution is given by equ. (122) with $c_s = 238$ m/sec. If we push equ. (123) and (124) to the limit of their applicability, $T \sim 2$ K, we find $\eta/s \sim 2$.

The computation of the shear viscosity in low temperature QCD also proceeds along similar lines. The Goldstone boson in QCD is the pion, and pion interactions are governed by the effective lagrangian given in equ. (45). The pion is not massless, $m_\pi = 139$ MeV. At very low temperature, $T \ll m_\pi$, the pion scattering amplitude is approximately constant and the viscosity is only weakly temperature dependent. At higher temperature we can set $m_\pi \simeq 0$ and the scattering amplitude is energy dependent. The main difference as compared to phonon scattering is that the four-pion interaction is of the form $(\phi\partial\phi)^2$ instead of $(\partial\phi)^4$, and that there is no three-pion interaction. As a consequence the $\pi\pi$ scattering matrix element scales as the second power of the external momenta. The pion entropy is given by equ. (122) with $c_s = c/\sqrt{3}$ and an isospin degeneracy factor 3. An approximate calculation of the ratio η/s gives [92, 93]

$$\frac{\eta}{s} = \frac{15}{16\pi}\frac{f_\pi^4}{T^4} \tag{125}$$

Variational solutions of the Boltzmann equation reported in [94] give η/s ratios that are about five times larger. Calculations based on the measured phase shifts and the role of higher hadronic resonances are discussed in [92].

3.5.3. Non-relativistic atoms: Dilute Fermi gases and ^4He The shear viscosity of the dilute Fermi gas at high temperature is determined by binary scattering between the atoms. The tree level scattering matrix follows from equ. (16),

$$\mathcal{M} = \frac{4\pi}{m}\frac{1}{1/a+iq}, \tag{126}$$

where q is the relative momentum. In the unitarity limit $a \to \infty$ the scattering amplitude diverges as $1/q$ in the limit of small momenta. For $T \gg T_F$ the infrared divergence is effectively cut off by the thermal momentum $(mT)^{1/2}$. The viscosity in the high temperature limit is [95, 96]

$$\eta = \frac{15}{32\sqrt{\pi}}(mT)^{3/2}. \tag{127}$$

This result is based on the variational function $g(p) \sim 1$. Corrections due to more complicated distribution functions are small, $\Delta\eta/\eta < 2\%$ [97]. The scaling of η with

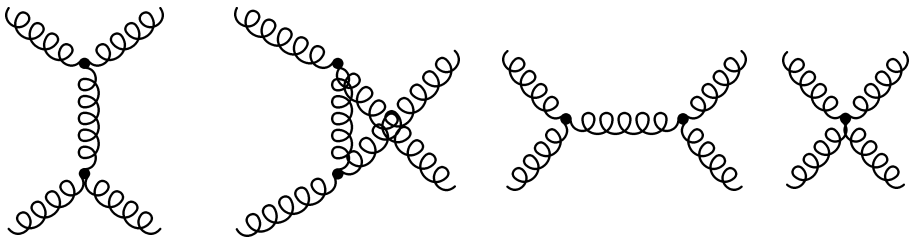

Figure 3. Leading order processes that contribute to the shear viscosity of a pure gluon plasma. The coefficient k defined in equ. (131) is determined by the t-channel diagram. The full leading order result, including the coefficient μ^*, requires the remaining diagrams, as well as gluon bremsstrahlung from the external legs (not shown).

temperature can be understood as a combination of the $T^{1/2}$ scaling of a dilute hard sphere gas (see Sect. 1) with an extra factor (mT) from the $1/q^2$ behavior of $|\mathcal{M}|^2$. The high temperature limit of the entropy density is that of a classical gas

$$s = \frac{2\sqrt{2}}{3\pi^2}(mT_F)^{3/2}\left[\log\left(\frac{3\sqrt{\pi}}{4}\frac{T^{3/2}}{T_F^{3/2}}\right)+\frac{5}{2}\right]. \tag{128}$$

Combining equ. (127) and (128) gives $\eta/s \sim x^{3/2}/\log(x)$ with $x = T/T_F$. The classical expression for the entropy becomes unphysical (negative) for $T \simeq T_c$. Extrapolating to $T \simeq 2T_c$ gives $\eta/s \simeq 0.5$.

The shear viscosity of helium is governed by scattering in the potential given in equ. (13). In the high temperature limit the dominant contribution does not come from the Van der Waals tail, but from the repulsive short range contribution. For a potential of the form $V \sim r^{-\nu}$ the viscosity scales as T^s with $s = \frac{1}{2} + \frac{2}{\nu-1}$ [98]. In the case of a Lennard-Jones (6-12) potential this implies $\eta \sim T^{0.68}$. A somewhat better fit to the data is provided by

$$\eta = \eta_0 \left(\frac{T}{T_0}\right)^{0.647} \tag{129}$$

with $\eta_0 = 1.88 \cdot 10^{-5}$ Pa·s and $T_0 = 273.15$ K. Very accurate calculations using realistic potentials can be found in [99]. These calculations are reliable down to about 10 K. The entropy density is given by the classical result, equ. (128). For $T = 10$ K we get $\eta/s \simeq 4$, and extrapolating to $T = 4$ K gives $\eta/s \simeq 1.5$.

3.5.4. Gauge fields in QCD The shear viscosity of a quark gluon plasma is determined by binary quark and gluon scattering. We first consider a pure gluon plasma. The leading order gluon-gluon scattering diagrams are shown in Fig. 4. The squared tree level amplitude is

$$|\mathcal{M}|^2 = \frac{9g^4}{2}\left(3 - \frac{ut}{s^2} - \frac{us}{t^2} - \frac{ts}{u^2}\right), \tag{130}$$

where g is the gauge coupling and s, t, u are the Mandelstam variables. The differential cross section diverges for small momentum transfer q as $1/q^4$. This is the standard

Rutherford behavior, which arises from t-channel gluon exchange. In the calculation of the shear viscosity the differential cross section is weighted by an extra factor q^2. The quantity $\sigma_T = \int dq^2 q^2 (d\sigma)/(dq^2)$ is known as the transport cross section. The transport cross section diverges logarithmically at small q. This divergence is regulated by medium corrections to the gluon propagator, see equ. (39,40). Electric gluon exchanges are screened at a distance $r_D \sim m_D^{-1}$, and the electric contribution to σ_T is proportional to $g^4 \log(m_D)$. There is no static magnetic screening, but gluons with energy ω are dynamically screened at a distance $r \sim (\omega m_D^2)^{-1/3}$. After integrating over energy the magnetic contribution also scales as $g^4 \log(m_D)$. Combining electric and magnetic t-channel exchanges gives [13, 14]

$$\eta = k \frac{T^3}{g^4 \log(\mu^*/m_D)} \,, \tag{131}$$

where $k = 27.13$. We will fix the coefficient μ^* below. This result corresponds to an optimized trial function $\chi(p) = A(p) p_{ij} v_{ij}$, but the simple approximation $A(p) \sim const$ agrees with the exact result to better than 1%. In order to compute the shear viscosity of a quark gluon plasma we have to include t-channel diagrams for quark-quark and quark-gluon scattering. The result is of the same form as equ. (131) with [14]

$$k(N_f) = (27.13, 60.81, 86.47, 106.67), \quad (N_f = 0, 1, 2, 3) \,. \tag{132}$$

Note that k increases with N_f faster than the total number of degrees of freedom. This is related to the fact that quarks have smaller color charges than gluons, which implies that quark-gluon scattering amplitudes are suppressed relative to gluon-gluon amplitudes.

In order to make an absolute prediction for the shear viscosity we need to determine the constant μ^* in equ. (131). This coefficient receives contributions from s and u-channel gluon exchanges. These contributions are straightforward to include. A more difficult problem arises from the fact that μ^* is sensitive to soft ($q \sim m_D$) binary $2 \to 2$ scattering followed by collinear $1 \to 2$ splitting. The inverse mean free time for this process is given by $\tau^{-1} \sim g^4/m_D^2 \times g^2 \times T^3 \sim g^4 T$, comparable to the mean free time for large angle $2 \to 2$ scattering. Collinear splitting does not directly contribute to shear viscosity (it contributes to bulk viscosity), but it degrades the momentum and assists in randomizing the momentum distribution in subsequent binary collisions.

The difficulty with collinear splitting is that the formation time of the emitted gluon is of order $1/(g^2 T)$. This is the same order of magnitude as the quasi-particle life time given in equ. (43), which implies that kinetic theory is breaking down. Arnold, Moore, and Yaffe showed that if interference between subsequent gluon emission processes, the Landau-Pomeranchuk effect, is taken into account an effective Boltzmann equation with $2 \to 2$ and $1 \to 2$ collision terms can be derived [100]. Arnold at al. find [15]

$$\mu^*(N_f = 0) = 2.765\, T \,. \tag{133}$$

They also show that μ^* is only weakly dependent on the number of flavors, $\mu^*(N_f = 3) = 2.957\, T$, and compute additional terms in an expansion in inverse logarithms of μ^*/m_D.

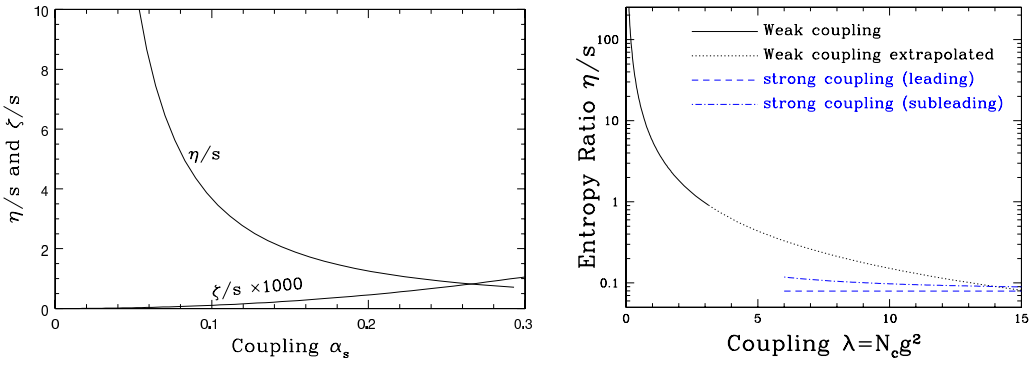

Figure 4. Shear and bulk viscosity to entropy density ratio in QCD (left panel) and $\mathcal{N} = 4$ supersymmetric Yang-Mills theory (right panel). The left panel shows the shear and bulk viscosity to entropy density ratio in QCD with $N_f = 3$ flavors as a function of the strong coupling constant α_s, from [103]. The right panel shows the ratio η/s in $\mathcal{N} = 4$ SUSY Yang Mills theory as a function of the 't Hooft coupling. The solid line shows the weak coupling result, the dotted line is an extrapolation of the weak coupling result to the strong coupling regime, the dashed lined is $\lambda \to \infty$ result from the AdS/CFT correspondence, and dash-dotted line is the leading correction to the strong coupling result, from [104].

The entropy density of the quark gluon plasma is given by

$$s = \frac{2\pi^2}{45}\left(2(N_c^2-1) + \frac{7}{8}4N_f\right) T^3 \,. \tag{134}$$

Higher order corrections to the entropy density are large, but the situation in the regime $T \geq 2T_c$ can be improved using resummation schemes, see Fig. 1. The resummed entropy differs from the free gas result by no more than 15% for $T > 2T_c$. The magnitude of higher order corrections to the viscosity is not known, but NLO results for the heavy quark diffusion constant suggest that higher corrections to transport coefficients are large [101].

The leading order QCD result is shown in Fig. 4. Clearly, η/s is strongly dependent on the coupling, and without performing higher order calculations it is not clear what value of α_s one should use at a given temperature. An interesting perspective is provided by exact results for η/s in the strong coupling limit of $\mathcal{N} = 4$ SUSY Yang-Mills theory, see Sect. 4. These results can be compared to weak coupling calculations based on kinetic theory [104]. The weak coupling result for η/s in the $\mathcal{N} = 4$ theory is smaller than the corresponding ratio in QCD by a factor $\sim 1/7$. This is related to the fact that in the $\mathcal{N} = 4$ theory all states are in the adjoint representation, and that the theory contains extra scalars. Both of these differences lead to larger cross sections. The leading order result for η/s in SUSY Yang-Mills theory is shown in the right panel of Fig. 4. We observe that η/s in the $\mathcal{N} = 4$ theory reaches the strong coupling limit when extrapolated to a 't Hooft coupling $\lambda = g^2 N_c \simeq 12$. This value is larger than the coupling $\lambda \sim 5$ at which the weak coupling expression for the entropy reaches the strong coupling limit $s/s_0 = 0.75$, see Fig. 1. If we consider $s/s_0 = 0.8$ to be the "QCD-like"

point, then we should restrict ourselves to $\lambda < 5$. In this case η/s does not drop below 0.5.

3.6. Kinetic theory: Other transport properties

3.6.1. Bulk viscosity The temperature dependence of bulk viscosity is quite different from that of shear viscosity. The bulk viscosity of a scale invariant system vanishes. In kinetic theory bulk viscosity is sensitive to deviations from conformality in the equation of state, and to the rate of processes that change the momentum distribution. Depending on the interplay between these two effects, the temperature dependence of bulk viscosity can differ dramatically between different fluids.

The Fermi gas at unitarity is exactly conformal and the bulk viscosity in the normal phase vanishes. In the low temperature phase conformal invariance requires $\zeta_1 = \zeta_2 = 0$, but ζ_3 can be non-zero [105]. This coefficient was recently computed in [102]. The result is sensitive to non-linearities in the phonon dispersion realtion. If $1 \to 2$ phonon splitting is kinematically allowed then $\zeta_3 \sim T^3$, where the constant of proportionality depends on the curvature of the dispersion relation. The bulk viscosity of liquid helium was calculated by Khalatnikov [22]. As in the case of shear viscosity the main contribution comes from phonons and rotons. Khalatnikov finds that ζ_2 is about an order of magnitude bigger than η. The other two bulk viscosities, ζ_1 and ζ_3, have different physical units, and cannot be directly compared to ζ_2. The linear combination that appears in the damping of second sound is $\alpha_\zeta = \zeta_2 + \rho^2\zeta_3 - 2\rho\zeta_1$. At normal density there are significant cancellations between these terms and $\zeta_2 \sim (\rho^2\zeta_3 - 2\rho\zeta_1)$. The bulk viscosity of helium vapor is small. Note that the bulk viscosity of most gases is dominated by internal excitations, like rotational and vibrational modes.

The bulk viscosity of a pion gas was computed by Chen and Wang [106]. They find that at low temperature bulk viscosity scales as $\zeta \sim T^7/f_\pi^4$ (up to logarithms). The bulk viscosity of the high temperature QGP phase was calculated by Arnold, Dogan, and Moore [103]. The result is

$$\zeta = \frac{A\alpha_s^2 T^3}{\log(\mu^*/m_D)}\,, \tag{135}$$

where $A = 0.443$ and $\mu^* = 7.14\,T$ in pure gauge QCD. In full QCD with $N_f = 3$ quark flavors $A = 0.657$ and $\mu^* = 7.77\,T$. We observe that ζ scales as $\alpha_s^4 \times \eta$. The trace anomaly $\epsilon - 3P$ is proportional to α_s^2, so bulk viscosity scales like the shear viscosity times the second power of the deviation from conformality. This is in agreement with an a simple formula proposed by Weinberg [107], $\zeta \sim (c_s^2 - \frac{1}{3})^2\eta$. However, Weinberg's relation is known to be violated in some theories, see [108] for an example.

3.6.2. Diffusion The diffusion of of impurities in liquid helium has been studied in some detail. Of particular interest is the behavior of dilute solutions of ^{3}He in ^{4}He. At low temperature the diffusion constant is determined by scattering off phonons and $D \sim 1/T^7$ [22, 109]. At high temperature diffusion is governed by scattering between

atoms and $D \sim T^{1+s}$ with $s = \frac{1}{2} + \frac{2}{\nu-1}$ for a $1/r^\nu$ potential [98]. We conclude that the temperature dependence of the diffusion constant is identical to that of the shear viscosity. The analogous problem for the unitary Fermi gas has not been studied, in part because of the lack of suitable impurities.

The diffusion constant for heavy quarks in a quark gluon plasma can be determined by computing the mean square momentum transfer per unit time, see Sec. 3.2. For approximately thermal heavy quarks the diffusion constant is dominated by heavy quark scattering on light quarks and gluons, $qQ \to qQ$ and $gQ \to gQ$. As in the case of shear viscosity the most important Feynman diagrams involve t-channel gluon exchanges. Since the heavy quark is slow the dominant interaction is electric gluon exchange and the cross section is regularized by Debye screening. The leading order result is [110, 111]

$$D = \frac{36\pi}{C_F g^4 T}\left[N_c\left(\log\left(\frac{2T}{m_D}\right)+c\right)+\frac{N_f}{2}\left(\log\left(\frac{4T}{m_D}\right)+c\right)\right]^{-1}, \tag{136}$$

where $C_F = (N_c^2-1)/(2N_c)$ and $c = 0.5-\gamma_E+\zeta'(2)/\zeta(2)$. The relaxation time η_D^{-1} scales as $M_Q/(T^2 g^4 \log(g)$, which is larger by a factor M_Q/T compared to the hydrodynamic relaxation time $\eta/(sT) \sim 1/(Tg^4\log(g))$. This is confirmed by numerical estimates, which give $\eta_D^{-1} \simeq 6.7/T \simeq 7$ fm for charm quarks at $T = 200$ MeV [111]. For comparison, the hydrodynamic relaxation time is $\eta/(sT) \simeq 1$ fm (for $\eta/s \simeq 1$).

3.6.3. Thermal conductivity Thermal conduction in superfluid helium is a complicated process. In a superfluid heat transport can take place by a process similar to internal convection where the superfluid moves relative to the normal fluid. As a consequence the heat flow observed in an experiment depends in part on the value of the shear viscosity. Also, the thermal conductivity of a weakly interacting phonon gas vanishes, and the dominant contribution comes from rotons or phonon-roton scattering [22]. The situation at high temperature is much simpler. Heat flow is a diffusive process, and the thermal conductivity is determined by scattering between atoms. The thermal conductivity scales as T^s where $s = \frac{1}{2} + \frac{2}{\nu-1}$, as in the case of shear viscosity. The ratio

$$Pr = \frac{\eta c_p}{\kappa} \tag{137}$$

of the shear and thermal diffusion constants is known as the Prandtl number. At large T the Prandtl number is a constant which in the case of helium is close to 2.5.

Most studies of the thermal conductivity of a quark gluon plasma have focused on the regime of very high baryon density. In the limit $\mu \gg T$, where μ is the quark chemical potential, the thermal conductivity scales as $\kappa \sim \mu^2/\alpha_s^2$ [112]. In the opposite limit $T \gg \mu$ there is an old relaxation time estimate $\kappa \sim T^4/(\alpha_s^2\mu^2)$ [7]. Note that while κ diverges as $\mu \to 0$, the dissipative contribution to the baryon current, equ. (79), is finite.

4. Holography

In kinetic theory conserved charges are carried by well defined quasi-particles. The time between collisions is long compared to the quantum mechanical scale, $\hbar/T$, and quantum mechanical interference between scattering events is not important. In the strong coupling limit quantum mechanical effects are large and quasi-particles lose their identity. A powerful new tool to study transport phenomena in this regime is the AdS/CFT correspondence [17, 113, 114, 115].

The AdS/CFT correspondence relates certain four dimensional gauge theories to higher dimensional string theories. The correspondence is simplest if the field theory is strongly coupled. In this limit the string theory reduces to a classical gravitational theory. The idea of a correspondence between field theories and higher dimensional gravity originated from developments within string theory, but there are precursors to the correspondence that come from the physics of black holes. It has been known for some time that black holes carry entropy, and that the entropy is proportional to the area, and not the volume of the black hole. It was also known that the evolution of black holes can be described by treating the event horizon as a physical membrane with well defined transport properties like electric conductivity and shear viscosity [116].

The best studied example of the AdS/CFT correspondence is the equivalence between $\mathcal{N} = 4$ Super Yang Mills theory (see Sect. 2.5) and type IIB supergravity on $\mathrm{AdS}_5 \times \mathrm{S}_5$. For our purposes the dynamics only involves AdS_5. This is a 5-dimensional space, which in AdS/CFT terminology is called the *bulk*. The dual field theory exists on the *boundary* of this space, which is 3+1 dimensional Minkowski space. The gauge gravity duality works as follows: Classical gravity equations of motion are solved in the $4 + 1$ dimensional curved geometry of AdS_5. Fluctuations of gravitational fields in the bulk induces charges on the $3 + 1$ dimensional boundary. The dynamics of $3 + 1$ dimensional boundary theory *is* the strongly coupled conformal field theory which we wish to study. Transport properties of the boundary theory can be determined by perturbing the boundary charges with an external field which then propagates into the bulk. The response of the induced charges to the applied field determines the transport coefficients. For each conserved charge of the field theory there is a corresponding field in the gravitational theory. The field corresponding to the stress tensor $T^{\mu\nu}$ is the graviton $h^{\mu\nu}$, and the field corresponding to the conserved R charge current J^μ_R is the five dimensional Maxwell field A^μ.

The AdS/CFT setup is analogous to a parallel plate capacitor. Electromagnetic fields in the bulk, the space between the plates, induce surface charges on the boundary. Fluctuations of the bulk field create fluctuations of the surface charges, and correlation functions of the surface charges can be related to normal modes of the bulk field. What is remarkable about the AdS/CFT correspondence is that the gravitational theory in the bulk defines a local field theory on the boundary, and that there are classical gravitational field configurations that correspond to field theories at finite temperature. These configurations can be used to study dissipative phenomena in the boundary field

theory.

The gravitational field configuration relevant to field theories at finite temperature is an AdS_5 black hole. In the black hole geometry the gravitational field is non zero as we approach the boundary of the $4+1$ dimensional space. This gravitational field is balanced by a non-zero stress tensor in the boundary field theory – the gravitational setup corresponds to the dynamics of a field theory with a non-zero density matrix. The event horizon of the back hole spans three spatial dimensions in the bulk and radiates at the Hawking temperature T_H. The black hole fills AdS_5 with a bath of gravitational radiation, and the temperature of the heat bath is identified with the temperature of the boundary field theory. The dynamics of graviton propagation in the black hole background determines stress tensor correlators at finite temperature in the boundary field theory. These correlators determine the shear viscosity according to Kubo formulas.

There is a vast amount of literature on the AdS/CFT correspondence. Here we will concentrate on a few selected issues that are relevant to this review. First, we will explain the calculation of the shear viscosity and the spectral weights of strongly coupled fluids. Then we will comment on the conjectured viscosity bound, and the calculation of other transport properties. Finally, we will review the derivation of higher order fluid dynamics using holography, and summarize some recent attempts to extend the correspondence to non-relativistic theories.

4.1. Shear viscosity and the stress tensor correlation function

The metric of $AdS_5 \times S_5$ is

$$ds^2 = \frac{r^2}{L^2}\left(-dt^2 + d\mathbf{x}^2\right) + \frac{L^2}{r^2}\,dr^2 + L^2 d\Omega_5^2\,. \tag{138}$$

The space is a direct product of a five dimensional sphere with metric $d\Omega_5^2$, and a five dimensional space with coordinates $(t, \mathbf{x}, r)$. The coordinate r is referred to as the "radial" AdS_5 coordinate. The limiting value $r \to \infty$ is the "boundary" of AdS_5. A fixed r slice of AdS_5 is a $3+1$ dimensional flat Minkowski space, but the five dimensional space is curved, with a constant negative curvature. L is the corresponding curvature radius. We require that L is large compared to the string length ℓ_s which guarantees the validity of the classical approximation. In the AdS/CFT correspondence L is related to the coupling constant of the $\mathcal{N}=4$ gauge theory, $\lambda \equiv g_{YM}^2 N_c$, through the relation $(L/\ell_s)^4 = \lambda$. The classical approximation to the gravitational theory is reliable if the field theory is strongly coupled. The classical fields can be expanded in S_5 spherical harmonics. At strong coupling higher harmonics are separated by a large gap, and we will ignore the S_5 from now on.

The metric of an AdS_5 black hole is

$$ds^2 = \frac{r^2}{L^2}\left(-f(r)dt^2 + d\mathbf{x}^2\right) + \frac{L^2}{f(r)r^2}\,dr^2\,, \tag{139}$$

where $f(r) = 1 - (r_0/r)^4$. The black hole horizon is a $3+1$ dimensional surface at $r = r_0$. The horizon radius is related to the Hawking temperature of the black hole by

$r_0\,\hbar/L^2 = \pi T_H$. This formula is an example of a general radius-energy relation in the AdS/CFT correspondence. A modification of the AdS geometry at radius r corresponds to a modification of the field theory at an energy scale $r\hbar/L^2$. It is convenient to perform a change variables $u \equiv (r_0/r)^2$ and write the metric as

$$ds^2 = \frac{(\pi TL)^2}{u}\left(-f(u)dt^2 + d\mathbf{x}^2\right) + \frac{L^2}{4u^2 f(u)}du^2\,, \tag{140}$$

where $f(u) = 1 - u^2$. Now the horizon is at $u = 1$. The boundary limit is found by evaluating all quantities at $u = \epsilon$ and then taking the boundary limit $\epsilon \to 0$.

As discussed above, the modified metric means that there is an induced stress at the boundary, $u = \epsilon$. The boundary metric $g_{\mu\nu}$ is related to the metric of the five dimensional theory $G_{\mu\nu}$ by the AdS scale factor

$$g_{\mu\nu} \equiv \frac{u}{(\pi TL)^2}\,G_{\mu\nu}\,. \tag{141}$$

Here and below Greek letters denote four dimensional indices $(x^\mu) = (t, x, y, z)$ while roman letters denote five dimensional indices $(x^M) = (x^\mu, u)$. Near the boundary the metric can be written

$$g_{\mu\nu} = g^o_{\mu\nu} + u^2\mathcal{B}_{\mu\nu} + O(u^4)\,, \tag{142}$$

where $g^o_{\mu\nu}$ is interpreted as the metric of $\mathcal{N} = 4$ gauge theory. Usually $g^o_{\mu\nu}$ is simply $\eta_{\mu\nu}$. The coefficient of u^2 ultimately determines the induced stress tensor in the boundary theory.

Specifically the induced stress is found by varying the action with respect to the boundary metric. This paragraph will focus on the mechanics of this process and the subsequent paragraph will discuss its physical interpretation. The induced stress is

$$\langle T_{\mu\nu}\rangle = \lim_{\epsilon\to 0}\frac{-2}{\sqrt{-g}}\frac{\delta S}{\delta g^{\mu\nu}}\bigg|_{u=\epsilon}\,, \tag{143}$$

where $\sqrt{-g} = (-\det g_{\mu\nu})^{1/2}$. The action is a sum of the Einstein-Hilbert action, the Gibbons-Hawking boundary term, and counter terms which are needed to render the action finite in the limit $u \to 0$,

$$S \equiv S_{EH} + S_{GH} + S_{CT}\,. \tag{144}$$

The Einstein-Hilbert action is

$$S_{EH} = \frac{1}{2\kappa_5^2}\int_{\mathcal{M}} d^5x\,\sqrt{-g}\,(\mathcal{R} + 2\Lambda)\,, \tag{145}$$

where $\mathcal{R}$ is the Ricci scalar and $\Lambda = 6/L^2$ is the cosmological constant. The five dimensional Newton constant $1/\kappa_5^2$ is related to the number of colors in the field theory, $1/\kappa_5^2 = N_c^2/(4\pi^2L^3)$. The Gibbons-Hawking-York [117, 118] boundary action is

$$S_{GH} = \frac{1}{2\kappa_5^2}\int_{\partial\mathcal{M}} d^4x\sqrt{-\gamma}\,2K\,, \tag{146}$$

where we have defined the boundary metric

$$\gamma_{\mu\nu} = G_{\mu\nu}|_{u=\epsilon}\,, \tag{147}$$

and K is the trace of the extrinsic curvature §. The boundary term guarantees that the variation of the action with respect to the 5-dimensional metric gives the Einstein equations in the bulk provided the variation vanishes on the boundary. Without the boundary action one also has to require that derivatives of the variation vanish on the boundary, see [119]. Finally, the counter term

$$S_{CT} = -\frac{6}{L}\int_{\partial\mathcal{M}} d^4x\sqrt{\gamma}\,, \tag{148}$$

is needed to render the action finite in the limit $u \to 0$. Notice that the counter term is independent of temperature. With these definitions, the variation relates the stress tensor to the extrinsic curvature

$$\langle T_{\mu\nu}\rangle = -\frac{1}{\kappa_5^2}\lim_{u\to 0}\frac{(\pi TL)^2}{u}\left[K_{\mu\nu} - K\gamma_{\mu\nu} + \frac{3}{L}\gamma_{\mu\nu}\right]. \tag{149}$$

Substituting the black hole metric equ. (140) and using the definition of the extrinsic curvature we have

$$\langle T_{\mu\nu}\rangle = \mathrm{diag}(\epsilon, p, p, p)\,, \qquad \frac{\epsilon}{3} = p = \frac{N_c^2}{8\pi^2}(\pi T)^4\,. \tag{150}$$

The pressure is three quarters of the Stefan Boltzmann value.

One may compare equ. (149) with the induced charge density on a capacitor plate. For instance if the plate spans the x, y plane, the surface charge density is related to the jump of electric field across the plate

$$\sigma = \left[E^z\right], \tag{151}$$

where $[E^z] = E^z_+ - E^z_-$ notates the jump. The analogous formulas in the gravitational theory are known as junction conditions [120]. Integrating the Einstein equations across a Gaussian pill box relates the surface stress $\tau^\mu{}_\nu$ to the jump in extrinsic curvature

$$\tau^\mu{}_\nu = -\frac{1}{\kappa_5^2}\left[K^\mu{}_\nu - K\delta^\mu{}_\nu\right]. \tag{152}$$

Thus the particular combination of extrinsic curvature plays an analogous role to the normal electric field, i.e. a combination of $-K_{\mu\nu} = n_u\Gamma^u_{\mu\nu}$ is the analogue of $\mathbf{n}\cdot\mathbf{E}$. If we have a semi-infinite metal block with surface charge density σ, then the outgoing electric field is related to the surface charge $E^z = \sigma$. By analogy, we associate the outgoing flux of extrinsic curvature at $u = \epsilon$ with the stress tensor in the gauge theory

$$\sqrt{-g}T^\mu{}_\nu = -\frac{1}{\kappa_5^2}\sqrt{\gamma}\left(K^\mu{}_\nu - K\delta^\mu{}_\nu\right). \tag{153}$$

Then taking the boundary limit $u \to 0$, we tentatively define the stress

$$T^\mu{}_\nu = -\frac{1}{\kappa_5^2}\lim_{u\to 0}\frac{(\pi TL)^4}{u^2}\left(K^\mu{}_\nu - K\delta^\mu{}_\nu\right). \tag{154}$$

§ More explicitly, $K = G^{\mu\nu}\nabla_\mu n_\nu$ with n^M an outward directed normal to the boundary of the AdS space, $n^M = -\sqrt{G^{55}}\delta^{5M}$. Note that $K_{\mu\nu} = \nabla_\mu n_\nu = -n_u\Gamma^u_{\mu\nu} = n^u\partial_u G_{\mu\nu}$.

Substituting the black hole AdS metric into this expression gives a divergent result. Nevertheless, the difference between this stress and the stress determined with the vacuum AdS metric equ. (138) is finite

$$\left\langle T^{\mu}{}_{\nu} \right\rangle - \left\langle T^{\mu}{}_{\nu} \right\rangle_{\rm vacuum} = -\frac{1}{\kappa_5^2} \lim_{u\to 0} \frac{(\pi T L)^4}{u^2} \left(K^{\mu}{}_{\nu} - K\delta^{\mu}{}_{\nu} + \frac{3}{L}\delta^{\mu}{}_{\nu} \right) . \qquad (155)$$

This equation is the same as derived previously in equ. (149).

So far we have computed a one point function of the conformal field theory, $\langle T^{\mu\nu}(\mathbf{x},t)\rangle$. To determine a retarded two point function, we follow the framework of linear response. Momentarily ignore the fifth dimension and consider turning on a time varying gravitational field $h^o_{xy}(\omega)$ in the usual four dimensional field theory. This time varying gravitational field induces a deviation from the equilibrium stress tensor in the same way that a time varying electric field induces a net current. According to linear response, the expectation value of the tress energy tensor is

$$\langle T_{xy}(\omega)\rangle_{h^o_{xy}} = T^{\rm eq}_{xy}(\omega) + G_R(\omega)\, h^o_{xy}(\omega)\,, \qquad (156)$$

where $T^{\rm eq}_{xy} = (\epsilon + p)u_x u_y + p g_{xy} = p h^o_{xy}(\omega)$ is the equilibrium stress tensor, and $G_R(\omega)$ is the equilibrium retarded correlator defined in equ. (97). The Kubo formula for the shear viscosity, equ. (98), dictates the functional form of this correlator in the small frequency limit, $G_R(\omega) = -i\omega\eta$. Thus the average stress tensor in the presence a time varying gravitational field is

$$\langle T_{xy}(\omega)\rangle_{h^o_{xy}} = p h^o_{xy} - i\omega\eta\, h^o_{xy}(\omega)\,. \qquad (157)$$

Now consider the small fluctuations of the metric field $H_{xy}(\omega,u)$ around the black hole metric equ. (140) of the five dimensional theory. The equation of motion for the gravitational fluctuation is found by linearizing the Einstein equations

$$\mathcal{R}_{MN} - \frac{1}{2} G_{MN} \left(\mathcal{R} + 2\Lambda\right) = 0\,. \qquad (158)$$

After a modest amount of algebra, the $\mathcal{R}_{xy}$ equation becomes an equation for $h_{xy} \equiv uH_{xy}(\omega,u)/(\pi T L)^2$

$$h''_{xy}(\omega,u) - \frac{1+u^2}{uf} h'_{xy}(\omega,u) + \frac{\omega^2}{(2\pi T)^2 u f^2} h_{xy}(\omega,u) = 0\,, \qquad (159)$$

where the primes denote derivatives with respect to u. This is a second order linear differential equation with regular singular points in the physical domain at the horizon $u = 1$ and the boundary $u = 0$. Solving equ. (159) near the black hole horizon $u = 1$, we determine that the graviton is a linear combination of two solutions, $h_{xy}(\omega,u) \sim (1-u)^{\mp i\omega/4\pi T}$. These solutions describe the gravitational wave propagating into $(-)$ and out of $(+)$ the black hole, respectively. The infalling solution is the physically relevant retarded solution. Near the boundary $u \to 0$ (or $r \to \infty$) the gravitational field is also a linear combination of two solutions

$$h_{xy}(\omega,u) = h^o_{xy}(\omega)\,(1 + \ldots) + \mathcal{B}(\omega)\, u^2\,(1 + \ldots)\,, \qquad (160)$$

where $\ldots$ denotes terms that vanish as $u \to 0$. The two modes are called the non-normalizable mode and the normalizable mode. The non-normalizable mode is constant

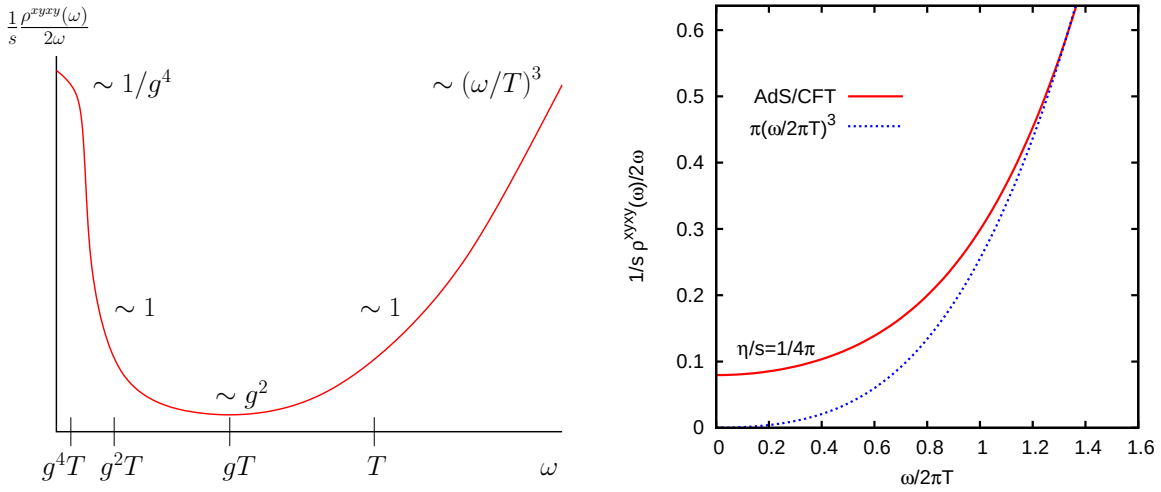

Figure 5. Spectral function $\rho^{xyxy}(\omega, \mathbf{k}=0)$ associated with the correlation function of the xy component of the energy momentum tensor. The spectral function is normalized to entropy density s. Left panel (Fig. (a)): Schematic picture of the spectral density in weak coupling QCD or SUSY Yang Mills theory [121, 122]. Right panel (Fig. (b)): Spectral density in strong coupling SUSY Yang-Mills theory calculated using the AdS/CFT correspondence, from [123].

as $r \to \infty$ while the normalizable mode falls as $1/r^4$. Inserting the metric perturbation equ. (160) into equ. (149) the average stress tensor is

$$\langle T_{xy}(\omega)\rangle = p\, h^o_{xy}(\omega) + (\epsilon + p)\, \mathcal{B}(\omega)\,, \tag{161}$$

with the previously defined energy density and pressure, equ. (150). We observe that the coefficient of the non-normalizable mode, h^o_{xy}, can be interpreted as the external gravitational field applied to the gauge theory, while the coefficient of the normalizable mode, $\mathcal{B}(\omega)$ is proportional to the induced stress tensor in the boundary theory.

For an arbitrary value of $\mathcal{B}(\omega)$ the general linear combination of solutions near the boundary would approach a linear combination of the infalling and outgoing solutions near the horizon. Thus the coefficient $\mathcal{B}(\omega)$ should be adjusted so that only the infalling solution $(1-u^2)^{-i\omega/4\pi T}$ is present near $u=1$. In general the required $\mathcal{B}(\omega)$ has to be determined numerically. For small ω however, a straightforward calculation shows that to linear order in ω the solution which is infalling at the horizon is

$$h_{xy} = h^o_{xy}(\omega)\,(1-u)^{-i\omega/4\pi T}\left[1 - \frac{i\omega}{4\pi T}\log(1+u) + O(\omega^2)\right]. \tag{162}$$

Expanding this functional form near the boundary we find $\mathcal{B}(\omega) = -i\omega/(4\pi T)$. Then using $\epsilon + p = sT$ and comparing the functional forms in equ. (157) and equ. (161) we conclude that $\langle T_{xy}(\omega)\rangle = p h^o_{xy} - i\omega\eta h^o_{xy}$ with

$$\frac{\eta}{s} = \frac{1}{4\pi}\,. \tag{163}$$

Remarkably, the strong coupling limit of the shear viscosity is small and independent of the coupling. The difference as compared to the weak coupling result becomes even

clearer if one considers the spectral function. As described in Sect. 3.4 the Kubo formula relates the shear viscosity to the zero energy limit of the stress-energy spectral function. In weak coupling QCD the spectral function has a narrow peak near zero energy which reflects the fact that momentum transport is due to quasi-particles that are almost on-shell. The height of the transport peak is governed by the kinetic theory result for the shear viscosity, and the width can be reconstructed from the f-sum rule

$$T\int_0^\Lambda \frac{d\omega}{\omega}\rho^{xyxy}(\omega) = \frac{T(\epsilon+P)}{5}\,, \tag{164}$$

where $g^4T \ll \Lambda \ll g^2T$. Since the height of the transport peak is $1/(g^4T)$, the width must be g^4T. The high energy part of the spectral density can be computed from the one-loop correlation function. The result is $\rho(\omega) \sim \omega^4$. A schematic picture of the spectral function is shown in Fig. 5(a).

In the strong coupling limit the width of the transport peak becomes bigger, and the height becomes smaller. In $\mathcal{N} = 4$ SUSY Yang Mills the infinite coupling limit can be determined as outlined above [123, 124]. Specifically, the spectral function may be found by determining $G_R(\omega)$ from the numerical coefficient $\mathcal{B}(\omega)$. The result is shown in Fig. 5(b). Clearly, the transport peak has completely disappeared, and there is no possibility of a quasi-particle interpretation of momentum transport. Whether the spectral function of the quark gluon plasma near T_c looks more like Fig. 5(a) or (b) will have to be settled by numerical calculations on the lattice, see Sect. 3.4. It is interesting to note that numerical calculations of the shear viscosity, which require the determination of the intercept of $\rho(\omega)/\omega$, are easier in the case of the strong coupling.

4.2. The KSS bound

The calculation of the shear viscosity has been extended to other strongly coupled field theories with gravitational duals. It was discovered that within a large class of theories the strong coupling limit of η depends on the theory, but the ratio η/s does not. This observation can be understood using Kubo's formula and the optical theorem. The optical theorem implies that the imaginary part of a correlation function can be related to the total cross section. As a consequence, the shear viscosity can be expressed in terms of the total graviton absorption cross section [16],

$$\eta = \frac{\sigma_{\rm abs}(0)}{2\kappa_5^2}\,. \tag{165}$$

The low energy limit of $\sigma_{\rm abs}$ is equal to the area A of the event horizon, and the entropy density is given by the Hawking-Bekenstein formula, $s = A/(4G)$ where $G = \kappa_5^2/(8\pi)$. The ratio η/s is independent of A and κ_5. More formal arguments for the universality of η/s in the strong coupling limit of field theories with holographic duals were given in [125, 25, 126]. Corrections to the infinite coupling limit of $\mathcal{N} = 4$ SUSY Yang Mills theory were studied in [18]. Buchel et al. find

$$\frac{\eta}{s} = \frac{1}{4\pi}\left\{1 + \frac{135\zeta(3)}{2(2\lambda)^{3/2}} + \ldots\right\}\,. \tag{166}$$

The first correction is positive, as one would expect from the fact that $\eta/s \to \infty$ as $\lambda \to 0$. Based on these observations, Kovtun, Son, and Starinets (KSS) conjectured that

$$\frac{\eta}{s} \geq \frac{1}{4\pi} \tag{167}$$

is a universal bound that applies to all fluids [19]. There is no proof of this conjecture, and a number of authors have attempted to construct counter examples. One possibility is a weakly interacting non-relativistic fluid with an exponentially large number of species or internal degrees of freedom, and therefore a very large entropy [19, 127, 128]. These systems are unusual because the time scale for thermal equilibration vastly exceeds the time scale for momentum equilibration, and because the fluid is not stable on very long time scales [129]. More recently, it was realized that theories with holographic duals described by higher derivative gravity may violate the KSS bound [130, 131, 132, 133]. An explicit example was constructed by Kats and Petrov [132]. They showed that in $\mathcal{N} = 2$ SUSY $Sp(N_c)$ gauge theory with a certain combination of matter fields

$$\frac{\eta}{s} = \frac{1}{4\pi}\left(1 - \frac{1}{2N_c}\right), \tag{168}$$

up to corrections of $O(\lambda^{-3/2})$. For $\lambda^{3/2} \gg N_c \gg \lambda \gg 1$ we find a violation of the KSS bound in a controlled calculation. However, there are bounds on the coefficients of higher derivative terms, and a modified bound on η/s may yet exist [133].

4.3. Other transport properties

There has been a large amount of work on applications of the AdS/CFT correspondence to transport properties other than the shear viscosity. Here we briefly summarize some results relevant to this review. $\mathcal{N} = 4$ SUSY Yang Mills theory has a conserved R-charge (see Sect. 2.5), and we can study transport in the presence of a finite R-charge density. Son and Starinets find that the shear viscosity and entropy density depend on the density, but the ratio η/s does not [134]. They also determine the thermal conductivity

$$\kappa = \frac{8\pi^2 T}{\mu^2}\,\eta\,, \tag{169}$$

as well as the R-charge diffusion constant. The heavy quark diffusion constant was calculated in [135, 136, 137]. The result is

$$D = \frac{2}{\pi T}\frac{1}{\sqrt{\lambda}}, \tag{170}$$

which depends on the value of the coupling λ, and goes to zero in the strong coupling limit. The functional dependence on λ is unusual from the point of view of perturbation theory, but typical of other AdS/CFT results. We also note that in the strong coupling limit the ratio of the heavy quark diffusion coefficient to the kinematic viscosity $\eta/(sT)$ goes to zero, whereas this ratio is independent of the coupling in the perturbative limit

The bulk viscosity of $\mathcal{N} = 4$ SUSY Yang Mills theory vanishes, but non-conformal deformations of the original AdS/CFT correspondence have been studied. Buchel proposed that in holographic models there is a lower bound on the bulk viscosity, $\zeta \geq 2(\frac{1}{3} - c_s^2)\eta$, where c_s is the speed of sound [138]. Note that the weak coupling formula involves the square of $(\frac{1}{3} - c_s^2)$. Gubser et al. considered a number of model geometries tuned to reproduce the QCD equation of state, and find that ζ/s has a maximum near the critical temperature where $\zeta/s \simeq 0.05$ [139]. Larger values of ζ/s near T_c have been suggested based on lattice data for the QCD trace anomaly [140].

4.4. Hydrodynamics and holography

Up to this point we have used the AdS/CFT correspondence to calculate the transport coefficients that appear in first order hydrodynamics. However, AdS/CFT can be used to compute the full correlation function, and not just the hydrodynamic limit. An example is the spectral function shown in Fig. 5, and similar calculations have been performed in other channels as well. In this section we wish to discuss how the stress tensor of the fluid relaxes to the Navier-Stokes form. This process can be described by the second order terms introduced in Sect. 3.1.3. We will follow the method outlined in [67].

A static fluid at temperature T corresponds to a black hole with a Hawking temperature $T_H = r_0/(\pi L^2)$. First we switch to Eddington Finkelstein coordinates, defining $v = t + \int^r dr\, L^2/fr^2$. Then the metric is regular at the event horizon of the black hole,

$$ds^2 = 2\, dv\, dr + \frac{r^2}{L^2}\left[-f(r)dv^2 + r^2 d\mathbf{x}^2\right] . \tag{171}$$

Introducing four dimensional coordinates $x^\mu = (x^0, x^1, x^2, x^3) = (v, \mathbf{x})$, a vector $u^\mu = (1, \mathbf{0})$ characterizing the local rest frame, and a scale parameter b characterizing the temperature the metric becomes

$$ds^2 = -2u_\mu dx^\mu dr + \frac{r^2}{L^2}\left[-f(br)u_\mu u_\nu dx^\mu dx^\nu + r^2 P_{\mu\nu} dx^\mu dx^\nu\right] , \tag{172}$$

where $P_{\mu\nu} = u_\mu u_\nu + \eta_{\mu\nu}$. The basic idea is to promote the variables u^μ and b to slowly varying functions of x^μ. The metric is then

$$\begin{aligned} ds^2 = & -2u_\mu(x)dx^\mu dr \\ & + \frac{r^2}{L^2}\left[-f(b(x)r)u_\mu(x)u_\nu(x)dx^\mu dx^\nu + r^2 P_{\mu\nu}(x)dx^\mu dx^\nu\right] \\ & + \text{ corrections due to gradients} . \end{aligned} \tag{173}$$

Variations in u_μ and b correspond to fluctuations in the local fluid velocity and temperature. Substituting this form into the Einstein equations, the corrections to the metric are determined order by order in the gradients of $u^\mu(x)$ and $b(x)$. These metric corrections lead to deviations of the boundary stress tensor from an ideal fluid of precisely the form required by hydrodynamics. Up to second order we can write

$$T^{\mu\nu} = T_0^{\mu\nu} + \delta^{(1)}T^{\mu\nu} + \delta^{(2)}T^{\mu\nu} + \dots , \tag{174}$$

and each term has physical significance. At zeroth order

$$T_0^{\mu\nu} = \frac{N_c^2}{8\pi^2}(\pi T)^4 \left(\eta^{\mu\nu} + 4u^\mu u^\nu\right) , \tag{175}$$

which shows that $\epsilon = 3P$ and that the pressure is 3/4 of the Stefan Boltzmann value. At first order

$$\delta^{(1)}T^{\mu\nu} = -\frac{N_c^2}{8\pi^2}(\pi T)^3\sigma^{\mu\nu} , \tag{176}$$

where $\sigma^{\mu\nu}$ is defined as in equ. (78). This results shows that $\eta = N_c^2\pi T^3/8$. Combined with the zeroth order stress tensor we find $\eta/s = 1/4\pi$, in agreement with previous results. Finally, at second order

$$\begin{aligned}\delta^{(2)}T^{\mu\nu} = \eta\tau_{II}\left[{}^{\langle}D\sigma^{\mu\nu\rangle} + \frac{1}{3}\sigma^{\mu\nu}(\partial\cdot u)\right] \\ + \lambda_1\sigma^{\langle\mu}{}_\lambda\sigma^{\nu\rangle\lambda} + \lambda_2\sigma^{\langle\mu}{}_\lambda\Omega^{\nu\rangle\lambda} + \lambda_3\Omega^{\langle\mu}{}_\lambda\Omega^{\nu\rangle\lambda} ,\end{aligned} \tag{177}$$

where $D = u\cdot\partial$, and the vorticity $\Omega_{\mu\nu}$ as well as the transverse traceless tensor $A^{\langle\mu\nu\rangle}$ are defined in Sect. 3.1.3. The form of $T^{\mu\nu}_{(2)}$ agrees with the general second order result for a conformal relativistic fluid derived in [65]. The second order coefficients are

$$\tau_\Pi = \frac{2-\ln 2}{\pi T} , \qquad \lambda_1 = \frac{2\eta}{\pi T} , \qquad \lambda_2 = \frac{2\eta\ln 2}{\pi T} , \qquad \lambda_3 = 0 . \tag{178}$$

We observe that the relaxation times are of order $(\pi T)^{-1}$, the shortest time scale characterizing the plasma.

4.5. Non-relativistic AdS/CFT correspondence

Given the role that the AdS/CFT correspondence has played in improving our understanding of conformal relativistic fluids it is natural to ask whether the correspondence can be extended to non-relativistic scale invariant fluids like the dilute Fermi gas at unitarity. The symmetry group of a non-relativistic conformal field theory in d spatial dimensions is known as the Schrödinger group $Sch(d)$, the symmetry group of the free Schrödinger equation. There has recently been significant progress in constructing holographic duals for non-relativistic field theories [141, 142, 143, 144].

The basic idea proposed in [141, 142] can be explained by looking at the metric of $d+2$ dimensional flat space

$$ds^2 = \eta_{\mu\nu}dx^\mu dx^\nu = -2dx^+dx^- + dx^i dx^i , \tag{179}$$

where we have introduced light cone coordinates (x^+, x^-, x^i) with $i = 1, \ldots, d$. Consider the evolution of a system with fixed light cone momentum P^- in light cone time x^+. In this case only the d dimensional Galilean subgroup of the Lorentz group is manifest. In the AdS/CFT correspondence the conformal symmetry of a $d+1$ dimensional field theory is realized by the isometries of the metric on AdS_{d+2}. The proposal is that the $Schr(d)$ symmetry of a non-relativistic $d+1$ dimensional conformal field theory can be mapped onto the isometries of the $d+3$ dimensional metric

$$ds^2 = r^2\left(-2dx^+dx^- - \beta^2r^2(dx^+)^2 + (dx^i)^2\right) + \frac{dr^2}{r^2}, \tag{180}$$

which reduces to the metric of AdS_{d+3} for $\beta \to 0$. This metric can be realized in string theory by starting from $AdS_5 \times \mathcal{X}_5$ (where $\mathcal{X}_5$ is an Einstein-Sasaki manifold) and applying a solution generating transformation (for example the "Null Melvin Twist" or the "TsT" transformation) [143, 144, 145]. The resulting field theory is a $2+1$ dimensional field theory with infinitely many bosonic and fermionic fields, and an unusual equation of state $P \sim T^4/\mu^2$ [145]. This is still quite far from the $3+1$ unitary Fermi gas, but the theory provides an explicit realization of a non-relativistic fluid which satisfies $\eta/s = 1/(4\pi)$.

The hydrodynamics of a holographic fluid with Schrödinger symmetry was studied in more detail in [146]. An interesting observation that was made in this paper is that the light cone reduction of a viscous relativistic stress tensor automatically leads to a $\vec{\nabla}T$ term in the non-relativistic energy current. The thermal conductivity is completely fixed by the shear viscosity and the equation of state,

$$\kappa = 2\eta \frac{\epsilon + P}{\rho T} \,. \tag{181}$$

This result can be expressed in terms of the Prandtl number $Pr = c_p \eta/\kappa$, see equ. (137). Using the equation of state of a non-relativistic conformal fluid we find $Pr = 1$. The Prandtl number of many gases is indeed close to one, see Sect. 3.6.3, but at strong coupling there is no obvious reason for $Pr = 1$ to hold.

5. Experimental determination of transport properties

In this section we will review experimental determinations of transport properties of liquid Helium, cold atomic gases, and the quark gluon plasma. We will focus on shear viscosity, since it is the main focus of this review, and since it is the only transport property for which good data is available for all three systems.

Liquid helium can be produced in bulk, and transport properties can be measured using methods that were developed for classical fluids. Cold atomic gases are produced in optical or magneto-optical traps. These traps typically contain $10^5 - 10^6$ atoms. Hydrodynamic behavior is observed when the trapping potential is modified, or if the local density or energy density is modified using laser beams. The quark gluon plasma can only be created for brief periods in collisions of ultra-relativistic heavy ions. The system typically contains on the order of $10^3 - 10^4$ quarks and gluons, and lasts for about 10 fm/c ($3 \cdot 10^{-23}$ sec). Hydrodynamic behavior may take place during the expansion of the system and is reflected in the momentum spectra of particles in the final state.

5.1. Liquid helium

There are a number of techniques for measuring the viscosity of fluids. Three popular instruments are:

(i) Capillary viscometers are based on Poiseuille flow. Poiseuille's formula states that the flow through a pipe is inversely proportional to the shear viscosity, and

proportional to the pressure drop as well as the fourth power of the diameter.

(ii) Rotation viscometers measure the torque on a rotating cylinder or disk. The torque per unit length exerted by a pair of coaxial infinitely long cylinders is proportional to the shear viscosity and the difference between the angular velocities, and proportional to the ratio $R_1 R_2/(R_1^2 - R_2^2)$, where $R_{1,2}$ are the two radii.

(iii) Vibration viscometers determine the damping of an oscillating sphere or plate. These devices have many advantages but the data are more difficult to interpret, because the damping depends not only on the viscosity, but also on the density of the fluid.

Initial measurements of the viscosity of superfluid liquid Helium lead to an apparent contradiction between the results obtained using different methods. Capillary flow viscometers indicated vanishing viscosity below T_c [147], oscillatory viscometers showed a drop of the shear viscosity [148], and experiments with rotation viscometers yielded a rise in viscosity below T_c [149]. The contradictions can be resolved using superfluid hydrodynamics. The flow through a narrow capillary is entirely a superflow, and not sensitive to viscosity. Oscillation viscometers measure the product of viscosity and normal density, which drops with temperature. Modern measurements confirm the rise of viscosity below T_c which is predicted by the phonon-roton theory. The minimum viscosity of Helium at normal pressure occurs just below the λ point where $\eta \simeq 1.2 \cdot 10^{-5}$ Poise. The minimum of η/s occurs at higher temperature, close to the liquid gas phase transition. Recent measurements confirm the (weak) divergence of the shear viscosity at the critical endpoint of the liquid gas phase transition predicted by dynamical universality [150]. Experiments also find the expected (much stronger) divergence of the heat conductivity near the lambda point [35].

Once the shear viscosity and the heat conductivity are determined sound attenuation experiments can be used to measure the bulk viscosity (ζ_2 in the superfluid phase) [151]. Below the λ point $\zeta_2 \simeq 10^{-4}$ Poise. Damping of second sound determines a linear combination of ζ_1 and ζ_3 in the superfluid phase [152], but the remaining linear combination is poorly constrained.

5.2. Cold atomic gases

Dilute Bose or Fermi gases are studied using optical traps that provide an approximately harmonic confinement potential

$$V = \frac{m}{2} \sum_i \omega_i^2 r_i^2. \tag{182}$$

The equilibrium density n_0 can be determined from the equation of hydrostatic equilibrium, $\boldsymbol{\nabla} P_0 = -n_0 \boldsymbol{\nabla} V$. This equation is equivalent to the well known Thomas-Fermi approximation. For dilute fermions at unitarity the equation of state at zero temperature is given by equ. (27) and

$$n_0(\mathbf{r}\,) = n_0(0) \left(1 - \sum_i \frac{r_i^2}{R_i^2}\right)^{1/\gamma}, \qquad R_i^2 = \frac{2\mu}{m\omega_i^2}, \tag{183}$$

where μ is the chemical potential and $\gamma = 2/3$. The chemical potential is related to the Fermi energy by the universal parameter ξ introduced in equ. (23). Transport properties of strongly interacting dilute Fermi gases can be extracted from a variety of experiments, free expansion from a deformed trap (elliptic flow) [153], damping of collective oscillations [154, 155, 41, 156, 157], sound propagation [158], and expansion out of rotating traps [159]. In the following we shall concentrate on damping of collective oscillations, as these experiments have been most carefully analyzed [160, 161, 162, 163].

We consider small oscillations around the equilibrium density, $n = n_0 + \delta n$. Since the damping is small, the motion is approximately described by ideal hydrodynamics. The compressibility at constant entropy is

$$\left(\frac{\partial P}{\partial n}\right)_S = (\gamma+1)\frac{P}{n}\ . \tag{184}$$

From the linearized continuity and Euler equation we get [164]

$$m\frac{\partial^2 \mathbf{v}}{\partial t^2} = -\gamma\left(\boldsymbol{\nabla}\cdot\mathbf{v}\right)\left(\boldsymbol{\nabla}V\right) - \boldsymbol{\nabla}\left(\mathbf{v}\cdot\boldsymbol{\nabla}V\right), \tag{185}$$

where we have dropped terms of the form $\nabla_i\nabla_j\mathbf{v}$ that involve higher derivatives of the velocity. This equation has simple scaling solutions of the form $v_i = a_i x_i \exp(i\omega t)$ (no sum over i). Inserting this ansatz into equ. (185) we get an equation that determines the eigenfrequencies ω. The experiments are performed using a trapping potential with axial symmetry, $\omega_1 = \omega_2 = \omega_0$, $\omega_3 = \lambda\omega_0$. In this case we find one solution with $\omega^2 = 2\omega_0^2$ and two solutions with [164, 165, 166]

$$\omega^2 = \omega_0^2\Bigg\{\gamma+1+\frac{\gamma+2}{2}\lambda^2 \pm \sqrt{\frac{(\gamma+2)^2}{4}\lambda^4 + (\gamma^2-3\gamma-2)\lambda^2 + (\gamma+1)^2}\Bigg\}. \tag{186}$$

In the limit of a very asymmetric trap ($\lambda \to 0$) the eigenfrequencies are $\omega^2 = 2\omega_0^2$ and $\omega^2 = (10/3)\omega_0^2$. The mode $\omega^2 = (10/3)\omega_0^2$ is a radial breathing mode with $\mathbf{a} = (a, a, 0)$ and the mode $\omega^2 = 2\omega_0^2$ corresponds to a radial quadrupole $\mathbf{a} = (a, -a, 0)$.

The prediction of ideal hydrodynamics for the frequency of the radial breathing mode agrees very well with experimental results [154]. Damping of collective modes is due to viscous effects. The dissipated energy is given by

$$\dot{E} = -\int d^3x\left\{\frac{\eta(x)}{2}\left(\nabla_i v_j + \nabla_j v_i - \frac{2}{3}\delta_{ij}\boldsymbol{\nabla}\cdot\mathbf{v}\right)^2 + \zeta(x)\left(\boldsymbol{\nabla}\cdot\mathbf{v}\right)^2 + \frac{\kappa(x)}{T}(\boldsymbol{\nabla}T)^2\right\}, \tag{187}$$

where $\eta(x), \zeta(x)$ and $\kappa(x)$ are the local shear viscosity, bulk viscosity, and thermal conductivity. In the unitarity limit the system is scale invariant and the bulk viscosity in the normal phase vanishes. In the superfluid phase $\zeta_1 = \zeta_2 = 0$ and the contribution of ζ_3 vanishes if $\mathbf{v}_s = \mathbf{v}_n$. For isentropic oscillations $\delta T \sim (\delta n/n)T$. The solutions of

equ. (185) satisfy $\delta n(x) \sim n_0(x)$. This implies that there are no temperature gradients, and that thermal conductivity does not contribute to dissipation.

We conclude that damping is dominated by shear viscosity. The energy dissipated by the radial scaling solutions is

$$\overline{\dot{E}} = -\frac{2}{3}\left(a_x^2 + a_y^2 - a_x a_y\right) \int d^3x\, \eta(x), \tag{188}$$

where $\overline{E}$ is a time average. The damping rate is given by the ratio of the energy dissipated to the total energy of the collective mode. The kinetic energy is

$$E_{kin} = \frac{m}{2} \int d^3x\, n(x) \mathbf{v}^2 = \frac{mN}{2}\left(a_x^2 + a_y^2\right) \langle x^2 \rangle. \tag{189}$$

In the case of a harmonic trapping potential the average $\langle x^2 \rangle$ can be extracted using a Virial theorem, $E = 2N\langle V \rangle$ [167]. The damping rate is

$$-\frac{1}{2}\frac{\overline{\dot{E}}}{E} = \frac{2}{3}\frac{a_x^2 + a_y^2 - a_x a_y}{a_x^2 + a_y^2}\frac{\int d^3x\, \eta(x)}{mN\langle x^2 \rangle}, \tag{190}$$

where the factor 1/2 takes into account that the experiments measure an amplitude, not energy, damping rate. We note that the second factor on the RHS is 1/2 for the radial breathing mode and 3/2 for the radial quadrupole mode. This dependence provides an important check for the assumption that damping is dominated by shear viscosity. Also note that if the shear viscosity is proportional to the density or the entropy density then $\dot{E}/E$ scales as $N^{-1/3}$. Near the surface the density is small and $\eta(x)$ will approach the Boltzmann limit, which is independent of density, see equ. (127). This is a problem, because the total volume of the system is infinite (at non-zero temperature the density has an infinite range tail). This difficulty is related to the breakdown of hydrodynamics near the surface of the cloud. An elegant solution to the problem is to include a finite relaxation time $\tau_\eta(r) = \eta/(n(r)k_B T)$ which diverges in the low density limit [168].

In order to compare with the proposed viscosity bound we will assume that the shear viscosity is proportional to the entropy density, $\eta(x) = \alpha s(x)$. Note that in general α is a function of T/T_F and varies across the trap (T_F depends on density). This means that we will extract an average value of $\alpha = \eta/s$. We can write

$$\frac{\eta}{s} = \frac{3}{4}\xi^{1/2}(3N)^{1/3}\left(\frac{\bar{\omega}\Gamma}{\omega_\perp^2}\right)\left(\frac{E}{E_{T=0}}\right)\left(\frac{N}{S}\right), \tag{191}$$

where $\Gamma/\omega_\perp$ is the dimensionless damping rate, $\bar{\omega} = \omega_\perp^{2/3}\omega_z^{1/3}$ is mean trap frequency, (S/N) is the entropy per particle, and $E/E_{T=0}$ is the equilibrium energy of the cloud in units of the zero temperature value. Fig. 6 shows η/s extracted from the experimental results of the Duke group [156]. The entropy per particle was also taken from experiment [170]. Similar results are obtained if the entropy is extracted from quantum Monte Carlo data. We observe that η/s in the vicinity of the transition temperature is about 1/2. We also note that the extracted shear viscosity roughly agrees with the high temperature, Fermion quasi-particle, kinetic theory result. The low temperature, phonon dominated, result is not seen in the data, presumably because the phonon mean free path is bigger than the system size.

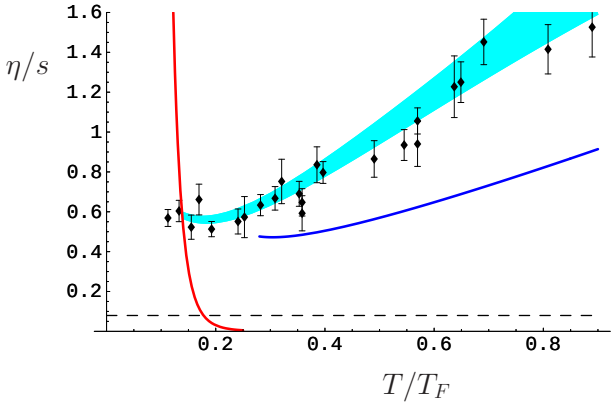

Figure 6. Viscosity to entropy density ratio of a cold atomic gas in the unitarity limit, from [162]. This data points are based on the damping data published in [156] and the thermodynamic data in [169, 170]. The light blue band is an estimate of the systematic uncertainty due to the breakdown of hydrodynamics near the surface of the cloud. The solid red and blue line show the low and high temperature limits of η/s, see equ. (121) and (127). The dashed line shows the conjectured viscosity bound $\eta/s = 1/(4\pi)$.

There are many caveats that one should keep in mind regarding this analysis. First, we assume that shear viscosity is the only source of dissipation. There is some evidence for this assumption from comparisons of the damping rate of different collective modes [171]. On the other hand, the dependence of the damping rate on particle number predicted by viscous hydrodynamics has never been demonstrated. Second, hydrodynamics can only be applied in a relatively narrow temperature regime $T < (2-3)T_c$. For higher temperatures the observed frequencies cross over from hydrodynamic behavior to a weakly collisional Boltzmann gas. This means that the kinetic theory prediction for the shear viscosity, equ. (127), is reliable but the frequency of the collective mode is too large for hydrodynamics to be applicable. Finally, there is an issue that is specific to the scaling flows ($v_i \sim a_{ij}x_j$) considered here. Since the velocity field is linear in the coordinates, the second derivative of the velocity vanishes. This means that the viscous term in the Navier Stokes equation, $\rho\dot{v}_i \sim \nabla_j[\eta(\nabla_i v_j + \ldots)]$, is only sensitive to the density dependent part of the viscosity. But for a dilute gas the viscosity is expected to be density independent, see equ. (127), so the dilute limit can not be verified using experiments that involve scaling flows.

There is clearly a need for additional experimental constraints. The first indication of almost ideal hydrodynamic behavior was the observation of elliptic flow by O'Hara et al. [153]. The experiment showed that if the trapping potential is removed the gas expands rapidly in the transverse direction while remaining nearly stationary in the axial. This is a consequence of the much larger pressure gradient in the short direction. The ideal hydrodynamics of this experiment was worked out in [172] but the effects of viscosity have not been carefully studied, in part because the data were taken at a single temperature. More recently Clancy et al. studied the expansion of a gas cloud

with an initial velocity field corresponding to a scissors mode [159]. This is an interesting system, because the initial velocity field is irrotational ($\nabla \times \mathbf{v} = 0$) but carries angular momentum. If the trapping potential is removed then the transverse size will grow initially, but if the gas remains irrotational then angular momentum conservation will force the transverse expansion to slow down (and the rotation to speed up) before the transverse and axial radii become equal [173]. This phenomenon was observed in the experiment, and an initial analysis leads to values of η/s close to $1/(4\pi)$ [174]. This result is very interesting, but some of the caveats mentioned above still apply.

5.3. The quark gluon plasma at RHIC

Cold quantum fluids can be studied in conditions that are very close to equilibrium. The quark gluon plasma, on the other hand, can only be created in relativistic heavy ion collisions. In these collisions the initial state is very far from equilibrium, and the system size is limited by the size of the heaviest stable nuclei. The applicability of hydrodynamics is not clear a priori. In this section we will summarize some of the evidence that has been obtained from experiments at the Relativistic Heavy Ion Collider (RHIC). These experiments indicate that local equilibration takes place, that nearly ideal fluid dynamics is applicable, and that the shear viscosity to entropy density ratio near T_c is within a factor of a few of the KSS bound.

The collision energy in Au+Au collisions at RHIC is 100 GeV per nucleon, and the nuclei are Lorentz contracted by a factor of $\gamma \simeq 100$. The transverse radius of a Au nucleus is approximately 6 fm and on the order of 7000 particles are produced overall. The motion of the particles is relativistic, and the duration of a heavy ion event is $\tau \sim 6$ fm. In order for hydrodynamics to be applicable this time has to be large compared to the equilibration time.

The main observables are the spectra dN/d^3p of produced particles. For momenta less than 2 GeV the spectra roughly follow Boltzmann distributions with a characteristic temperature close to the QCD critical temperature. The first hint that the system is behaving collectively is the existence of radial flow. Heavy particle spectra have apparent temperatures that are larger than the temperatures extracted from light particles. This can be understood if there is a collective transverse expansion velocity $v_\perp$ which boosts the observed transverse momenta by an amount $p_\perp \sim m v_\perp$.

More dramatic evidence for hydrodynamics is provided by the observation of elliptic flow in non-central heavy ion collisions. The centrality of the collision is characterized by the impact parameter b, the transverse separation of the two nuclei. The magnitude of b can be determined experimentally by selecting events with a given multiplicity of produced particles. The uncertainty in the impact parameter determination is small except in very peripheral bins [175]. The direction of the impact parameter can be determined on an event by event basis using the azimuthal dependence of the spectra. Imagine that the impact parameter direction is already known. This defines a coordinate system where z is along the beam axis and x is along the impact parameter direction.

We write $(p_x, p_y, p_z) = (p_\perp \cos(\phi), p_\perp \sin(\phi), p_z)$, and the particle distribution can be expanded in Fourier components of ϕ,

$$p_0 \frac{dN}{d^3p}\bigg|_{p_z=0} = v_0(p_\perp)\Big(1 + 2v_2(p_\perp)\cos(2\phi) + 2v_4(p_\perp)\cos(4\phi) + \dots\Big). \quad (192)$$

For a typical mid-central collision with $b \simeq 6\,\mathrm{fm}$ the v_2 harmonic, called the elliptic flow coefficient, is approximately 6%. In an actual event the reaction plane can be determined (in principle) by plotting the distribution in ϕ relative to an arbitrarily chosen axis, and then requiring that the distribution has a maximum at $\phi = 0$. This intuitive method to determine the reaction plane forms the basis of the event plane method. The result can be corrected for v_2 fluctuations and additional correlations among the produced particles. Current analyses are not based on the event plane method but use two, four, and higher particle cumulants – see [176] and references therein for a complete review. The scaling of these cumulants with multiplicity demonstrates that one can reliably extract collective flow down to small system sizes. These measurements provide a unique opportunity to study the approach to hydrodynamic behavior in a controlled fashion [177].

Elliptic flow represents the collective response of the system to pressure gradients in the initial state. At finite impact parameter the initial state has the shape of an ellipse, with the short axis along the x direction, and the long axis along the y direction. This implies that pressure gradients along the x axis are larger than along the y axis. Hydrodynamic evolution converts the initial pressure gradients to velocity gradients in the final state. Elliptic flow is a direct measure of collectivity. In particular, if the nucleus nucleus event were a simple superposition of proton proton collisions then the particle distribution would be azimuthally symmetric.

5.3.1. The Bjorken model The application of hydrodynamics to relativistic heavy ion collisions goes back to the work of Landau [178] and Bjorken [179]. Bjorken discovered a simple scaling solution that provides a natural starting point for more elaborate solutions in the ultra-relativistic domain. Consider two highly relativistic nuclei moving with equal but opposite momenta in the z direction. In the relativistic regime the natural variable to describe the motion in the z direction is the rapidity

$$y = \frac{1}{2}\log\left(\frac{E + p_z}{E - p_z}\right). \quad (193)$$

At RHIC the energy of the colliding nuclei is 100+100 GeV per nucleon, and the separation in rapidity is $\Delta y = 10.6$. Bjorken suggested that the two highly Lorentz contracted nuclei pass through each other and create a longitudinally expanding fireball in which particles are produced. In the original model the number of produced particles is independent of rapidity, and the subsequent evolution is invariant under boosts along the z axis. The evolution in proper time is the same for all comoving observers. The flow velocity is

$$u_\mu = \gamma(1, 0, 0, v_z) = (t/\tau, 0, 0, z/\tau), \quad (194)$$

where γ is the boost factor and $\tau = \sqrt{t^2 - z^2}$ is the proper time. The velocity field (194) solves the relativistic Euler equation (76). In particular, there is no longitudinal acceleration. The remaining hydrodynamic variables are determined by entropy conservation. Equ. (75) gives

$$\frac{d}{d\tau}\left[\tau s(\tau)\right] = 0 \tag{195}$$

and $s(\tau) = s_0\tau_0/\tau$. For an ideal relativistic gas $s \sim T^3$ and $T \sim 1/\tau^{1/3}$. Typical parameters at RHIC are $\tau_0 \simeq (0.6-1.6)$ fm and $T_0 \simeq (300-425)$ MeV. The combination $\tau_0 T_0^3$ is constrained by the final multiplicity, but individually τ_0 and T_0 are not well constrained. We note that the corresponding initial temperature is significantly larger than the critical temperature for the QCD phase transition.

The temperature drops as a function of τ and eventually the system becomes to dilute for the hydrodynamic evolution to make sense. At this point, the hydrodynamic description is matched to kinetic theory,

$$T_{\mu\nu}^{hydro} \equiv T_{\mu\nu}^{kin} = \int d\Gamma\, p_\mu p_\nu f(\mathbf{x}, \mathbf{p}, t)\,. \tag{196}$$

For an ideal fluid the distribution function is parameterized by the local temperature and flow velocity

$$f(\mathbf{x}, \mathbf{p}, t) = \sum_i \frac{d_i}{\exp(p \cdot u/T) \pm 1}\,, \tag{197}$$

where i labels different particle species, and d_i are the corresponding degeneracies. Finally, the observed particle spectra are given by

$$\left(p_0 \frac{dN}{d^3p}\right)_i = \frac{1}{(2\pi)^3} \int d\Sigma_\mu\, p^\mu f_i(\mathbf{x}, \mathbf{p}, t)\,, \tag{198}$$

where Σ_μ is the normal vector on the "freezeout" hypersurface, the surface on which the matching between the hydrodynamics and kinetic descriptions is performed.

In order to quantitatively describe the observed particle distributions several improvements of the simple Bjorken model are necessary. First, one has to include the transverse expansion of the system. Transverse expansion becomes important at a proper time $\tau \sim R/c_s$, where R is the (rms) size of the nucleus, and c_s is the speed of sound. At very late times the expansion becomes three dimensional,

$$s(\tau) \sim \frac{1}{\tau^3}\,, \tag{199}$$

and $T \sim 1/\tau$. Transverse expansion is caused by transverse pressure gradients. These gradients are sensitive to the initial energy density of the system. One simple model for the initial energy density (or entropy density) in the transverse plane is the Glauber model. In the Glauber model the entropy density is

$$\begin{aligned} s(\mathbf{x}_\perp, b) \propto\; & T_A(\mathbf{x}_\perp + \mathbf{b}/2)\Big[1 - \exp\left(-\sigma_{NN}\, T_A(\mathbf{x}_\perp - \mathbf{b}/2)\right)\Big] \\ & +\; T_A(\mathbf{x}_\perp - \mathbf{b}/2)\Big[1 - \exp\left(-\sigma_{NN}\, T_A(\mathbf{x}_\perp + \mathbf{b}/2)\right)\Big]\,, \end{aligned} \tag{200}$$

where **b** is the impact parameter

$$T_A(\mathbf{x}_\perp) = \int dz\, \rho_A(\mathbf{x}) \tag{201}$$

is the thickness function, and $\sigma_{NN}(\sqrt{s})$ is the nucleon-nucleon cross section. Here, $\rho_A(\mathbf{x})$ is the nuclear density. The idea behind the Glauber model is that the initial entropy density is proportional to the number of nucleons per unit area which actually collide. Other variants exist. For instance, one can distribute the energy density according to the number of binary nucleon-nucleon collisions – see Ref. [180] for a comparison. A more sophisticated theory of the initial energy density is provided by the Color Glass Condensate (CGC) [181, 182]. This model leads to somewhat steeper initial transverse energy density distributions.

Gradients in the transverse pressure lead to transverse acceleration and generate collective transverse flow. The collective expansion leads to a blue-shift of the transverse momentum spectra of produced particles. For an azimuthally symmetric source with temperature T and radial flow velocity $u^r(r)$ we get [183]

$$\left(p_0 \frac{dN}{d^3p}\right)_i = \frac{2d_i}{(2\pi)^2} r m_\perp \int r dr\, K_1\left(\frac{m_\perp u^\tau}{T}\right) I_1\left(\frac{p_\perp u^r}{T}\right), \tag{202}$$

where $m_\perp = \sqrt{p_\perp^2 + m_i^2}$ is the transverse "mass", and $K_1(z), I_1(z)$ are generalized Bessel functions. Using the asymptotic form of the Bessel functions one can show that the spectrum has the form

$$\frac{dN}{dm_\perp^2} \sim \exp\left(-\frac{m_\perp}{T_{\mathit{eff}}}\right), \quad T_{eff} = T\sqrt{\frac{1+v_r}{1-v_r}}. \tag{203}$$

This effect of transverse flow on the spectra is seen in the data. At RHIC, transverse velocities at freezeout reach $0.6\,c$. At finite impact parameter the initial energy density in the transverse plane is not azimuthally symmetric. The pressure gradient along the direction of the impact parameter is larger than the gradient in the orthogonal direction. The resulting anisotropy of the transverse flow can be characterized by the elliptic flow parameter v_2 defined in equ. (192). The observed elliptic flow is remarkable because v_2 is a very direct measure of transverse pressure. The observed radial flow is proportional to the radial pressure and the expansion time, but elliptic flow has to be generated early, when the system is still deformed.

5.3.2. Estimates of viscous corrections We are now in a position to discuss the role of dissipative effects. We begin with the effect of shear and bulk viscosity on the Bjorken solution. The scaling flow given in equ. (194) is a solution of the relativistic Navier-Stokes equation. Viscosity only modifies the entropy equation. We get

$$\frac{1}{s}\frac{ds}{d\tau} = -\frac{1}{\tau}\left(1 - \frac{\frac{4}{3}\eta + \zeta}{sT\tau}\right). \tag{204}$$

We observe that dissipation is governed by the sound attenuation length Γ_s, see equ. (82). The applicability of the Navier-Stokes equation requires that the viscous correction is

small [7]

$$\frac{\eta}{s} + \frac{3}{4}\frac{\zeta}{s} \ll \frac{3}{4}(T\tau)\,. \tag{205}$$

For the Bjorken solution $T\tau \sim \tau^{2/3}$ grows with time, and this condition is most restrictive during the initial phase. Using $\tau_0 = 1$ fm and $T_0 = 300$ MeV gives $\eta/s < 0.6$. For a three dimensional expansion $T\tau$ is independent of time. At very late time the fluid is composed of hadrons, or pre-formed hadronic resonances. In that case $\eta \sim T/\sigma$, where σ is a hadronic cross section. Then, for a three dimensional expansion, the viscous correction $\eta/(sT\tau)$ grows with proper time as τ^2. This shows that the system has to freeze out at late time.

It is instructive to study the viscous contribution to the stress tensor in more detail. At central rapidity we have (for $\zeta = 0$)

$$T_{zz} = P - \frac{4}{3}\frac{\eta}{\tau}, \quad T_{xx} = T_{yy} = P + \frac{2}{3}\frac{\eta}{\tau}\,. \tag{206}$$

This means that shear viscosity decreases the longitudinal pressure and increases the transverse one. In the Bjorken scenario there is no acceleration, but if pressure gradients are taken into account shear viscosity will tend to increase radial flow. A similar effect will occur at finite impact parameter. Shear viscosity reduces the pressure along the impact parameter direction, increases the pressure in the all orthogonal direction, and suppresses elliptic flow. This is the basic observation that motivates attempts to extract shear viscosity from the observed elliptic flow.

Viscosity modifies the stress tensor, and via the matching condition (196) this modification changes the distribution functions of produced particles. In Ref. [184] a simple quadratic ansatz for the leading correction δf to the distribution function was proposed

$$\delta f = \frac{3}{8}\frac{\Gamma_s}{T^2} f_0(1+f_0) p_\alpha p_\beta \nabla^{\langle\alpha} u^{\beta\rangle}\,, \tag{207}$$

where $\nabla^{\langle\alpha} u^{\beta\rangle}$ is a symmetric traceless tensor, see equ. (84). This form summarizes the results of more involved kinetic calculations [14]. The modified distribution function leads to a modification of the single particle spectrum. For a simple Bjorken expansion and at large $p_\perp$ we find

$$\frac{\delta(dN)}{dN_0} = \frac{\Gamma_s}{4\tau_f}\left(\frac{p_\perp}{T}\right)^2\,, \tag{208}$$

where τ_f is the freezeout time. We observe that the dissipative correction to the spectrum is controlled by the same parameter Γ_s/τ that appeared in equ. (204). We also note that the viscous term grows with $p_\perp$. At RHIC transverse momentum spectra are in agreement with hydrodynamic predictions out to transverse momenta several times larger than the temperature. In equ. (208) this is partially compensated by the fact that τ_f/τ_0 is a large number, but typically the requirement $\delta(dN)/(dN_0) < 1$ provides a more stringent bound on η/s than equ. (205). We can also include transverse expansion and study the leading dissipative correction to v_2 [184]. The viscous correction tends

to reduce v_2 and grows with $p_\perp$. At $p_\perp = 1$ GeV an estimate using formulas similar to equ. (208) finds $(\delta v_2)/v_2 \sim 1$ for $\Gamma_s/\tau_f \sim 0.2$. Using $\tau_f \sim 5$ fm this translates into $\eta/s \leq 0.5$.

5.3.3. Hydrodynamic Simulations There have been a number of recent numerical studies devoted to extracting the shear viscosity of the quark gluon plasma [185, 186, 187, 188, 189]. Here, we will follow the work of Dusling and Teaney [185], and refer the reader to the recent review by Heinz [26] for a more detailed comparison between different strategies for implementing relativistic viscous hydrodynamics for heavy ion collisions at RHIC. Dusling and Teaney considered a $2+1$ dimensional boost invariant model. They used a second order fluid model studied by Öttinger [190]. For this purpose we introduce an additional dynamical tensor $c^{\mu\nu}$, related to $\delta T^{\mu\nu}$, which obeys the constraint

$$c_{\mu\nu} u^\nu = u_\mu \,. \tag{209}$$

This tensor can be decomposed as

$$c_{\mu\nu} = -u_\mu u_\nu + \mathring{c}_{\mu\nu} + \overline{c}_{\mu\nu} \,, \tag{210}$$

$$\overline{c}_{\mu\nu} = \frac{1}{3}\left(c_\lambda{}^\lambda - 1\right)\left(\eta_{\mu\nu} + u_\mu u_\nu\right) \,, \tag{211}$$

and the shear stress tensor is parameterized as

$$\delta T^{\mu\nu} = -P(\epsilon)\alpha\, \mathring{c}^{\mu\nu} \,. \tag{212}$$

The tensor $c_{\mu\nu}$ obeys the equation of motion

$$u^\lambda(\partial_\lambda c_{\mu\nu} - \partial_\mu c_{\lambda\nu} - \partial_\nu c_{\mu\lambda}) = -\frac{1}{\tau_0}\,\overline{c}_{\mu\nu} - \frac{1}{\tau_2}\,\mathring{c}_{\mu\nu} \,. \tag{213}$$

The constraint equ. (209) is preserved under time evolution. In the limit that the relaxation times τ_0 and τ_2 are small the evolution equation leads to the following solution for $c^{\mu\nu}$ in the local rest frame

$$c^{ij} = \tau_2\left(\partial^i u^j + \partial^j u^i - \frac{2}{3}\delta^{ij}\partial_k u^k\right) + \frac{2}{3}\,\tau_0 \delta^{ij}\partial_k u^k \,. \tag{214}$$

Comparing with the Navier-Stokes equation we see that

$$\eta = \tau_2\, P\, \alpha \,, \qquad \zeta = \frac{2}{3}\,\tau_0\, P\, \alpha \,. \tag{215}$$

Dusling and Teaney used these relations (with $\alpha = 0.7$) to fix (τ_0, τ_2) in terms of η and ζ, and they studied the sensitivity to the parameter α. They considered a simple conformal equation of state $P = \epsilon/3$, and set $\zeta = 0$.

An advantage Öttinger's approach is that equ. (213) is relatively simple to solve. One just evolves the spatial components of c_{ij} and then uses the constraints (209) to solve for the time components c_{00} and c_{0i}. As hydrodynamics is universal, any fluid model can be recast in terms of the first and second order formalism described in Sec. 3.1.3.

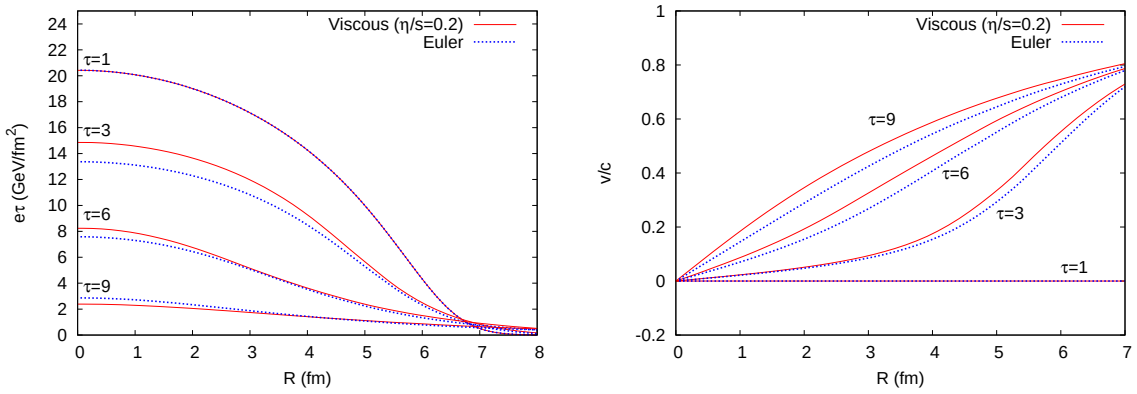

Figure 7. Plot of the energy density per unit rapidity $e\tau$ (left) and of the transverse velocity (right) at times of $\tau = 1, 3, 6, 9$ fm/c, for $\eta/s = 0.2$ (solid red line) and for ideal hydrodynamics (dotted blue line), from [185].

For the Öttinger fluid model, expanding out the equations of motion to second order leads to the relation

$$\pi^{\mu\nu} = -\eta\sigma^{\mu\nu} - \tau_2\left[\langle D\pi^{\mu\nu\rangle} + \frac{4}{3}\pi^{\mu\nu}(\partial\cdot u)\right] + \frac{\tau_2}{\eta}\pi^{\langle\mu}{}_{\lambda}\pi^{\nu\rangle\lambda} + \tau_2\pi^{\langle\mu}{}_{\lambda}\Omega^{\nu\rangle\lambda} - \frac{2}{3}\tau_2\pi_{\mu\nu}(\partial\cdot u)\,. \tag{216}$$

The last term in this expression differs from the general result in equ. (216), which indicates that at second order in gradients this model contains terms that break conformal symmetry.

The hydrodynamic equations were solved for several fixed values of the shear viscosity to entropy density ratio η/s. At the initial time $\tau_0 = 1$ fm the entropy per participant is adjusted and closely corresponds to the results of full hydrodynamic simulations [191, 192, 193]. The maximum initial temperature is $T_0 = 420$ MeV at an impact parameter $b = 0$. The initial components of the stress tensor are set to the Navier Stokes values.

Numerical results are shown in Fig. 7. The effect of viscosity is twofold. The longitudinal pressure is initially reduced and the viscous case does less longitudinal PdV work as in the simple Bjorken expansion. This means that at early times the energy per rapidity decreases more slowly in the viscous case. The reduction of longitudinal pressure is accompanied by a larger transverse pressure. This causes the transverse velocity to grow more rapidly. The larger transverse velocity causes the energy density to deplete faster at late times in the viscous case. The net result is that a finite viscosity, even as large as $\eta/s = 0.2$, does not integrate to give major deviations from the ideal equations of motion.

Freezeout happens when the viscous terms become large compared to the ideal terms. Thus freezeout is much less arbitrary in viscous hydrodynamics as compared to

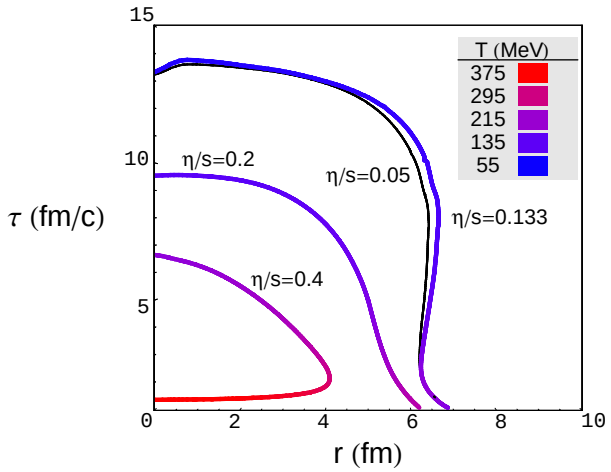

Figure 8. Location of freezeout surfaces for for central Au-Au collisions. The surfaces are determined by the condition $\frac{\eta}{p}\,(\partial\cdot u) = 0.6$, slightly larger than the value 0.5 discussed in the text. Different surfaces correspond to different values of η/s. The shading corresponds to the freezeout temperature. The thin solid black curve shows the contour set by $\frac{\eta}{p}\,(\partial\cdot u) = 0.225$ for comparison.

ideal hydrodynamics. Specifically, freezeout is signaled when

$$\frac{\eta}{P}\,\partial\cdot u \simeq \frac{1}{2}\,. \tag{217}$$

This combination of parameters can be motivated from kinetic theory. The pressure is of order $P \sim \epsilon\,\langle v_{\rm th}^2\rangle$ where $\langle v_{\rm th}^2\rangle$ is the typical quasi particle velocity and ϵ is the energy density. The viscosity is of order $\eta \sim \epsilon\,\langle v_{\rm th}^2\rangle\,\tau_R$ where τ_R is the relaxation time. Thus the freezeout condition is $\frac{\eta}{P}\,(\partial\cdot u) \sim \tau_R(\partial\cdot u) \sim \frac{1}{2}$. Typical freezeout surfaces are shown in Fig. 8. We note that hydrodynamics breaks down both at late and also at early times. The latter is most clearly see from the $\eta/s = 0.4$ curve. If η/s is very small then freezeout will occur at very late proper time. In the following, we shall therefore use a simpler criterion $\chi \equiv \frac{1}{T}(\partial\cdot u) = \text{const}$ which is independent of η/s. Taking $\chi = 3$ roughly corresponds to the $\eta/s = 0.2$ freezeout surface in Fig. 8.

Finally, we need to compute the spectra of produced particles. We follow the procedure outlined above, see equ. (207), and write the distribution function as $f = f_0 + \delta f$ with

$$\delta f = \frac{1}{2(\epsilon+P)T^2}\,f_0(1+f_0)\,p^\mu p^\nu \delta T_{\mu\nu}\,. \tag{218}$$

The spectrum is determined by integrating the distribution function over the freezeout surface as in equ. (198), and the elliptic flow parameter v_2 is computed from the definition in equ. (192). A comparison with the data obtained by the STAR collaboration is shown in Fig. (9). There are several curves here and we will go through them one by one:

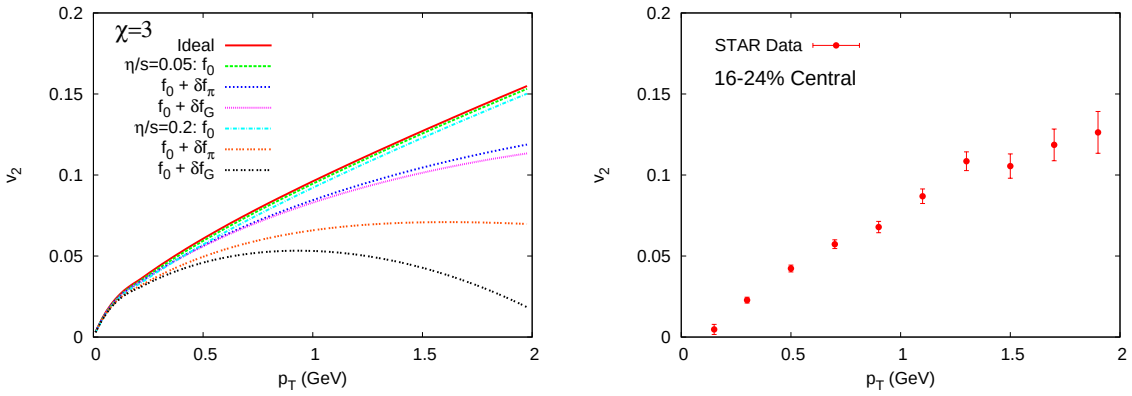

Figure 9. Left: $v_2(p_T)$ for massless Bose particles for simulations using $\eta/s = 0, 0.05, 0.2$ at an impact parameter of $b = 6.5\,\mathrm{fm}$. Right: Four-particle cumulant data as measured in Au-Au collisions at $\sqrt{s} = 200$ GeV for a centrality selection of 16% to 24% [194].

- For the two different values of η/s, 0.05 and 0.2, there are three curves each. Our best estimates for the elliptic flow as a function of p_T are labeled $f_0 + \delta f_\pi$ and are shown by the blue ($\eta/s = 0.05$) and orange ($\eta/s = 0.2$) lines.
- To disentangle what part of the viscous modification is due to the distribution function δf and what part of it is due to changes in the flow, we also compute $v_2(p_T)$ with f_0 only. We see that the effect on v_2 from viscous modifications of the flow is relatively minor. This may be the largest obstacle to reliably extracting the shear viscosity from the heavy ion data. However, it is important to realize that the modification to the distribution function reflects the viscous correction to the stress tensor itself. In hydrodynamic simulations the p_T integrated v_2 tracks the asymmetry of the stress tensor [195]. In the context of viscous hydrodynamics this is nicely illustrated in Fig. 8 of Ref. [188]. Nevertheless, in contrast to the atomic physics experiments discussed in Sect. 5.2, the observed viscous corrections to the elliptic flow do not reflect a resummation of secular terms in the gradient expansion.
- Finally instead of showing the spectrum computed with $\delta T^{\mu\nu}$, we show $v_2(p_T)$ computed with velocity gradients directly. For this purpose $\delta T^{\mu\nu}$ in equ. (218) is replaced by $-\eta\sigma^{\mu\nu}$ where $\sigma^{\mu\nu}$ is computed from the flow velocities. $v_2(p_T)$ computed in this way is denoted by $f_0 + \delta f_G$ in the figure and corresponds to the magenta and black curves. To first order in gradients this is an identity and the difference between f_π and f_G is a measure of the magnitude of second order terms. For the smallest viscosity $\eta/s = 0.05$ the differences are quite small, but the effect is more noticeable for $\eta/s = 0.2$.

We conclude that for small values of $\eta/s \lesssim 0.2$ the gradient expansion is working. There are, however, a number of issues that have to be considered in order to extract reliable values for η/s:

- The constraints on η/s are sensitive to the initial values for the transverse energy

density. In particular, using color glass initial conditions produces higher transverse pressure gradients, and allows for values of η/s about twice larger than Glauber model initial conditions [188].

- Near the edge of the nucleus the gradient expansion breaks down completely. It is important to quantify the extent to which the effects of the edge propagate into the interior and invalidate the hydrodynamic description. One way to do this is by comparing the results of hydrodynamic simulations to kinetic theory. For strongly coupled plasmas kinetic theory is not an appropriate description of the microscopic interactions. However, hydrodynamics is independent of the microscopic details. Thus extrapolating kinetic theory into the strongly coupled domain is good way to construct a model which gracefully transitions from a hydrodynamic description in the interior to a kinetic description near the edge. There are several important developments in this direction [189, 196].
- Viscous effects in the hadronic phase are very important [191, 182]. These effects can be taken into account by coupling the hydrodynamic evolution to a hadronic cascade.
- Effects due to bulk viscosity may reduce both radial and elliptic flow [197, 198]. Bulk viscosity is likely to be much smaller than shear viscosity in the plasma phase, but it is expected to grow near the phase transition. The magnitude of this growth is not clear.

Some of these effects have yet to be carefully studied. However, even if one conservatively assumes that all uncertainties tend to increase the bound on η/s, one still has to conclude that for a shear viscosity of $\eta/s > 0.4$ it will be impossible to reproduce the observed flow. The question now is whether it will be possible to describe the large set of available data on energy, impact parameter, rapidity, transverse momentum, and species dependence of flow using viscous hydro, and whether it is possible to extract a reliable value, with controlled error bars, for η/s of the quark gluon plasma.

6. Outlook

In this review we summarized theoretical and experimental information on the behavior of nearly perfect fluids. We characterized the "perfectness" in terms of the shear viscosity of the fluid. Shear viscosity is special because

- shear viscosity is the "minimal" transport property of a fluid. Both bulk viscosity and thermal conductivity may vanish – bulk viscosity in the case of scale invariant fluids, thermal conductivity in the absence of a conserved charge – but there is no symmetry that would cause the shear viscosity to vanish. Other transport properties, like diffusion constants and conductivities, depend on the presence of additional conserved charges. The "perfectness" of any fluid can be characterized by the dimensionless ratio η/s. If factors of $\hbar$ and k_B are reinstated the dimensionless measure of fluidity is $[\eta/\hbar]/[s/k_B]$.

- a small shear viscosity is uniquely associated with strong interactions. Other transport coefficients may vanish even if the interaction strength remains weak. For example, bulk viscosity vanishes if the theory is conformal, and the diffusion constant goes to zero at the a localization phase transition, but the shear viscosity of a weakly coupled fluid is always large.

Note that the reverse of the last statement is not true: The viscosity can be large, even if the interaction is strong. One possible scenario is that the interaction is so strong that it leads to the breakdown of a continuous symmetry, and the emergence of a new set of weakly coupled quasi-particles. Note that the $\mathcal{N} = 4$ super-conformal fluid is special in this regard: There is no symmetry breaking in the strong coupling limit. Another example is the liquid-gas phase transition. There are no weakly coupled quasi-particles, but the viscosity diverges because of critical fluctuations.

We summarized the main theoretical approaches to transport coefficients: kinetic theory, holography, and non-perturbative approaches based on the Kubo formula.

- Kinetic theory applies whenever the fluid can be described in terms of quasi-particles. For many fluids this is the case in both the high and the low temperature limit. Typically, at high temperature the quasi-particles are the "fundamental" degrees of freedom (quarks, gluons, atoms) whereas the low temperature degrees of freedom are composite (phonons, rotons, pions). In the regime in which kinetic theory applies the ratio η/s is always parametrically large. This leads to a characteristic "concave" temperature dependence of η/s. Kinetic theory is useful in constraining the location of the viscosity minimum (usually, near the crossover between the high and low temperature regimes). Also, despite the weak coupling restriction, kinetic theory is quantitatively accurate for many quantum fluids in the whole temperature range covered by experiment.
- Holography is a new method for studying the transport behavior of quantum fluids. It is most useful in the strong coupling limit of certain model field theories (like $\mathcal{N} = 4$ super-conformal field theory), but the range of field theories that have known holographic duals has grown significantly over the years. More importantly, holographic dualities have led to important new insights into the transport properties of strongly coupled fluids. This includes the proposed universal bound on η/s, consistent higher order hydrodynamic theories, computations of the spectral function associated with the shear and other transport modes, etc. Holography has also been used to study specific solutions to the hydrodynamic equations, like the wake of a moving heavy quark, or the approach to equilibrium after the collision of two highly Lorentz contracted sources.
- The Kubo formula connects non-perturbative calculations of equilibrium correlation functions with non-equilibrium transport coefficients. Possible non-perturbative approaches include Euclidean lattice, large-N, exact renormalization group, and Dyson-Schwinger calculations. Significant progress has been made in computing the shear viscosity of the quark gluon plasma on the lattice. The results are close to the

proposed bound. Future calculations will answer the question whether transport phenomena in the QCD plasma can be understood in terms of quasi-particles.

Finally, we summarized the experimental situation for the three most strongly coupled fluids that can be prepared in the laboratory.

- Liquid helium has been studied for many years and its shear viscosity is well determined. The minimum value of η/s is about 0.8 and is attained near the endpoint of the liquid gas phase transition. The ratio η/n has a minimum closer to the lambda transition. Even though $\eta/s < 1$ the transport properties of liquid helium can be quantitatively understood using kinetic theory.
- Strongly interacting cold atomic Fermi gases were first created in the laboratory in 1999. These systems are interesting because the interaction between the atoms can be controlled, and a large set of hydrodynamic flows (collective oscillations, elliptic flow, rotating systems) can be studied. Current experiments involve 10^5-10^6 atoms, and the range of temperatures and interaction strengths over which hydrodynamic behavior can be observed is not large. There are also some difficulties in extracting the viscosity that are related to the nature of the flow profiles that have been studied. A conservative estimate is $\eta/s < 0.5$.
- The quark gluon plasma has been studied in heavy ion collisions at a number of facilities, AGS (Brookhaven), SPS (CERN), RHIC (Brookhaven). Almost ideal hydrodynamic behavior was observed for the first time in 200 GeV per nucleon (in the center of mass) Au on Au collisions at RHIC. These experiments are difficult to analyze - the initial state is very far from equilibrium and not completely understood, final state interactions are important, and the size and lifetime of the system are not very large. Important progress has nevertheless been made in extracting constraints on the transport properties of the quark gluon plasma. A conservative bound is $\eta/s < 0.4$, but the the value of η/s that provides the best fit to the data is smaller, $\eta/s \sim 0.1$.

Acknowledgments: This work was supported in parts by the US Department of Energy grant DE-FG02-03ER41260 (T.S.) and DE-FG02-08ER41540 (D.T.). D.T. is also supported by the Alfred P. Sloan foundation. We would like to thank Gordon Baym for providing the impetus to write this review. We would like to acknowledge useful discussions with Dam Son, Edward Shuryak, and John Thomas.

[1] O. Darrigol, Worlds of Flow, Oxford University Press (2005).
[2] S. G. Brush, The kind of motion we call heat, North Holland (1986).
[3] J. Frenkel, Kinetic theory of liquids, Dover Publications (1955).
[4] P. J. Linstrom, W. G. Mallard, Eds., NIST Chemistry WebBook, NIST Standard Reference Database Number 69, National Institute of Standards and Technology; http://webbook.nist.gov.
[5] J. D. Cox, D. D. Wagman, V. A. Medvedev, CODATA Key Values for Thermodynamics, Hemisphere Publishing Corp., New York (1989); http://www.codata.org.

[6] J. Wilks, "The Properties of Liquid and Solid Helium", Clarendon (1966).
[7] P. Danielewicz and M. Gyulassy, Phys. Rev. D **31**, 53 (1985).
[8] B. DeMarco, D. S. Jin, Science **285.5434**, 1703 (1999).
[9] K. M. O'Hara, S. R. Granade, M. E. Gehm, T. A. Savard, S. Bali, C. Freed, and J. E. Thomas, Phys. Rev. Lett. **82**, 4204 (1999).
[10] S. S. Adler *et al.* [PHENIX Collaboration], Phys. Rev. Lett. **91**, 182301 (2003) [arXiv:nucl-ex/0305013].
[11] B. B. Back *et al.* [PHOBOS Collaboration], Phys. Rev. C **72**, 051901 (2005) [arXiv:nucl-ex/0407012].
[12] J. Adams *et al.* [STAR Collaboration], Phys. Rev. C **72**, 014904 (2005) [arXiv:nucl-ex/0409033].
[13] G. Baym, H. Monien, C. J. Pethick and D. G. Ravenhall, Phys. Rev. Lett. **64**, 1867 (1990).
[14] P. Arnold, G. D. Moore and L. G. Yaffe, JHEP **0011**, 001 (2000) [arXiv:hep-ph/0010177].
[15] P. Arnold, G. D. Moore and L. G. Yaffe, JHEP **0305**, 051 (2003) [arXiv:hep-ph/0302165].
[16] G. Policastro, D. T. Son and A. O. Starinets, Phys. Rev. Lett. **87**, 081601 (2001) [arXiv:hep-th/0104066].
[17] J. M. Maldacena, Adv. Theor. Math. Phys. **2**, 231 (1998) [Int. J. Theor. Phys. **38**, 1113 (1999)] [arXiv:hep-th/9711200].
[18] A. Buchel, J. T. Liu and A. O. Starinets, Nucl. Phys. B **707**, 56 (2005) [arXiv:hep-th/0406264].
[19] P. Kovtun, D. T. Son and A. O. Starinets, Phys. Rev. Lett. **94**, 111601 (2005) [arXiv:hep-th/0405231].
[20] S. Giorgini, L. P. Pitaevskii, S. Stringari, Rev. Mod. Phys. **80** 1215 (2008) [arXiv:0706.3360].
[21] E. Shuryak, Prog. Part. Nucl. Phys. **62**, 48 (2009) [arXiv:0807.3033 [hep-ph]].
[22] I. M. Khalatnikov, "Introduction to the Theory of Superfluidity", W. .A. Benjamin, Inc. (1965).
[23] G. Baym, C. Pethick, "Landau Fermi Liquid Theory", Wiley, New York (1991).
[24] P. Arnold, Int. J. Mod. Phys. E **16**, 2555 (2007) [arXiv:0708.0812 [hep-ph]].
[25] D. T. Son and A. O. Starinets, Ann. Rev. Nucl. Part. Sci. **57**, 95 (2007) [arXiv:0704.0240 [hep-th]].
[26] U. W. Heinz, arXiv:0901.4355 [nucl-th].
[27] P. Romatschke, arXiv:0902.3663 [hep-ph].
[28] P. Arnold and G. D. Moore, Phys. Rev. Lett. **87**, 120401 (2001) [arXiv:cond-mat/0103228].
[29] R. A. Aziz, M. J. Slaman, J. Chem. Phys. **94**, 8047 (1991).
[30] K. T. Tang, J. P. Toennies, C. L. Yiu, Phys. Rev. Lett. **74**, 1546 (1995).
[31] E. Braaten and H. W. Hammer, Annals Phys. **322**, 120 (2007) [arXiv:cond-mat/0612123].
[32] D. M. Ceperley, Rev. Mod. Phys. **67**, 279 (1995).
[33] H. R. Glyde, R. T. Azuah, W. G. Stirling, Phys. Rev. B **62**, 14337 (2000).
[34] M. Campostrini, M. Hasenbusch, A. Pelissetto, E. Vicari, Phys. Rev. B **74**, 144506 (2006) [arXiv:cond-mat/0605083].
[35] J. A. Lipa, D. R. Swanson, J. A. Nissen, T. C. P.'Chui, U. E. Israelsson, Phys. Rev. Lett. **76**, 944 (1996).
[36] R. P. Feynman, Phys. Rev. **94**, 262 (1954).
[37] C. Regal, Ph. D. Thesis, University of Colorado (2005), cond-mat/0601054.
[38] L. P. Gorkov and T. K. Melik-Barkhudarov, Sov. Phys. JETP **13**, 1018 (1961).
[39] P. Nozieres, S. Schmitt-Rink, J. of Low Temp. Phys. **59**, 195 (1984).
[40] S.-Y. Chang, V. R. Pandharipande, J. Carlson, and K. E. Schmidt, Phys. Rev. **A** 70, 043602 (2004).
[41] M. Bartenstein, A. Altmeyer, S. Riedl, S. Jochim, C. Chin, J. Hecker Denschlag, and R. Grimm, Phys. Rev. Lett. **92**, 203201 (2004) [cond-mat/0412712];
[42] T. Mehen, I. W. Stewart and M. B. Wise, Phys. Lett. B **474**, 145 (2000) [arXiv:hep-th/9910025].
[43] D. T. Son and M. Wingate, Annals Phys. **321**, 197 (2006) [cond-mat/0509786].
[44] E. Burovski, N. Prokof'ev, B. Svistunov, M. Troyer, Phys. Rev. Lett. **96**, 160402 (2006) [cond-mat/0602224].
[45] J. Carlson, S.-Y. Chang, V. R. Pandharipande, and K. E. Schmidt, Phys. Rev. Lett. **91**, 050401,

(2003). [physics/0303094].
[46] L. Luo, J. E. Thomas, J. Low Temp. Phys. in press (2009), [arXiv:0811.1159[cond-mat.other]].
[47] G. E. Astrakharchik, J. Boronat, J. Casulleras, S. Giorgini, Phys. Rev. Lett. 93, 200404 (2004) [cond-mat/0406113].
[48] M. G. Alford, A. Schmitt, K. Rajagopal and T. Schäfer, Rev. Mod. Phys. **80**, 1455 (2008) [arXiv:0709.4635 [hep-ph]].
[49] E. V. Shuryak, Sov. Phys. JETP **47**, 212 (1978) Zh. Eksp. Teor. Fiz. **74**, 408 (1978)].
[50] M. LeBellac, "Thermal Field Theory", Cambridge University Press, Cambridge (1996).
[51] E. Braaten and R. D. Pisarski, Phys. Rev. D **42**, 2156 (1990).
[52] J. P. Blaizot, E. Iancu and A. Rebhan, "Thermodynamics of the high-temperature quark gluon plasma", in Quark Gluon Plasma 3, R. Hwa, X.-N. Wang, eds., (2003) [hep-ph/0303185].
[53] E. Braaten and A. Nieto, Phys. Rev. D **51**, 6990 (1995) [arXiv:hep-ph/9501375].
[54] A. Hietanen, K. Kajantie, M. Laine, K. Rummukainen and Y. Schroder, Phys. Rev. D **79**, 045018 (2009) [arXiv:0811.4664 [hep-lat]].
[55] E. Laermann and O. Philipsen, Ann. Rev. Nucl. Part. Sci. **53**, 163 (2003) [arXiv:hep-ph/0303042].
[56] F. Karsch, J. Phys. G **34**, S627 (2007) [arXiv:hep-ph/0701210].
[57] Y. Aoki, Z. Fodor, S. D. Katz and K. K. Szabo, Phys. Lett. B **643**, 46 (2006) [arXiv:hep-lat/0609068].
[58] J. Terning, "Modern supersymmetry: Dynamics and duality," Oxford, UK: Clarendon (2006).
[59] S. S. Gubser, I. R. Klebanov and A. A. Tseytlin, Nucl. Phys. B **534**, 202 (1998) [arXiv:hep-th/9805156].
[60] A. Fotopoulos and T. R. Taylor, Phys. Rev. D **59**, 061701 (1999) [arXiv:hep-th/9811224].
[61] A. Nieto and M. H. G. Tytgat, arXiv:hep-th/9906147.
[62] J. P. Blaizot, E. Iancu, U. Kraemmer and A. Rebhan, JHEP **0706**, 035 (2007) [arXiv:hep-ph/0611393].
[63] M. Greiter, F. Wilczek and E. Witten, Mod. Phys. Lett. B **3**, 903 (1989).
[64] D. T. Son, preprint, hep-ph/0204199.
[65] R. Baier, P. Romatschke, D. T. Son, A. O. Starinets and M. A. Stephanov, JHEP **0804**, 100 (2008) [arXiv:0712.2451 [hep-th]].
[66] M. A. York and G. D. Moore, arXiv:0811.0729 [hep-ph].
[67] S. Bhattacharyya, V. E. Hubeny, S. Minwalla and M. Rangamani, JHEP **0802**, 045 (2008) [arXiv:0712.2456 [hep-th]].
[68] W. Israel and J. M. Stewart, Annals Phys. **118**, 341 (1979).
[69] R. P. Geroch and L. Lindblom, Phys. Rev. D **41**, 1855 (1990).
[70] D. Burnett, Proc. Lond. Math. Soc. **39** 385 (1935).
[71] D. Burnett, Proc. Lond. Math. Soc. **40** 382 (1936).
[72] L. S. Garcia-Colina, R. M. Velascoa, F. J. Uribea, Phys. Rep. **465** 149 (2008).
[73] H. Grad, Comm. Pure and Appl. Math. **2** 331 (1949).
[74] J. Foch, G. E. Uhlenbeck Phys. Rev. Lett. **19** 1025 (1967).
[75] J. D. Foch, G. W. Ford, In: J. deBoer and G.E. Uhlenbeck, Editors, Studies in Statistical Mechanics part B, vol. V, North-Holland (1970).
[76] I. M. Khalatnikov, V. V. Lebedev, Phys. Lett. A **91**, 70 (1982).
[77] B. Carter, I. M. Khalatnikov, Phys. Rev. D **45**, 4536 (1992).
[78] D. T. Son, Int. J. Mod. Phys. A **16S1C**, 1284 (2001) [arXiv:hep-ph/0011246].
[79] M. Mannarelli and C. Manuel, Phys. Rev. D **77**, 103014 (2008) [arXiv:0802.0321 [hep-ph]].
[80] P. C. Hohenberg and B. I. Halperin, Rev. Mod. Phys. **49**, 435 (1977).
[81] A. Onuki, Phys. Rev. E **55**, 403 (1997).
[82] D. T. Son and M. A. Stephanov, Phys. Rev. D **70**, 056001 (2004) [arXiv:hep-ph/0401052].
[83] F. Karsch and H. W. Wyld, Phys. Rev. D **35**, 2518 (1987).
[84] H. B. Meyer, Phys. Rev. D **76**, 101701 (2007) [arXiv:0704.1801 [hep-lat]].
[85] H. B. Meyer, Phys. Rev. Lett. **100**, 162001 (2008) [arXiv:0710.3717 [hep-lat]].

[86] S. Sakai and A. Nakamura, PoS **LAT2007**, 221 (2007) [arXiv:0710.3625 [hep-lat]].
[87] G. Aarts, PoS **LAT2007**, 001 (2007) [arXiv:0710.0739 [hep-lat]].
[88] H. B. Meyer, JHEP **0808**, 031 (2008) [arXiv:0806.3914 [hep-lat]].
[89] L. D. Landau, E. M. Lifshitz, "Physical Kinetics", Course of Theoretical Physics, Vol.X, Pergamon Press (1981).
[90] G. Rupak and T. Schäfer, Phys. Rev. A **76**, 053607 (2007) [arXiv:0707.1520 [cond-mat.other]].
[91] H. J. Maris, Phys. Rev. **A**, 1980 (1973).
[92] M. Prakash, M. Prakash, R. Venugopalan and G. Welke, Phys. Rept. **227**, 321 (1993).
[93] L. P. Csernai, J. I. Kapusta and L. D. McLerran, Phys. Rev. Lett. **97**, 152303 (2006) [arXiv:nucl-th/0604032].
[94] J. W. Chen and E. Nakano, Phys. Lett. B **647**, 371 (2007) [arXiv:hep-ph/0604138].
[95] P. Massignan, G. M. Bruun, H. Smith, Phys. Rev. A **71**, 033607 (2005) [cond-mat/0409660].
[96] G. M. Bruun, H. Smith, Phys. Rev. A **72**, 043605 (2005) [cond-mat/0504734].
[97] G. M. Bruun, H. Smith, Phys. Rev. A **75**, 043612 (2007) [cond-mat/0612460].
[98] S. Chapman and T. G. Cowling, "The Mathematical Theory of Non-Uniform Gases", Cambridge University Press, 3rd ed. (1970).
[99] R. A. Aziz, A. R. Janzen, M. R. Moldover, Phys. Rev. Lett. **74**, 1586 (1995).
[100] P. Arnold, G. D. Moore and L. G. Yaffe, JHEP **0301**, 030 (2003) [arXiv:hep-ph/0209353].
[101] S. Caron-Huot and G. D. Moore, JHEP **0802**, 081 (2008) [arXiv:0801.2173 [hep-ph]].
[102] M. A. Escobedo, M. Mannarelli and C. Manuel, preprint (2009).
[103] P. Arnold, C. Dogan and G. D. Moore, Phys. Rev. D **74**, 085021 (2006) [arXiv:hep-ph/0608012].
[104] S. C. Huot, S. Jeon and G. D. Moore, Phys. Rev. Lett. **98**, 172303 (2007) [arXiv:hep-ph/0608062].
[105] D. T. Son, Phys. Rev. Lett. **98**, 020604 (2007) [arXiv:cond-mat/0511721].
[106] J. W. Chen and J. Wang, arXiv:0711.4824 [hep-ph].
[107] S. Weinberg, "Gravitation and Cosmology", Wiley & Sons (1972).
[108] S. Jeon, Phys. Rev. D **52**, 3591 (1995) [arXiv:hep-ph/9409250].
[109] R. M. Bowley, Europhys. Lett. **58** 725 (2002).
[110] B. Svetitsky, Phys. Rev. D **37**, 2484 (1988).
[111] G. D. Moore and D. Teaney, Phys. Rev. C **71**, 064904 (2005) [arXiv:hep-ph/0412346].
[112] H. Heiselberg and C. J. Pethick, Phys. Rev. D **48**, 2916 (1993).
[113] E. Witten, Adv. Theor. Math. Phys. **2**, 253 (1998) [arXiv:hep-th/9802150].
[114] S. S. Gubser, I. R. Klebanov and A. M. Polyakov, Phys. Lett. B **428**, 105 (1998) [arXiv:hep-th/9802109].
[115] O. Aharony, S. S. Gubser, J. M. Maldacena, H. Ooguri and Y. Oz, Phys. Rept. **323** (2000) 183 [arXiv:hep-th/9905111].
[116] K. S. Thorne, R. H. Price, D. A. MacDonald, "Black Holes: The Membrane Paradigm", Yale University Press, 1986.
[117] G. W. Gibbons and S. W. Hawking, Phys. Rev. D **15**, 2752 (1977).
[118] J. W. . York, Phys. Rev. Lett. **28**, 1082 (1972).
[119] R. M. Wald, "General Relativity", University of Chicago Press (1984).
[120] C. W. Misner, K. S. Thorne and J. A. Wheeler, "Gravitation", W. H. Freeman (1973).
[121] G. Aarts and J. M. Martinez Resco, JHEP **0204**, 053 (2002) [arXiv:hep-ph/0203177].
[122] G. D. Moore and O. Saremi, JHEP **0809**, 015 (2008) [arXiv:0805.4201 [hep-ph]].
[123] D. Teaney, Phys. Rev. D **74**, 045025 (2006) [arXiv:hep-ph/0602044].
[124] P. Kovtun and A. Starinets, Phys. Rev. Lett. **96**, 131601 (2006) [arXiv:hep-th/0602059].
[125] A. Buchel and J. T. Liu, Phys. Rev. Lett. **93**, 090602 (2004) [arXiv:hep-th/0311175].
[126] N. Iqbal and H. Liu, Phys. Rev. D **79**, 025023 (2009) [arXiv:0809.3808 [hep-th]].
[127] T. D. Cohen, Phys. Rev. Lett. **99**, 021602 (2007) [arXiv:hep-th/0702136].
[128] A. Dobado and F. J. Llanes-Estrada, Eur. Phys. J. C **51**, 913 (2007) [arXiv:hep-th/0703132].
[129] D. T. Son, Phys. Rev. Lett. **100**, 029101 (2008) [arXiv:0709.4651 [hep-th]].
[130] M. Brigante, H. Liu, R. C. Myers, S. Shenker and S. Yaida, Phys. Rev. D **77**, 126006 (2008)

[arXiv:0712.0805 [hep-th]].
[131] M. Brigante, H. Liu, R. C. Myers, S. Shenker and S. Yaida, Phys. Rev. Lett. **100**, 191601 (2008) [arXiv:0802.3318 [hep-th]].
[132] Y. Kats and P. Petrov, JHEP **0901**, 044 (2009) [arXiv:0712.0743 [hep-th]].
[133] A. Buchel, R. C. Myers and A. Sinha, arXiv:0812.2521 [hep-th].
[134] D. T. Son and A. O. Starinets, JHEP **0603**, 052 (2006) [arXiv:hep-th/0601157].
[135] C. P. Herzog, A. Karch, P. Kovtun, C. Kozcaz and L. G. Yaffe, JHEP **0607**, 013 (2006) [arXiv:hep-th/0605158].
[136] J. Casalderrey-Solana and D. Teaney, Phys. Rev. D **74**, 085012 (2006) [arXiv:hep-ph/0605199].
[137] S. S. Gubser, Phys. Rev. D **74**, 126005 (2006) [arXiv:hep-th/0605182].
[138] A. Buchel, Phys. Lett. B **663**, 286 (2008) [arXiv:0708.3459 [hep-th]].
[139] S. S. Gubser, S. S. Pufu and F. D. Rocha, JHEP **0808**, 085 (2008) [arXiv:0806.0407 [hep-th]].
[140] F. Karsch, D. Kharzeev and K. Tuchin, Phys. Lett. B **663**, 217 (2008) [arXiv:0711.0914 [hep-ph]].
[141] D. T. Son, Phys. Rev. D **78**, 046003 (2008) [arXiv:0804.3972 [hep-th]].
[142] K. Balasubramanian and J. McGreevy, Phys. Rev. Lett. **101**, 061601 (2008) [arXiv:0804.4053 [hep-th]].
[143] C. P. Herzog, M. Rangamani and S. F. Ross, JHEP **0811**, 080 (2008) [arXiv:0807.1099 [hep-th]].
[144] J. Maldacena, D. Martelli and Y. Tachikawa, JHEP **0810**, 072 (2008) [arXiv:0807.1100 [hep-th]].
[145] A. Adams, K. Balasubramanian and J. McGreevy, JHEP **0811**, 059 (2008) [arXiv:0807.1111 [hep-th]].
[146] M. Rangamani, S. F. Ross, D. T. Son and E. G. Thompson, arXiv:0811.2049 [hep-th].
[147] P. L. Kapitza, Nature **74**, 141 (1938).
[148] W. H. Keesom and G. E. Mac Wood, Physica **5**, 737 (1938).
[149] A. D. B. Woods and A. C. Hollis-Hallet, Can. J. Phys. **41**, 596 (1963).
[150] C. C. Agosta, S. Wang, L. H. Cohen, H. Meyer, J. Low Temp. Phys. **67**, 237(1987).
[151] S. J. Putterman, "Superfluid hydrodynamics", North-Holland, Amsterdam (1974).
[152] W. B. Hanson and J. R. Pellam, Phys. Rev. **95**, 321 (1954).
[153] K. M. O'Hara, S. L. Hemmer, M. E. Gehm, S. R. Granade, J. E. Thomas, Science **298**, 2179 (2002) [cond-mat/0212463].
[154] J. Kinast, S. L. Hemmer, M. E. Gehm, A. Turlapov, and J. E. Thomas, Phys. Rev. Lett. **92**, 150402 (2004).
[155] J. Kinast, A. Turlapov, J. E. Thomas, Phys. Rev. A **70**, 051401(R) (2004).
[156] J. Kinast, A. Turlapov, J. E. Thomas, Phys. Rev. Lett. **94**, 170404 (2005) [cond-mat/0502507].
[157] A. Altmeyer, S. Riedl, C. Kohstall, M. Wright, R. Geursen, M. Bartenstein, C. Chin, J. Hecker Denschlag, R. Grimm, preprint, cond-mat/0609390.
[158] J. Joseph, B. Clancy, L. Luo, J. Kinast, A. Turlapov, J. E. Thomas, Phys. Rev. Lett. **98**, 170401 (2007) [cond-mat/0612567].
[159] B. Clancy, L. Luo, J. E. Thomas Phys. Rev. Lett. **99** 140401 (2007) [arXiv:0705.2782 [cond-mat.other]].
[160] G. M. Kavoulakis, C. J. Pethick, H. Smith, Phys. Rev. A **57**, 2938 (1998) [cond-mat/9710130];
[161] B. A. Gelman, E. V. Shuryak, and I. Zahed, Phys. Rev. A **72**, 043601 (2005) [nucl-th/0410067].
[162] T. Schäfer, Phys. Rev. A **76**, 063618 (2007) [arXiv:cond-mat/0701251].
[163] A. Turlapov, J. Kinast, B. Clancy, L. Luo, J. Joseph, J. E. Thomas, J. Low Temp. Phys. **150**, 567 (2008) [arXiv:0707.2574].
[164] H. Heiselberg, Phys. Rev. Lett. **93**, 040402 (2004) [cond-mat/0403041];
[165] S. Stringari, Europhys. Lett. **65**, 749 (2004) [cond-mat/0312614].
[166] A. Bulgac and G. F. Bertsch, Phys. Rev. Lett. **94**, 070401 (2005) [cond-mat/0404687].
[167] J. E. Thomas, J. Kinast, A. Turlapov, Phys. Rev. Lett. **95**, 120402 (2005) [cond-mat/0503620].
[168] G. M. Bruun, H. Smith Phys. Rev. A **76**, 045602 (2007) [arXiv:0709.1617].
[169] J. Kinast, A. Turlapov, J. E. Thomas, Q. Chen, J. Stajic, and K. Levin, Science **307**, 1296 (2005) [cond-mat/0502087].

[170] L. Luo, B. Clancy, J. Joseph, J. Kinast, J. E. Thomas, preprint, cond-mat/0611566.
[171] S. Riedl, E. R. Sanchez Guajardo, C. Kohstall, A. Altmeyer, M. J. Wright, J. Hecker Denschlag, R. Grimm, G. M. Bruun, H. Smith, Phys. Rev. A **78**, 053609 (2008) [arXiv:0809.1814[cond-mat.other]].
[172] C. Menotti, P. Pedri, S. Stringari, Phys. Rev. Lett. **89**, 250402 (2002) [cond-mat/0208150].
[173] M. Edwards, C. W. Clark, P. Pedri, L. Pitaevskii, S. Stringari, Phys. Rev. Lett. **88** 070405 (2002).
[174] B. Clancy, Ph.D. Thesis, Duke University (2008).
[175] M. L. Miller, K. Reygers, S. J. Sanders and P. Steinberg, Ann. Rev. Nucl. Part. Sci. **57**, 205 (2007) [arXiv:nucl-ex/0701025].
[176] S. A. Voloshin, A. M. Poskanzer and R. Snellings, arXiv:0809.2949 [nucl-ex].
[177] C. Gombeaud and J. Y. Ollitrault, Phys. Rev. C **77**, 054904 (2008) [arXiv:nucl-th/0702075].
[178] L. D. Landau, Izv. Akad. Nauk Ser. Fiz. **17**, 51 (1953).
[179] J. D. Bjorken, Phys. Rev. D **27**, 140 (1983).
[180] P. F. Kolb, U. W. Heinz, P. Huovinen, K. J. Eskola and K. Tuominen, Nucl. Phys. A **696**, 197 (2001) [arXiv:hep-ph/0103234].
[181] L. D. McLerran and R. Venugopalan, Phys. Rev. D **49**, 2233 (1994) [arXiv:hep-ph/9309289].
[182] T. Hirano, U. W. Heinz, D. Kharzeev, R. Lacey and Y. Nara, Phys. Lett. B **636**, 299 (2006) [arXiv:nucl-th/0511046].
[183] E. Schnedermann, J. Sollfrank and U. W. Heinz, Phys. Rev. C **48**, 2462 (1993) [arXiv:nucl-th/9307020].
[184] D. Teaney, Phys. Rev. C **68**, 034913 (2003) [nucl-th/0301099].
[185] K. Dusling and D. Teaney, Phys. Rev. C **77**, 034905 (2008) [arXiv:0710.5932 [nucl-th]].
[186] P. Romatschke and U. Romatschke, Phys. Rev. Lett. **99**, 172301 (2007) [arXiv:0706.1522 [nucl-th]].
[187] H. Song and U. W. Heinz, Phys. Rev. C **77**, 064901 (2008) [arXiv:0712.3715 [nucl-th]].
[188] M. Luzum and P. Romatschke, Phys. Rev. C **78**, 034915 (2008) [arXiv:0804.4015 [nucl-th]].
[189] P. Huovinen and D. Molnar, Phys. Rev. C **79**, 014906 (2009) [arXiv:0808.0953 [nucl-th]].
[190] H. C. Öttinger, Physica A **254** 433 (1998).
[191] D. Teaney, J. Lauret and E. V. Shuryak, Phys. Rev. Lett. **86**, 4783 (2001) [arXiv:nucl-th/0110037].
[192] P. F. Kolb, P. Huovinen, U. W. Heinz and H. Heiselberg, Phys. Lett. B **500**, 232 (2001) [arXiv:hep-ph/0012137].
[193] P. Huovinen, P. F. Kolb, U. W. Heinz, P. V. Ruuskanen and S. A. Voloshin, Phys. Lett. B **503**, 58 (2001) [arXiv:hep-ph/0101136].
[194] C. Adler *et. al.* [STAR Collaboration], Phys. Rev. C **66**, 034904 (2002).
[195] P. F. Kolb, J. Sollfrank and U. W. Heinz, Phys. Lett. B **459**, 667 (1999) [arXiv:nucl-th/9906003].
[196] I. Bouras, E. Molnar, H. Niemi, Z. Xu, A. El, O. Fochler, C. Greiner, D. H. Rischke, arXiv:0902.1927 [hep-ph].
[197] H. Song and U. W. Heinz, arXiv:0812.4274 [nucl-th].
[198] G. S. Denicol, T. Kodama, T. Koide and Ph. Mota, arXiv:0903.3595 [hep-ph].